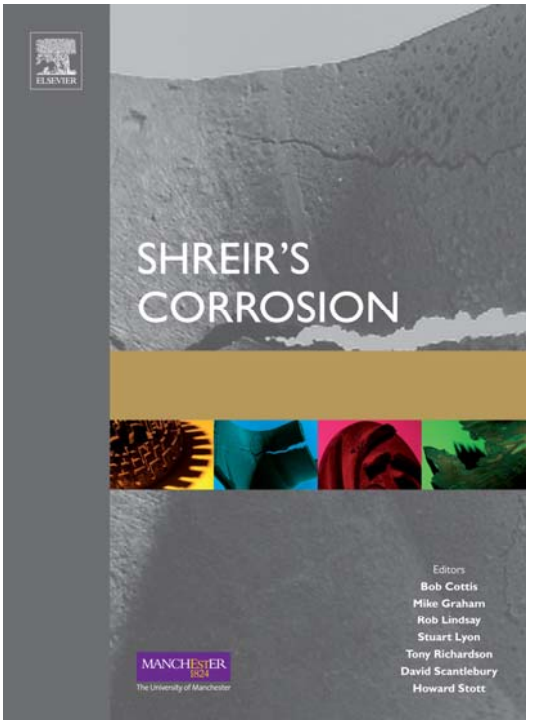

Macdonald D D and Engelhardt G R 2010 Predictive Modeling of Corrosion. In: Richardson J A et al. (eds.) Shreir's Corrosion, volume 2, pp. 1630-1679 Amsterdam: Elsevier.

2.39 Predictive Modeling of Corrosion

D. D. Macdonald
Center for Electrochemical Science and Technology, Department of Materials Science and Engineering, Pennsylvania State University, University Park, PA 16802, USA
G. R. Engelhardt
OLI Systems, Inc., 108 The American Road, Morris Plains, NJ 07950, USA

Abbreviations

BWR Boiling water reactor
CDF Cumulative distribution function
CEFM Coupled environment fracture model
CEM Coupled environment model
CEP Corrosion evolutionary path
CF Corrosion fatigue
CGR Crack growth rate
CT Compact tension
DAH Differential aeration hypothesis
DFA Damage function analysis
ECL Electrochemical crack length
ECP Electrochemical corrosion potential
EVD Extreme value distribution
HWX Hydrogen water chemistry
IGSCC Stress corrosion cracking
LPST Low-pressure steam turbines
MCL Mechanical crack length
MPM Mixed potential model
NWC Normal water chemistry
PDM Point defect model
SCC Stress corrosion cracking

Symbols

a Depth of a corrosion event
a_{max} Deepest corrosion event
a_{cr} Critical depth
b Bulk
b Inverse Tafel constant
C_k Concentration of species k
d Thickness of the wall
$\bar{D}$ Average diffusivity of breakdown sites
D_k Diffusion coefficient of species k
D_t Turbulent diffusion coefficient
E Potential
E_{corr} Corrosion potential

Shreir's Corrosion, Fourth Edition (2010), vol. 2, pp. 1630-1679

E_{crit} Critical potential for localized corrosion
E_{rp} Repassivation potential
E_0 Equilibrium potential
F Faraday's constant
F_k Integral damage function for corrosion event, k
f_k Differential damage function for corrosion event, k
G^{ex} Excess Gibbs energy
I Current density
I_{ss} Steady-state passive current density
i_a Anodic current density
i_c Cathodic current density
i_{corr} Corrosion current density
i_p Passive current density
i_0 Exchange current density
i^0_{corr} Current density on the bare surface
i^* Current density calculated in the absence of a potential drop in the cell
J_{ca} Flux of cation vacancies
J_m Annihilation flux of metal vacancies
j_k Flux of species k
K Constant in eqn [70]
k_i Reaction rate for ith reaction
K Equilibrium constant
K_I Stress intensity factor
K_{ISCC} Critical stress intensity factor
k_m Rate of chemical reaction m
K_v Electrochemical equivalent volume
L Thickness of barrier layer
L_{ss} State thickness of barrier layer
m Constant in eqn [70]
N Total number of nucleated stable pits
n_k Rate of nucleation of defect k
Q Quasipotential
P_f Probability of failure
R Gas constant
R_k Rate of production or depletion of species k
Re Reynolds number
s Surface
S Surface area
Sc Schmidt number
T Temperature
t Time
t_s Service time
t_{in} Incubation time
t_{pr} Propagation time
u Central parameter
u_i Mobility of species i
U_0 Open circuit potential
v Hydrodynamic velocity
V_k Rate of propagation of corrosion defect k
V_0 Initial pit propagation rate
$\overline{V}_0$ Mean initial pit propagation rate
V_{app} Applied voltage
V_c Critical voltage
V_m Electrode potential
X_i Internal independent variable
X_m Average depth of the largest pit
x Depth of penetration
x_0 Characteristic depth
Y_i External independent variable
z Direction perpendicular to the surface
z_k Charge of species k
α (1) Anodic transfer coefficient, (2) scale parameter, (3) polarizability of the barrier layer/solution (outer layer) interface
β (1) Tafel coefficient using natural logarithms, (2) dispersion in Laplace's distribution
ΔG^0_S Standard Gibbs energy change for the chloride absorption reaction
ΔG^0_S Change of Gibbs energy for the Schottky-pair reaction
ΔK Stress intensity factor range
ε (1) Dielectric permittivity, (2) electric field strength within the barrier layer
$\dot{\varepsilon}_{ct}$ Crack tip strain rate
ε_f Fracture strain
γ Delay repassivation constant
γ_k Activity coefficient of species k
Γ Ratio of the bare surface of the crack tip to the total geometric surface
η Dynamic viscosity
ΔK_{th} Threshold stress intensity factor range
κ Conductivity
λ (1) Constant in eqn [83], (2) function defined by eqn [97]
μ_k Chemical potential of species k
ν Kinematic viscosity
ν_k Stoichiometric coefficient of species k
ρ Density
ξ Critical areal concentration of vacancies
ζ Survival probability
σ Standard deviation
τ Dissolution time
Φ Cumulative distribution function
φ Electrical potential
Ψ Extreme value distribution
ψ Laplace's distribution function
Ω Mole volume of the barrier layer per cation

2.39.1 Introduction

As our industrial and infrastructure systems (refineries, power plants, pipelines, etc.) age, there is a considerable economic incentive to avoid unscheduled outages and to extend operation beyond the design lifetime. The avoidance of unscheduled outages is of particular interest, because the failure of even a minor component can result in the complete shutdown of a facility. For example, the unscheduled shutdown of a 1000 MWe nuclear power plant due to the failure of a valve may cost the operator between $1 million and $3 million per day, depending upon the cost of replacement power and other factors. However, if component failures could be accurately predicted, maintenance could be performed during scheduled outages, the cost of which has already been built into the price of the product, thereby minimizing the economic impact of the failure. With regard to life extension, the successful extension of operation beyond the design life translates into enhanced profits and the avoidance of costly licensing and environmental impact assessments associated with the development and construction of a new facility. However, in this case as well, the key to successful operation is the ability to avoid unscheduled downtime and hence maintain continuity of production. However, eventually, the frequency and severity of unscheduled outages render continued operation uneconomic and, at that point, replacement of the facility becomes necessary.

Corrosion is a major cause of component failure, and hence the occurrence of unscheduled downtime, in complex industrial systems. In particular, the various forms of localized corrosion, including pitting corrosion, crevice corrosion, stress corrosion cracking (SCC), and corrosion fatigue (to name the common forms), are particularly deleterious, because they frequently occur without any outward sign of accumulating damage and because they often result in sudden and catastrophic failures. Thus, the development of effective general and especially localized corrosion damage prediction technologies is essential for the successful avoidance of unscheduled downtime and for the successful implementation of life extension strategies.

There are two main approaches for predicting corrosion damage – empiricism and determinism. ('Determinism' is used here in the physics sense to describe a model whose predictions are constrained to the 'physically viable' realm by the natural laws. The term 'determinism' is often used in engineering disciplines to indicate a model that provides a definite output in response to a definite input.) Empiricism is the philosophy that everything we can ever know must have been experienced. On the other hand, determinism is the philosophy that we may predict the future from the past via the natural laws. Within these two classes, there exist numerous subclasses. For example, within the empirical class, there are functional models, in which (discrete) data are represented by continuous mathematical functions; statistical models; and artificial neural networks, to name a few. Within the broad class of 'deterministic' models, there can exist 'definite' models that yield a single output for a given set of input values; and probabilistic models, in which the inputs are distributed resulting in a distributed output from which the probability of an event occurring can be estimated.

It must be noted that, up to now, the prediction of corrosion damage has been largely based on the application of empirical models and only in the past decade, or so, have deterministic models been developed.

It is important to note that there are particular difficulties in using purely empirical models for predicting corrosion damage in real industrial systems, caused by the following factors: (i) Empirical models are generally expensive, because of the need for large databases covering many independent variables for calibration. Complex industrial systems are unique, even when they are of the same design, because they endure different operating conditions and histories. Thus, for example, an airplane that has been operating in a hot, humid environment might require more inspection and maintenance than an identical aircraft based in a desert environment. (ii) Failures are rare events. Accordingly, it is generally impossible to develop an effective database for model calibration based on the failure statistic of any given system. (iii) Empirical models also fail to capture the mechanism of failure.

Of course, deterministic models also pose many challenges. The most important of these are as follows: (i) Corrosion is an extremely complex phenomenon that depends on a multitude of factors, including the chemistry of the environment, metallurgy, and thermomechanical history of the corroding metal, hydrodynamics of multiphase flow, geometry, stress, temperature, pressure, and so on; (ii) the lack of information on kinetic parameters of the corroding system; and (iii) the need to define the corrosion evolutionary path (CEP). Because any model that is developed to describe the damaging process, and on which the deterministic prediction of damage is based, is only a figment of our imagination, and is based upon inputs from imperfect senses that are interpreted through an imperfect intellect, it is clear

that a working deterministic model can yield only an approximate description of a real system. Accordingly, pure 'determinism' is an ideal concept that is probably never achieved in reality, and the complementary, use of deterministic and empirical model provides the most effective method for predicting corrosion damage. Nevertheless, through the application of the 'scientific method,' in which a model is continually revised as it is cyclically tested against new observations, many deterministic models evolve toward providing accurate descriptions of real systems.

At this point, it is necessary to contrast the philosophical bases of 'mechanistic models' and 'deterministic models,' because great confusion exists in the literature on this issue. A mechanistic model is based upon a realistic mechanism for the process that is underpinned by a valid theory that, ideally, accounts for all of the observed properties. There is no requirement that the output must be constrained by the natural laws, as is the case for a deterministic model. Frequently, it is found that the values of unknown parameters are simply determined by calibration, whereas, in a deterministic model those same parameter values would be determined by the constraints. Given sufficient complexity and enough unknown parameters, a mechanistic model can be made to fit any data set imaginable and then yield predictions that are frequently at odds with reality. This cannot happen in the case of a deterministic model because the constraints, which are expressions of scientific generality (i.e., the 'natural laws'), limit the predictions to a realm that is consistent with the constraints themselves (i.e., to physical 'reality').

The need to define the CEP has been explained above. The CEP is defined as the path taken by the system in terms of those independent variables that have a significant impact on the rate of damage accumulation in transitioning from the present state to the future state. This path must be continuous and is required for both deterministic and empirical damage prediction models. Examples of defining the CEP are given later in this chapter, when we discuss the prediction of damage in practical systems.

In this article, we review recent advances in the development of some deterministic models for predicting corrosion damage (the review of some empirical models, including statistical models and artificial neural networks can be found in other articles in this volume). This subject is much too broad for justice to be done in a single chapter of the current length, but, by limiting the scope, the authors wish to illustrate the essential elements of theory and deterministic model-building and to demonstrate how the models can make useful predictions. The cases discussed have been chosen to address practical problems in current science and engineering, and, where possible, applications of the models to real engineering problems have been selected.

2.39.2 Definition of Corrosion Damage

As is well known, corrosion damage can be classified into two categories: uniform (general) corrosion and localized corrosion, and the quantitative description of these two cases are quite different. In this review, principal attention will be devoted to the case of localized corrosion. However, it must be noted that, in the general case, it is impossible to describe the propagation of localized corrosion damage without having reliable deterministic models for general corrosion, because the latter models yield the most important value for predicting the rate of localized corrosion; namely, the corrosion potential, E_{corr}.

In the case of general corrosion, it is natural to define corrosion damage at a given point on a metal surface as being the thickness of the metal layer that has corroded, a. This definition means that we can predict general corrosion damage if we can calculate a as a function of time and of the independent variables controlling the damaging process, that is, a is predicted in the form:

$$a = a(t, X_i, Y_i) \qquad [1]$$

Here, X_i and Y_i are internal and external independent variables, respectively, that determine the damage propagation rate. Examples of internal variables are grain size and orientation, texture, electrochemical kinetic parameters, and other microstructural properties. The external variables include loading and environmental conditions.

Even the term 'uniform corrosion' shows that, usually, the corroding layer thickness, a, depends slightly on the coordinates on the metal surface, if internal and external variables can be considered to be approximately constant for different parts of the system. In other words, it is assumed that, for a given set of conditions, uniform corrosion damage can be characterized for a given time and for given environmental conditions by a single value – average thickness of the corroded layer. Accordingly, for the case of general corrosion, the service life of the system, t_s, can be defined as the duration before the corroding

layer thickness achieves some average critical thickness, a_{cr}, (or reaches some minimum allowed value). Usually, the uniform corrosion data are analyzed by using the normal distribution. It is also assumed that the standard deviation of the thickness of the corroded layer, σ, can be estimated by using eqn [1], if the standard deviations of values X_i and Y_i are known by using, for example, the standard method for calculating the propagation of error.

In the case of localized corrosion, the situation becomes more complicated. Generally speaking, the accumulation of localized corrosion damage in a system is completely defined if we know how many pits or other corrosion events (per square centimeter) have depths between x and $x + dx$ for a given observation time, t, at a given location on the metal surface. We will denote this quantity as $f_k(x, t)dx$ where $f_k(x, t)$ is the so-called differential damage function.[1] Here, the index k denotes different types of localized defects, such as active and passive pits, cracks, crevices, and so on.

However, in the overwhelming majority of practical cases, such complete information is not required to effectively predict the failure time due to the penetration of the deepest event. Thus, very often, it is sufficient to obtain information about only the deepest corrosion event (pit, crack), because failure in the system commonly occurs when the depth of the deepest corrosion event a_{max} exceeds some critical value, a_{cr}. Usually, a_{cr} is the thickness of the wall of a pipe, for example, or the depth of a pit transitioning into an unstable crack. With regard to the first case, in order to describe the damage, we can use an equation of the previous form, that is,

$$a_{max} = a_{max}(t, X_i, Y_i) \quad [2]$$

Accordingly, the service life of the system, t_s (that is sometimes denoted as being the time to failure, t_f) can be expressed as the sum of incubation period, t_{in}, and propagation period, t_{pr}, in order for the defect to attain a critical depth:

$$t_s = t_{in} + t_{pr} \quad [3]$$

The period of propagation, t_{pr}, can be divided into periods corresponding to different forms of propagating of the corrosion defect; for example, in the form of pit, t_{pit}, or in the form of crack, t_{cr}, if the crack nucleates from the pit. In turn, for example, t_{cr} can be subdivided into the period $t_{cr,c}$ (the time required for the surface crack to grow into a through crack) and $t_{cr,g}$ (the time for a through crack to grow to a prescribed critical length), and so on.

It is important to understand that even if relation [2] can be obtained, its applicability would be questionable. The problem is that eqn [2] yields a single number for a_{max} for a given value for t and for other parameters of the system. However, in the general case, it is impossible to describe available experimental data by a single number. Thus, **Table 1** shows typical data for the depths of the deepest pits experimentally measured[2] on 20 sampled areas of 300×300 mm on the bottom outer surface near the periphery of a circular tank made of SS41 carbon steel, storing heavy petroleum, after 7 years of service; all of the pit depths not smaller than 0.5 mm were recorded, and the maximum pit depth in each sampled area was noted. The experimental data were taken from Harlow and Wei.[3–7]

We see that the difference between the observed values is greater than 280%. It is clear that, in the general case, prediction of corrosion damage can be done only in probabilistic terms. Apparently, the best form of predicting localized corrosion damage would be prediction of the probability of failure, P_f:

$$P_f = P_f(a_{cr}, t, X_i, Y_i, S) \quad [3]$$

that is, the probability that at least one corrosion event of any form (pit, stress corrosion crack, fatigue crack) reaches some critical depth, a_{cr}, at a given observation time, t, for any given set of environmental conditions. It is essential that P_f must be a function of the total area of the system, because the larger the area of the system, the larger will be the number of corrosion events and hence the greater the probability that a deeper event will exist. Accordingly, P_f must increase with area.

Table 1 Maximum pit depth distribution, $a_{max,i}$ (in ascending order) for oil storage tank

	i								
	12	***13***	***14***	***15***	***16***	***17***	***18***	***19***	***20***
$a_{max,i}$ (mm)	0.65	0.71	0.75	0.84	0.90	1.07	1.18	1.25	1.82

Index i numerates samples. Samples with $i < 12$ have maximum pit depth of <0.5 mm.

Let us consider possible ways for theoretically estimating this probability. The most intensive work that has been reported on predicting corrosion (in aluminum alloys) is that of Harlow and Wei,[3–7] whose important achievement has been to insert into prediction technology the realization that an analytical description (not necessarily a deterministic description) of the accumulation of damage is possible. Their approach is as follows: It is assumed that a pit is nucleated at an initial moment, $t = 0$, with an initial depth of a_0, and that the depth increases with increasing observation time, t. At some critical depth, a_{tr}, the pit transitions into a crack. By using mechanically-based models for calculating pit or crack propagation rates, an analytical expression for the depth of the corrosion event, a (in the form of a pit or crack), as a function of time is found in analytical form, as described by eqn [1]. All variables X_i and Y_i (where only temperature has been included in the environmental variables) are subdivided into two parts: deterministic parameters (in the engineering sense, i.e., parameters with fixed values) and random parameters, with the latter obeying, for example, the Weibull distribution. Subsequently, eqn [1], together with the change-of-variable theorem, or standard Monte Carlo technique, may be used to estimate the probability of failure, $Pr(a > a_{cr},t)$, that is, the probability that the crack length, a, exceeds the prescribed critical length of the crack, a_{cr}, at given observation time, t. The obvious problem with this approach is that it is completely devoid of environmental effects, such as those of potential, pH, $[Cl^-]$, and solution conductivity on pit and crack nucleation and growth, even though these effects have been established experimentally and are consistent with field observations. Accordingly, the underlying model for damage propagation fails to explain all of the experimental observations and hence is not viable. The second problem is that, by selecting a single pit, the significant literature demonstrating that pitting, which leads to cracking, is a progressive phenomenon in which new pits nucleate as existing pits grow and die (repassivate), is ignored. Thus, by selecting a particular pit initially, there is no way of knowing, *a priori*, whether that pit will survive to grow to a critical depth and hence, nucleate a crack. Indeed, the approach taken by Harlow and Wei is, in form, very similar to that employed by Liu and Macdonald[8,9] in the early 1990s to describe the failure of low pressure steam turbines, except that the latter study incorporated environmental effects, and the predictions of the component models were constrained by the appropriate natural laws (including the conservation of charge, recognizing the electrochemical nature of the damaging processes).

The question then arises whether the models of Harlow and Wei, for example, can be generalized by including the influence of environmental parameters, other than temperature, in explicit form. Even if they were able to do so, which, in itself, would require a massive reformulation of the models to incorporate environmental effects, in our opinion, the applicability of their approach would remain highly questionable, because environmental effects cannot be included in an *ad hoc* fashion. In addition, as noted above, the current Harlow and Wei[3–7] models consider only a single event, whereas it is well known that corrosion damage due to pitting, stress corrosion cracking, and corrosion fatigue accumulates progressively (that is, new pits/cracks nucleate while existing pits/cracks grow and die). In other words, it is impossible, in the general case, to attribute corrosion damage to a single corrosion event on the surface in isolation from all other events. Instead, the development of damage must be described in terms of an ensemble of localized corrosion events.

This thesis is confirmed by the following: The probability that any particular pit will repassivate (die) during the service life of a system is generally very high. Thus, let us consider the classical measurements of pit depth distribution versus time performed by Aziz[10] on Alcan aluminum alloy 2S-O in Kingston tap water (**Figure 1**). This study showed that by the end of 2 months, the bulk of the pits represented by the bell-shaped curve had ceased to grow (i.e., they had 'died') and only the deeper pits continued to propagate. In other words, by the end of two months from the beginning of the corrosive attack (in this particular case), the overwhelming majority of the pits repassivate (die). Accordingly, there is no way of knowing whether the pit selected had the necessary characteristics to grow to the critical length. In the general case, the probability that the depth of the deepest pit will exceed some critical value depends on the number of nucleated, stable pits and on the probability of repassivation. In some extreme cases, the probability that the depth of the deepest pit increases beyond some critical value is vanishingly small,[11] with the result that cracks will not nucleate. Obviously, this is a scenario that can only be described in terms of a large ensemble of events, rather than in terms of a single event.

In addition, the interaction between growing pits must be taken into account. The presence of existing

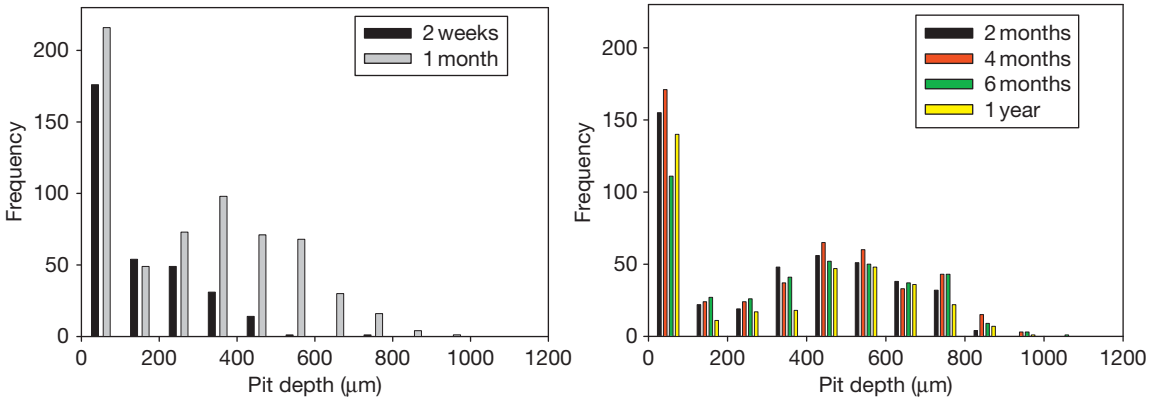

Figure 1 Pit depth distributions for Alcan 2S-O aluminum alloy immersed in Kingston water for different periods of time. The increment in pit depth is 100 μm. Reproduced from Aziz, P. M. *Corrosion* **1956**, *12*, 35–46.

pits impacts the probability of nucleation of other stable pits within the neighboring region. This phenomenon has been experimentally reported by Macdonald[12] and is explained by the competition of the pits for the available resources on the external surfaces (oxygen reduction) or because the existing pit cathodically protects the neighboring surface and hence inhibits the nucleation of the second pit. The interaction between the 'hemispheres of influence' (subtending the external area over which the cathodic reaction occurs) of growing, stable pits can also reduce the propagation rate of each of the pits, simply by reducing the metal potential at the pit bottom. Finally, we also have to take into account the overlapping between growing pits that also influences the shape and propagation rate. All of this shows that any method for estimating the probability of failure on the basis of the propagation of a single corrosion event (pit or crack) cannot be general.

2.39.3 Damage Function Analysis

One of the approaches that considers the accumulation of corrosion damage in terms of the evolution of an ensemble of pits and cracks is damage function analysis (DFA).[1,13,14] (The other possible method, that based on the Monte Carlo simulation of movement of ensemble of corrosion events will also be described below). As mentioned above, the differential damage function, $f_k(x,t)$ yields the complete description of corrosion damage. It is easy to obtain the differential equation for this function. The function f_k has a dimension of $\#/(\mathrm{cm}^2\ \mathrm{cm}) = \#/\mathrm{cm}^3$, analogous to the concentration of particles. Accordingly, it is very convenient to regard each defect as a 'particle' that moves in the x direction (perpendicular to the surface, with $x = 0$ being at the metal surface). The coordinate of this particle, x, coincides with the depth of penetration into the surface. Accordingly, f_k must obey the law of mass conservation

$$\frac{\partial f_k}{\partial t} + \frac{\partial j_k}{\partial x} = R_k, \quad k = 1, 2, \ldots, K \qquad [4]$$

where j_k and R_k are the flux density and the bulk source (sink) of the 'particle' k respectively. Thus, the subscript k enumerates the corrosion defect (e.g., pit or crack) and K is the total number of different corrosion defects in the system. By definition, $R_k(x,t)\mathrm{d}x\mathrm{d}t$ yields the number of defects k (per square centimeter) with depths between x and $x + \mathrm{d}x$ that arise (or disappear) during the period of time between t and $t + \mathrm{d}t$, due to transformation (repassivation, in the case of pits).

The system of eqns [4] can be solved with the appropriate boundary and initial conditions.

$$j_k = n_k(t) \quad \text{at } x = 0, t > 0 \qquad [5]$$

and

$$f_k = f_{k0}(x) \quad \text{at } x \geq 0, t = 0 \qquad [6]$$

where $f_{k0}(x)$ is the initial distribution of defect k (usually we can assume that $f_{k0}(x) = 0$, i.e., no damage exists at zero time) and $n_k(t)$ is the nucleation rate of the same defect (i.e., $n_k(t)\ \mathrm{d}t$ is the number of stable defects (per square centimeter) that nucleate in the induction time interval between t and $t + \mathrm{d}t$).

Thus, because the defect propagation flux, j_k, must be nonnegative (the depth of a corrosion event can only increase with time), the following, simplest numerical upwind finite difference scheme can be used for numerically solving eqns [4]–[6].

$$f_{k,m}^{n+1} = f_{k,m}^{n} - \frac{\Delta t}{\Delta x}\left(j_{k,m}^{n} - j_{k,m-1}^{n}\right) + R_k^n \Delta t \qquad [7]$$

Here, we use the straightforward approach of choosing equally spaced points along both the t- and x-axes: $x_j = x_0 + m\Delta x$, $m = 0, 1, \ldots, \mathcal{J}$ and $t_j = t_0 + n\Delta x$, $n = 0, 1, \ldots, N$, and we denote $f_{k,m}^{n} = f_k(t_n, x_m)$. The values $f_{k,0}^{n}$ and $f_{k,m}^{0}$ are calculated from the boundary and initial conditions [4] and [5]. Of course, it is assumed that we know (i.e., can calculate) fluxes, j_k, and sources/sinks, R_k, as functions of the spatial coordinates and time, and, in nonlinear cases, as functions of the unknown values of f_k.

It is important to note that, sometimes, the equation of continuity is presented in the simplified form[15,16]

$$\frac{\partial f_k}{\partial t} + \frac{\partial [V_k(x) f_k]}{\partial x} = R_k, k = 1, 2, \ldots, K \qquad [8]$$

This expression implies that the rate of kth defect, V_k, depends only on the depth of penetration, x, and accordingly, for the flux density, j_k, we have

$$j_k(x, t) = f_k(x, t) V_k(x) \qquad [9]$$

In the simplest cases, it is even possible to obtain analytical solutions for the damage functions. As an example, let us consider the case of pitting corrosion under constant external conditions. In this instance, we have two kinds of defects ($K = 2$): active pits with the damage function, f_a, and passivated pits (i.e., those that have 'died' through delayed repassivation) with the damage function, f_p. Let us assume that the flux density of active pits is described by eqn [8] with $V_a(x) = V(x)$. By definition, the flux of passivated pits is zero (i.e., these pits are 'dead'). It is evident that functions R_a and R_p must obey the relation $R_p = -R_a$ (a pit must be either alive or dead). If, in addition, we assume that the pit repassivation process obeys a first order decay law, the function R_a has the form

$$R_a(x, t) = -\gamma f_a(x, t) \qquad [10]$$

where γ is the delayed repassivation ('death') constant (i.e., the rate constant for repassivation of stable pits). In the general case, γ depends on the depth of the pit, x, and on time, t, when the external conditions depend on time. However, in this example, we assume that γ is a constant, that is, we suppose that pits repassivate accidentally and that the probability of repassivation does not depend on pit depth. (This is clearly a gross oversimplification, since the probability of delayed repassivation is expected to increase with pit age, but this does not change the logic of the argument). Accordingly, the system of equations for calculating the DFs has the form

$$\frac{\partial f_a}{\partial t} + \frac{\partial [V(x) f_a]}{\partial x} = -\gamma f_a \qquad [11]$$

and

$$\frac{\partial f_p}{\partial t} = \gamma f_a \qquad [12]$$

The boundary and initial conditions are given as

$$V f_a = n(t) \text{at } x = 0, t > 0 \text{ and } f_a = f_p = 0 \quad \text{at } t = 0 \qquad [13]$$

where $n(t)$ is the nucleation rate of pits on the surface. Analytical solutions to this system of linear partial first-order differential equations can be obtained by using the characteristic method[17] and have the following form:

$$f_a = \frac{\exp[-\gamma\theta(x)] n[t - \theta(x)]}{V(x)} \text{ and}$$
$$f_p = \frac{\gamma \exp[-\gamma\theta(x)] N[t - \theta(x)]}{V(x)} \qquad [14]$$

where

$$\theta_{pit}(x) = \int_0^x \frac{dx'}{V(x')} \qquad [15]$$

is the age of a pit with depth x and

$$N(t) = \int_0^t n(t')dt' \qquad [16]$$

is the number of stable pits (per square centimeter) that nucleate in the time interval between 0 and t.

In some cases, it is convenient to use the so-called integral damage function

$$F_k(x, t) = \int_x^\infty f_k(x', t)dx' \qquad [17]$$

which yields the number (per square centimeter) of corrosion events with depths larger than x for a given observation time, t. It is important to note that, experimentally, only the sum of the damage functions for active and passive pits $f = f_a + f_p$ is determined and in many instances the integral damage function only is measured. Accordingly, it is important for practical reasons to obtain the equation for the integral damage function, $F = F_a + F_p$, for the sum of the active and passive pits. Note that, for the considered case, the integral damage function corresponds to the

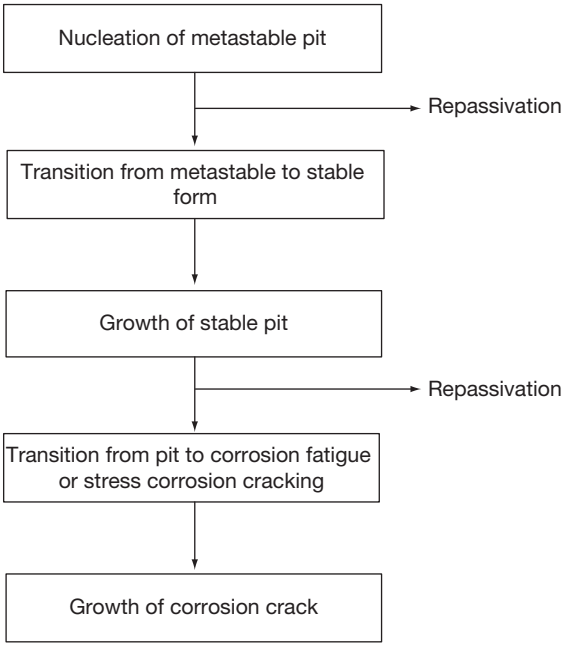

Figure 2 Schematic history of the nucleation and propagation of corrosion damage.

number of remaining pits on a surface, as the surface is removed layer by layer in preestablished increments. From eqns [14] and [17], we therefore have

$$F(x,t) = \exp[-\gamma\theta(x)]N[t-\theta(x)] \qquad [18]$$

According to the theory outlined above, calculation of the damage functions requires the determination of three independent functions for each kind of corrosion defect, k: (1) the rate of defect nucleation, n_k; (2) the flux density (growth rate) of the defect, j_k; and (3) the rate of transition of one kind of defect into another, R_k (e.g., the transition of an active pit into a passivated pit or the transition of a pit into a crack). In other words, we need to have quantitative models for describing each stage of corrosion damage as indicated in Figure 2. Below, we will discuss the feasibility of calculating each of these three functions. However, as noted above, the detailed deterministic description of any phase of corrosion propagation is impossible without reliable information about the corrosion potential of the system, E_{corr}. Accordingly, in the first step, the methods for calculating E_{corr} will be considered.

2.39.4 Mixed Potential Model

In 1937, Wagner and Traud[18] formulated their mixed potential theory in electrochemistry, in which the potential adopted by an electrode in contact with an aqueous solution containing both oxidizing and reducing species is determined by a balance of the cathodic (reduction) and anodic (oxidation) partial processes occurring at the surface. If the electrode is inert, the resulting potential is known as the redox potential, E_{redox}. On the other hand, if the electrode is electroactive and undergoes electrooxidation (corrosion), thereby contributing to the total partial anodic current, the potential is known as the electrochemical corrosion potential, ECP (or E_{corr}), of the substrate. Thus, if the partial current densities do not depend on the coordinate on the metal surface, the charge conservation condition for the interface may be written as

$$\sum_k i_{a,k} + \sum_m i_{c,m} = 0 \text{ at } E = E_{corr} \qquad [19]$$

where $i_{a,k}$ and $i_{c,m}$ are partial anodic and cathodic current densities, corresponding to the kth anodic and mth cathodic reaction correspondingly. This simple theory has proved to have a profound impact on how we interpret the corrosion of metals and alloys in a wide variety of systems.

As an example, let us consider one of the first comprehensive applications of the mixed potential theory in corrosion science to an industrial system, namely the calculation of ECP in the coolant circuits of water-cooled nuclear reactors, particularly boiling water reactors (BWRs), using a mixed potential model (MPM).[19,20] In this complex chemical system (the reactor coolant circuit), radiolysis of the coolant water by ionizing radiation (γ-photons and neutrons) produces a myriad of electroactive species, some of which are oxidizing species (e.g., O_2, H_2O_2, OH) and others that are reducing species (H_2, H). These species all contribute to the current flow across the interface, but the mixed potential theory predicts that the contribution that any given species can make to the potential is roughly proportional to its concentration. Thus, in BWR primary coolant circuits, the only species of practical importance are O_2, H_2O_2, and H_2, since the concentrations of these species are orders of magnitude greater than those of the other radiolytic species. The reactions describing each of the electroactive species are described as redox reactions, which can be written in the general form as

$$R \leftrightarrow O + ne^- \qquad [20]$$

where R and O are reduced and oxidized species, respectively, with the kinetics of the reaction being

described in terms of the generalized Butler–Volmer equation

$$i_{R/O,j} = \frac{e^{b_{a,j}\eta_j} - e^{-b_{c,j}\eta_j}}{\frac{1}{i_{0,j}} + \frac{e^{b_{a,j}\eta_j}}{i_{l,f,j}} - \frac{e^{-b_{c,j}\eta_j}}{i_{l,r,j}}} \quad [21]$$

where b_a and b_c are the anodic (oxidation) and cathodic (reduction) inverse Tafel constants, i_0 is the exchange current density, $i_{l,f}$ and $i_{l,r}$ are the mass transport limiting current densities, and η is the overpotential that is defined as the difference between the potential and the equilibrium potential for reaction j. The parameters b_a and b_c are normally measured in separate experiments, but in principle can be calculated *ab initio*. The exchange current density, i_0, is almost always measured directly, as theory is not sufficiently well developed to calculate this quantity from first principles. In addition to the redox partial reactions (oxidation and reduction processes), the anodic oxidation of the substrate also contributes to the total current density. In this case, the point defect model (PDM)[21] (the PDM will be considered in detail in the next section) provides the functional form of the anodic oxidation current density as

$$i_a = A + Be^{CE} \quad [22]$$

where A, B, and C are constants that depend upon the values of fundamental parameters in the model and upon the properties of the system (e.g., pH). For metals and alloys that form n-type passive films, in which cation interstitials and/or oxygen vacancies are the dominant defects, $B = 0$, and the anodic oxidation current density is independent of potential, unless there is a change in the oxidation state of the metal ion (cation or interstitial) being ejected from the barrier oxide layer at the barrier layer–solution interface. Systems of this type include iron and carbon steel, the stainless steels, and the chromium-containing, nickel-based alloys, such as Alloys 600 and 22. On the other hand, for metals that form p-type passive films (e.g., nickel), $A = 0$, and B and C are greater than zero. In this case, the passive current density is described by the Tafel equation.

The conservation of charge requires that the sum of the partial current densities at the interface be zero, with this condition being expressed as

$$i_a(E) + \sum_{j=1}^{\mathcal{J}} \frac{e^{b_{a,j}\eta_j} - e^{-b_{c,j}\eta_j}}{\frac{1}{i_{0,j}} + \frac{e^{b_{a,j}\eta_j}}{i_{l,f,j}} - \frac{e^{-b_{c,j}\eta_j}}{i_{l,r,j}}} = 0 \quad [23]$$

where $\mathcal{J}$ is the total number of redox reactions in the system. Note that in eqn [19], the summation takes place over the anodic and cathodic reactions separately, whereas in eqn [23], index j enumerates the redox reactions, each comprising conjugate partial anodic and cathodic partial reactions. Solution of eqn [23] yields the ECP or the corrosion potential, $E_{corr.}$ Note that $\eta_j = E - E_j^e$, where E_j^e is the equilibrium potential for the jth redox reaction. The limiting currents can be written in terms of the mass transfer correlations for the flow geometry and flow regime of interest.[22]

$$i_{l,j} = \pm n_j F A' Re^{\lambda} Sc^{\gamma} C_{O/R}^{b} \quad [24]$$

where n_j is the number of electrons involved in the reaction, A' is a constant, $Re = dV/v$ is Reynolds number, d is the hydrodynamic diameter of the channel, V is the flow velocity, $v = \hat{\eta}/\rho$ is the kinematic viscosity, $\hat{\eta}$ and ρ are the dynamic viscosity and the density, respectively, of the medium, and $C_{O/R}^{b}$ is the concentration of the reactive species in the bulk environment. The Schmidt number is defined as $Sc = v/D$, where D is the diffusivity of the reacting species. The sign convention is '+' for the forward direction (left to right) of the reaction [20], as written, and '−' for the reverse direction. Mass transfer correlations of the type expressed by eqn [24] are available in the literature for a wide variety of flow geometries and regimes (Selman and Tobias,[22] and citations therein), with the latter corresponding to specific ranges in Re and Sc. Once the corrosion potential is known (by solving eqn [23]), the corrosion current density is readily calculated using eqn [22].

As noted above, the MPM has been used extensively to calculate the corrosion potentials of stainless steel components in the coolant circuits of BWRs, and we will use this case to illustrate the power of this model in defining the response of metals and alloys to the properties of the environment in a complex industrial system. The typical measured and calculated ECP data for a cell attached to the recirculation piping of the Liebstadt BWR in Switzerland as a function of the amount of hydrogen added to the feedwater are plotted in **Figure 3**. This represents a 'double blind' comparison in that those who performed the calculations[19,23] did not have access to the data measured on the reactor, and those who measured the ECP on the reactor (Sierra Nuclear) did not have access to the calculated values. As shown, the measured and predicted corrosion potential data are in good agreement, except for the initial point (zero added hydrogen). However, in this case, it was found that the level of agreement could be greatly improved by changing the mass transport parameters (flow velocity, hydrodynamic diameter, etc.).

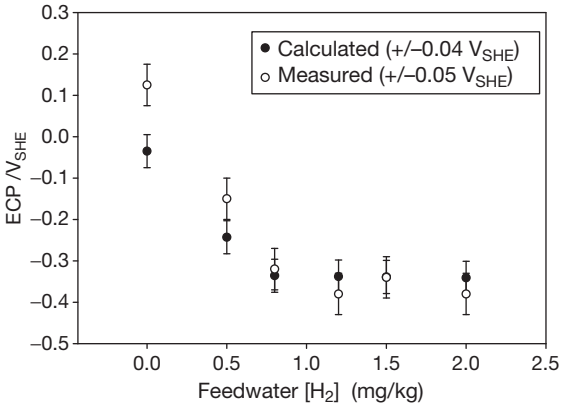

Figure 3 Comparison of calculated and measured ECP for the Leibstadt BWR in Switzerland. The 'measured' data were acquired in a test cell attached to the recirculation piping. The data employed in the calculation are summarized in Macdonald and Urquidi-Macdonald[19] and Macdonald *et al.*[23] The estimated accuracies of the calculated and measured data are indicated in the box in the figure.

Since these parameters are poorly characterized for an autoclave at very low flow rates, the disagreement in the absence of added hydrogen is of little consequence.

The accuracy of any MPM model for predicting E_{corr} and the rate of uniform corrosion depends on the accuracy of modeling of the rates of particular electrochemical reactions along with the completeness of the set of reactions included in the summation in eqn [19]. A detailed review of different models for the kinetics of corrosion can be found in the corresponding chapter of this book **Chapter 2.38, Modeling of Aqueous Corrosion**. Here we would only like to mention that already existing commercial software yields reliable prediction of the corrosion potential and, correspondingly, the rate of uniform corrosion under relatively complicated conditions, including the influence of adsorption, active–passive transition effects, scaling, transport in porous media, and so on.

Thus, the models of Anderko *et al.*[24–26] and those of others[8,9,19–21,23] have been developed for simulating the rates of general corrosion of selected metals (including carbon steels, stainless steels, aluminum, and nickel-based alloys) in aqueous solutions. The model consists of thermophysical and electrochemical modules. The thermophysical module is used to calculate the speciation of aqueous solutions and to obtain concentrations, activities, and the transport properties of individual species. The electrochemical module simulates partial oxidation and reduction processes on the surface of the metal. It is capable of reproducing the active–passive transition and the effect of solution species on passivity. The model has been implemented in a program that can be used to simulate the effects of various conditions, such as temperature, pressure, pH, component concentrations, and flow velocity on the corrosion potential and corrosion rate. The model clearly demonstrates the influence of inhibitors on corrosion rate. Good agreement with experimental data has been obtained.

Other comprehensive models have been developed for describing general corrosion under specific conditions. Thus, Nordsveen *et al.*[27] developed a mechanistic model of uniform carbon dioxide (CO_2) corrosion that takes into account such phenomena as diffusion of species between the metal surface and the bulk including diffusion through porous surface films, migration due to the establishment of potential gradients, and the existence of homogenous chemical reactions, including the precipitation of surface films. Nešić *et al.*[28] developed a comprehensive model for calculating internal uniform corrosion rates under multiphase flow conditions in mild steel pipelines.

However, it is important to note that, in the general case, for calculating ECP and uniform corrosion rate, where extensive localized corrosion may exist on a surface, thereby imparting significant nonuniformity in the current densities, we have to use, instead of eqn [19], the following equation.

$$\int_S \sum_m i_{a,m}\, dS + \int_S \sum_k i_{c,k}\, dS = 0 \quad \text{at } E = E_{corr} \quad [25]$$

It is evident that eqn [25] reduces to eqn [19] when we can assume that the partial current densities do not depend on the coordinates (location) on the metal surface, or if we can neglect any such dependencies. Thus, let us consider the case of pitting corrosion. Of course, the anodic current density inside pits can exceed the passive corrosion current density by several orders of magnitude. However, if the area of the active dissolution (area of pit surfaces) is much smaller than the total area of the metal surface (active corrosion current is much smaller than the passive corrosion current), it may be possible to use eqn [19] instead of eqn [25]; otherwise, such a simplification would be incorrect.

Experiments show that, often, both possibilities can be realized in an industrial system.[29,30] Thus, in the case of the corrosion of Alloy 20Kh13 (the Russian analog of Type 403 SS) in NaCl solutions, the corrosion potential is observed to decrease with time.[30] This reduction occurs due to the intensive growth of corrosion pits, because the total cathodic partial current has

to increase in order to compensate the increasing total partial anodic current, to conserve charge in the system. At some point, this growth stops due to the transport limitation for the cathodic reactant (oxygen), that is, the system is now limited by the lack of cathodic resources to support the ever-increasing corrosion current. On the other hand, such reduction is not observed in cases where the total area of observed pits is very small and hence, the nonuniformity in the partial current densities is minor and can be ignored.

These examples clearly show that, in the general case, eqn [25] must be used for predicting corrosion potential, at least in the case of steels that are not highly resistant to localized corrosion in the prevailing environment. It is evident that because of the statistical character of pit distribution in size and position, the imposition of charge conservation can be done correctly only by considering propagation of pitting damage as the evolution of an ensemble of pits that initiate, propagate, and repassivate on the metal surface.

2.39.5 Rate of Pit Nucleation

2.39.5.1 Empirical Models

It would be natural to assume, and experiment confirms this at least for the case of stainless steels, that the rate of nucleation of stable pits, n, is proportional to the rate of nucleation of metastable pits, n_{mp},[31–33] that is,

$$n = \varsigma n_{mp} \qquad [26]$$

where coefficient, ς, can be considered as the probability of nucleation of a stable pit from a metastable pit and is termed the 'survival probability.' This parameter can be measured experimentally. Thus, for example, for Type 304L stainless steel in chloride-containing solution, the experimentally measured survival probability has a value of the order of 10^{-2} to 10^{-4},[31,32] depending upon the potential and solution conditions. Accordingly, the most probable number of stable pits (per square centimeter), N_0, will be $N_0 = \varsigma N_{mp,0}$, where $N_{mp,0}$, is the most probable number of available sites (per square centimeter) for metastable pits.

In many practical cases, it is possible to assume that all stable pits on a given surface nucleate during an initial period of time that is much smaller than the observation time, t, or the service life of the system, t_s. In this case, the process is termed 'instantaneous nucleation.' For example, for the case of the pitting corrosion of aluminum in tap water, as described by Aziz,[10] practically all the pits were found to nucleate within the first 2 weeks (see **Figure 1**). Under these conditions, the total number of nucleated stable pits (per square centimeter) that nucleate in the time interval between 0 and t can be simply represented as

$$N(t) = N_0 U_+(t) \qquad [27]$$

where $U_+(t)$ is the asymmetrical unit function ($U_+ = 0$ at $t \leq 0$ and $U_+ = 1$ at $t > 0$).

If pit nucleation cannot be regarded as being 'instantaneous,' the simplest assumption concerning the pit nucleation rate of metastable sites, $n_{mp}(t) = dN_{mp}/dt$, is that $n_{mp}(t)$ is proportional to the number of available metastable sites, that is, $dN_{ms}/dt = [N_{mps,0} - N_{mp}(t)]/t_0$,[32] which yields

$$N(t) = N_0[1 - \exp(-t/t_0)] \qquad [28]$$

where t_0 is some characteristic time. It is evident that t_0 must depend on the corrosion potential, temperature, and electrolyte composition, and some experimental data indicating such dependencies can be found in the literature.[31–34] However, no theoretical (deterministic) model has been reported for estimating t_0 as a function of the environmental conditions and the kinetic parameters of the system.

2.39.5.2 Point Defect Model

A comprehensive model, in the form of the PDM[35–39] has been developed for estimating the nucleation rate of metastable pits which, when combined with eqn [26], yields the sought-after nucleation rate of stable pits. (Note that only the growth of stable pits gives rise to pitting damage on a surface.) The PDM was originally developed in the early 1980s to provide an atomic scale description of the growth of passive films on a metal surface, but was subsequently expanded to describe metastable passivity breakdown. Thus, it is clearly evident that any deterministic model for describing pit nucleation rate must simultaneously describe the properties of passive films existing on the metal surface and clearly specify the criteria for passivity breakdown itself. The conditions under which passive films exist on metal surfaces are a matter of great theoretical and practical interest, because the phenomenon of passivity is the enabler for our current, metals-based civilization.[21] Thus, our industrial systems and machines are fabricated primarily from the reactive metals and their alloys, including iron, nickel, chromium, aluminum, titanium, copper, zinc, zirconium, stainless steels, nickel-base alloys, and

aluminum alloys, to name a few. Although the phenomenon of 'passivity' has been known for about 170 years,[40] and the conditions under which metals and alloys become passive have been systematically explored over the past 70 years, until recently no reasonably unifying theoretical treatment of the limits of passivity has emerged. While many theories and models for the passive state have been developed,[21] most of the presently available models describe an already existing passive film and do not address the conditions under which the film may form or disappear. One of the few attempts to address this issue is the one by Engell,[41] who postulated that passive films can be thermodynamically stable or metastable, with film formation being governed by equilibrium thermodynamics in the first case and by the relative rates of formation and dissolution in the second. While Engell's work[41] made a valuable contribution to the theory of passivity, it did not resolve the theoretical issues with sufficient precision to allow specification of the exact conditions under which passivation/depassivation might occur (see below).

A comprehensive review of the conditions under which passivity may occur and be lost has been explored within the framework of the PDM by using phase–space analysis (PSA) and can be found in Macdonald.[42] It has been shown that the PDM provides a comprehensive basis for describing the formation and destruction of passive films and hence allows specification of the conditions for the use of reactive metals in our metals-based civilization. A brief description of some results is given below.

The PDM postulates that passive films that form on metal and alloy surfaces in contact with oxidizing environments are bilayer structures comprising a highly (point) defective barrier layer, which grows into the metal and an outer layer that forms via the hydrolysis of cations transmitted through the barrier layer and the subsequent precipitation of a hydroxide, oxyhydroxide, or oxide, depending upon the formation conditions, or by transformation of the outer surface of the barrier layer itself (an 'Ostwald ripening' process). In many systems (e.g., Ni and Cr), the barrier layer appears to be substantially responsible for the phenomenon of passivity. In other systems, such as the valve metals and their alloys (Al, Ta, Ti, Nb, Zr), and iron (particularly at elevated temperatures), for example, the outer layer may form a highly resistive coating that effectively separates the reactive metal and the barrier layer from the corrosive environment. The 'sealing' of anodized aluminum is an example of how the outer layer may be manipulated to achieve high corrosion resistance. In the present analysis, only the barrier layer is considered, because the passivity of chromium-containing alloys appears to be due to a thin barrier layer of defective Cr_2O_3 that forms on the surface in contact with the alloy. Thus, in these cases, the barrier layer is clearly 'the last line of defense.'

The PDM further postulates that the point defects present in a barrier layer are, in general, cation vacancies ($V_M^{\chi'}$), oxygen vacancies ($V_O^{\bullet\bullet}$), and cation interstitials ($M_i^{\chi+}$), as designated by the Kroger–Vink notation (**Figure 4**). Cation vacancies are electron acceptors, which result in doping the barrier layer

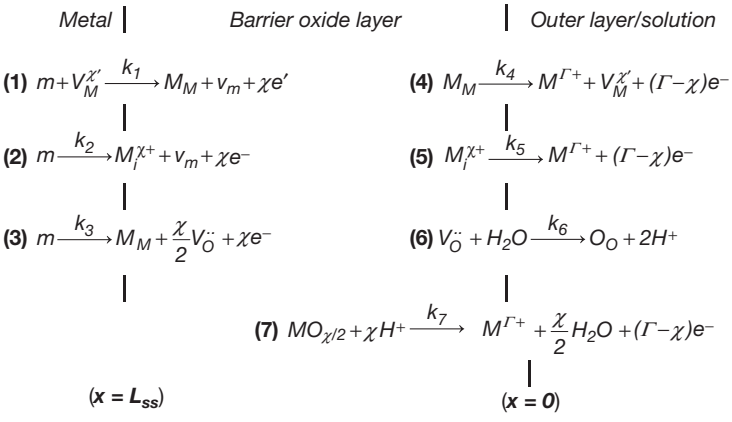

Figure 4 Interfacial defect generation/annihilation reactions that are postulated to occur in the growth of anodic barrier oxide films according to the point defect model.[35] M, metal atom; $V_M^{\chi'}$, cation vacancy on the metal sublattice of the barrier layer; $M_i^{\chi+}$, interstitial cation; M_M, metal cation on the metal sublattice of the barrier layer; $V_O^{\bullet\bullet}$, oxygen vacancy on the oxygen sublattice of the barrier layer; O_O, oxygen anion on the oxygen sublattice of the barrier layer, $M^{\Gamma+}$, metal cation in solution.

p-type, whereas oxygen vacancies and metal interstitials are electron donors, resulting in n-type doping. Thus, on both pure metals and alloys, the barrier layer is essentially a highly doped, point defect semiconductor, as demonstrated by Mott–Schottky analysis[21] for example. Not unexpectedly, the situation with regard to alloys is somewhat more complicated than that for the pure metals. Thus, while the barrier layers on pure chromium and on Fe–Cr–Ni alloys (including the stainless steels) are commonly described as being 'defective Cr_2O_3,' those on pure chromium are normally p-type in electronic character[43] and those on the stainless steels[44] are n-type. The latter can be described as $Cr_{2+x}O_{3-y}$, recognizing that the barrier layer may be metal rich (via metal interstitials) or oxygen-deficient (via oxygen vacancies), or both, whereas that on pure chromium apparently is metal- and oxygen-deficient, or $Cr_{2-x}O_{3-y}$, with the cation vacancy being the dominant defect in the system. It is not known whether the apparent differences in the barrier layers on pure chromium and on chromium-containing alloys are due to doping of the barrier layer by other alloying elements, or the inhibition of cation vacancy generation relative to the generation of oxygen vacancies and metal interstitials, in the barrier layer on the alloys compared with that on pure chromium.

The defect structure of the barrier layer can be understood in terms of the set of defect generation and annihilation reactions occurring at the metal–barrier layer interface and at the barrier layer–outer layer (solution) interface, as depicted in **Figure 4**.[42] Regardless of the electronic type, that is, irrespective of the identity of the dominant defect in the system, reactions [3] and [7] (**Figure 4**) are responsible for the growth and destruction of the barrier layer and any analysis of the stability of the layer must focus on these two reactions. That the barrier layer always contains oxygen vacancies is self-evident, since the rate of dissolution at the barrier layer–solution interface is always finite.

As noted elsewhere,[21,42] the rate of change of the barrier layer thickness for a barrier layer that forms irreversibly on a metal or alloy surface can be expressed as

$$\frac{dL}{dt} = \Omega k_3^0 e^{a_3 V} e^{b_3 L} e^{c_3 \mathrm{pH}} - \Omega k_7^0 (C_{H^+}/C_{H^+}^0)^n e^{a_7 V} e^{c_7 \mathrm{pH}} \quad [29]$$

where $a_3 = \alpha_3(1-\alpha)\chi\gamma, a_7 = \alpha_7\alpha(\Gamma-\chi)\gamma, b_3 = -\alpha_3\chi\varepsilon\gamma$, $c_3 = -\alpha_3\chi\beta\gamma$, and $c_7 = \alpha_7\beta(\Gamma-\chi)\gamma$. In these expressions, Ω is the mole volume of the barrier layer per cation, ε is the electric field strength within the barrier layer (postulated to be a constant and independent of the applied voltage in the steady state, because of the buffering action of Esaki tunneling),[21] k_i^0 and α_i are the standard rate constant and transfer coefficient, respectively, for the appropriate reactions depicted in **Figure 4** (i.e., reactions [3] and [7]), α is the polarizability of the barrier layer–solution (outer layer) interface (i.e., the dependence of the voltage drop across the interface, $\phi_{f/s}$, on the applied voltage, V), β is the dependence of $\phi_{f/s}$ on pH (assumed to be linear), $\gamma = F/RT$, χ is the oxidation state of the cation in the barrier layer, Γ is the corresponding quantity for the cation in solution, C_{H^+} is the concentration of hydrogen ion, $C_{H^+}^0$ is the standard state hydrogen ion concentration, and n is the kinetic order of the barrier layer dissolution reaction with respect to H^+.

By setting the left side of eqn [29] equal to zero, the steady state thickness of the barrier layer, L_{ss}, is readily derived as

$$L_{ss} = \left[\frac{1-\alpha}{\varepsilon} - \frac{\alpha\alpha_7}{\alpha_3\varepsilon}\left(\frac{\Gamma}{\chi}-1\right)\right]V + \left[\frac{2.303n}{\alpha_3\varepsilon\chi\gamma} - \frac{\alpha_7\beta}{\alpha_3\varepsilon}\left(\frac{\Gamma}{\chi}-1\right) - \frac{\beta}{\varepsilon}\right]\mathrm{pH} + \frac{1}{\alpha_3\varepsilon\chi\gamma}\ln\left(\frac{k_3^0}{k_7^0}\right) \quad [30]$$

Note that in deriving these expressions, the convention has been adopted that, for the rate of barrier layer dissolution, C_{H^+} and $C_{H^+}^0$ have units of mol cm^{-3}, but when used for defining pH, the units are the conventional mol 1^{-1}. Thus, the standard states for the dissolution reaction (second term on the right side of eqn [39]) and for the pH are 1.0 mol cm^{-3} and 1.0 mol 1^{-1}, respectively. The introduction of a standard state into the dissolution rate renders the units of k_7^0 independent of the kinetic order, n, without altering the numerical value of the rate.

The steady state passive current density is readily derived[21] as

$$I_{ss} = \Gamma F\left[k_2^0 e^{a_2 V} e^{b_2 L_{ss}} e^{c_2 \mathrm{pH}} + k_4^0 e^{a_4 V} e^{c_4 \mathrm{pH}} + k_7^0 e^{a_7 V} e^{c_7 \mathrm{pH}} \cdot (C_{H^+}/C_{H^+}^0)^n\right] \quad [31]$$

where the first, second, and third terms arise from the generation and transport of cation interstitials, cation vacancies, and oxygen vacancies, respectively, with the term due to the latter being expressed in terms of the rate of dissolution of the barrier layer.[21] This expression is derived, in part, by noting that the fluxes of a given defect at the two interfaces under steady-state conditions are equal; in this way, the

expression for the current can be formulated so as to avoid the defect concentrations at the interfaces.

The passive state is not perfectly protective and, for a variety of reasons, passivity breakdown occurs, resulting in enhanced corrosion rates. Of particular concern is localized passivity breakdown, which results in the nucleation and growth of pits and subsequently, the nucleation and growth of cracks if, the requisite tensile stress is present in the system. A review of the literature reveals the following generalizations of the experimental data for passivity breakdown of metals and alloys in a wide variety of environments[21]:

1. Localized corrosion is initiated by passivity breakdown and occurs on a wide variety of passive metals and alloys in a wide variety of environments.
2. Certain species (e.g., Cl^- and Br^-) induce passivity breakdown by interacting with the barrier layer. These aggressive species apparently do not penetrate through the barrier layer but may be incorporated into the precipitated outer layer.
3. Passivity breakdown occurs at a wide variety of sites on metal and alloy surfaces.
4. Passivity breakdown is a dynamic deterministic process, being predetermined and (in principle) predictable on the basis of known physical laws.
5. The transition of a metastable event to a stable event is a rare event.
6. Two fundamentally different repassivation phenomena may be identified: (i) 'Prompt' repassivation and (ii) 'delayed' repassivation (sometimes referred to as 'stifling').
7. A single passivity breakdown site is characterized by a critical voltage (V_c) and induction time (t_{ind}). V_c is found to be near-normally distributed while t_{ind} displays a left acute distribution. The parameters V_c (and $\bar{V}_c$) and t_{ind} exhibit highly characteristic dependencies on the activities of the breakdown-inducing aggressive species (a_x) and on the applied voltage (t_{ind} only) for a wide variety of systems, suggesting commonality in mechanism.
8. V_c (and $\bar{V}_c$) is found to depend on the identity of the aggressive ion within a homologous series. Thus, in the case of iron and nickel, the propensities of the halide ions for inducing passivity breakdown lie as $F^- < Cl^- > B^- < I^-$, whereas, in the case of titanium, bromide ion is the most aggressive. These trends are readily explained by the absorption of the halide into oxygen vacancies in the surface of the barrier layer, with the extent of absorption being determined by the competitive needs to dehydrate the ion and expand the vacancy.[21]
9. The mean breakdown voltage, $\bar{V}_c$ is found to decrease linearly with $\log(a_X)$ with a slope that exceeds $2.303RT/F$, which is attributed to the value of the polarizability of the barrier layer–solution interface lying between 0 and 1, for essentially all systems (metal–solution) that have been investigated. Likewise, the induction time for essentially all systems investigated display a common form of the dependencies of $\log(t_{ind})$ on potential and $[X^-]$. These relationships strongly suggest commonality in breakdown mechanism.
10. Certain oxyanions (e.g., nitrate, borate, and nitrite) strongly inhibit passivity breakdown, with the effect being accounted for by competitive absorption with the aggressive anion into surface oxygen vacancies in the barrier layer.[21]
11. In many systems (e.g., Al, Ga, Zr, stainless steel), blister formation is observed to be the precursor to passivity breakdown.
12. Certain alloying elements (e.g., Mo in Ni) cause a positive shift in V_c (and $\bar{V}_c$) and in a lengthening of the induction time. The effect is greater for a larger difference in the oxidation states between the solute and host.
13. Incident electromagnetic radiation, with a photon energy that is greater than the bandgap of the barrier layer oxide also results in a positive shift in V_c (and $\bar{V}_c$) and in a lengthening of the induction time. The defect (electronic and crystallographic) structures of the barrier layer are modified by irradiation.

It has been shown that PDM is able to explain all the experimental data for passivity breakdown of metals and alloys mentioned above and accordingly, can be considered as providing a suitable theoretical basis for a deterministic model treatment of passivity breakdown and the nucleation of metastable pits in a metal surface.[21]

The PDM, as it relates to passivity breakdown, postulates that certain aggressive anions, for example, F^-, Cl^-, Br^-, and I^- absorb into oxygen vacancies in the surface of the barrier layer, resulting in the generation of cation vacancies and hence, to an enhanced flux of the same species across the barrier layer toward the metal–barrier layer interface, as depicted in **Figure 5**. The PDM postulates that if the cation vacancies arriving at the metal–barrier layer interface

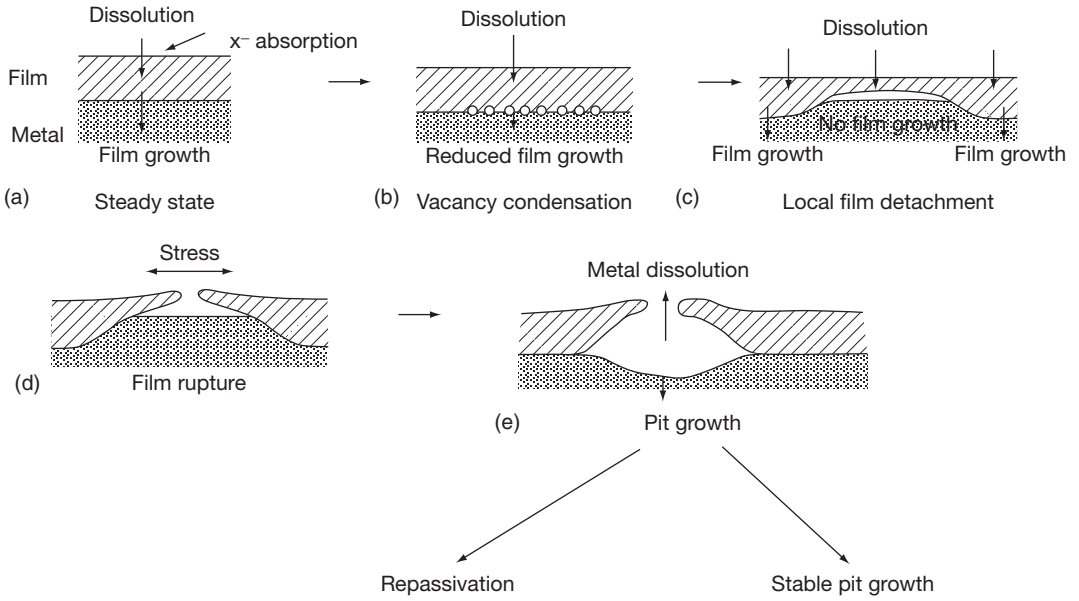

Figure 5 Sequence of events in passivity breakdown, according to the point defect model.[21] Note that the initial event is the absorption of an aggressive anion into an oxygen vacancy at the film–solution interface (a), resulting in an enhanced flux of cation vacancies across the film and eventually in condensation of cation vacancies at the metal–film interface (b). The film stops growing into the metal beneath the cation vacancy condensate while it continues to dissolve at the film–solution interface (c), eventually resulting in rupture (d) and repassivation or the formation of a stable pit (e).

cannot be annihilated at a sufficiently high rate via reaction [1] (**Figure 5**), the excess vacancies will condense locally and hence cause local separation of the barrier layer from the substrate metal. Once separation has occurred, reaction [3] (**Figure 5**) can no longer occur so that the barrier layer at that locale is prevented from growing into the metal. However, the barrier layer continues to grow into the metal at the periphery of the cation vacancy condensate and also continues to dissolve at the barrier layer–solution interface. This results in local thinning of the 'cap' over the cation vacancy condensate with the cap eventually rupturing because of the growth stresses in the film and in the near-surface substrate. The 'weak points' on the surface where passivity breakdown is predicted to occur correspond to regions of high cation vacancy flux. These regions are assumed to be regions of high local discontinuity in the barrier layer, such as the points of intersection of the barrier layer with precipitates, inclusions (e.g., MnS), and other 'second phase' particles. Support for this mechanism stems from the almost general observation of the formation of blisters ('cation vacancy condensate') as precursors to passivity breakdown on a wide variety of metals and alloys, the passivity breakdown on liquid versus solid gallium, and the potential sweep rate dependence of the apparent breakdown voltage.[21] The latter evidence is particularly convincing because the test involves no adjustable parameters and yields a quantity (the concentration of condensed vacancies) that can be compared with the same quantity calculated from fundamental principles (crystal structure of the barrier layer).

The description of possible mechanisms for the generation of cation vacancies at the barrier layer–solution interface upon the absorption of the aggressive anion into a positively charged oxygen vacancy in the surface of the barrier layer can be found in Macdonald.[21]

Mathematically, the condition for the initial formation of the cation vacancy condensate can be expressed as[35]

$$(\mathcal{J}_{ca} - \mathcal{J}_m)(t - \tau) \geq \xi \qquad [32]$$

where $\mathcal{J}_{ca}$ is the flux of cation vacancies across the barrier layer at the breakdown site, $\mathcal{J}_m$ is the annihilation flux (i.e., the rate of reaction [1], **Figure 5**), t is the time, τ is the dissolution time (see below), and ξ is the critical areal concentration of vacancies ($\#/cm^2$). Noting that $\mathcal{J}_{ca}$ is voltage dependent, the critical breakdown voltage corresponds to that at which breakdown takes an infinite time to occur that is, when $\mathcal{J}_{ca} = \mathcal{J}_m$. This condition, in turn, leads to the following expressions for the breakdown voltage and

the induction time for passivity breakdown at a single site on the metal surface as[35]

$$V_C = \frac{4.606RT}{\chi\alpha F}\log\left[\frac{\mathcal{J}_m}{\mathcal{J}^O u^{-\chi/2}}\right] - \frac{2.303RT}{\alpha F}\log a_X \quad [33]$$

$$t_{ind} = \xi'\left[\exp\left(\frac{\chi\alpha F\Delta V}{2RT}\right) - 1\right]^{-1} + \tau \quad [34]$$

where

$$\mathcal{J}^O = \chi KD[N_v/\Omega]^{1+\chi/2}\exp[-\Delta G_S^0/RT] \quad [35]$$

and

$$u = (N_A/\Omega)\exp[\Delta G_A^0/RT]\exp[-F(\beta pH + \varphi_{f/s}^0)/RT] \quad [36]$$

where N_A is the Avogadro number, ΔG_S^0 is the Gibbs energy change for the Schottky-pair reaction, β is the dependence of the potential drop across film–solution interface on pH, $\varphi_{f/s}^0$ is a constant (potential drop at the film–solution interface for $V_{app} = 0$, and pH = 0) and ΔG_A^0 is the standard Gibbs energy change for the chloride–oxygen vacancy absorption reaction.

Additionally, the 'relaxation' time, τ, which is now identified with the time taken for the cap over the vacancy condensate to thin sufficiently for rupture to occur[21] from the point of initial cation vacancy condensation, can be expressed as

$$\tau \le L_{ss}/(dL/dt)_{dissolution} = L_{ss}/\Omega k_s\left(C_{H^+}/C_{H^+}^0\right)^n \quad [37]$$

In these expressions, L_{ss} is the steady-state thickness of the barrier layer at the voltage at which cation vacancy condensation just begins. This value is given by eqn [30]. The other parameters are as defined above.

Typical plots of breakdown voltage versus chloride activity, plotted in accordance with eqn [33] are presented in **Figure 6**. The data labeled 'PDM' were calculated from eqn [33] using parameter values estimated by different experiments (primarily from electrochemical impedance spectroscopy, EIS). It should be noted that the PDM has been subjected to numerous experimental tests and, to the authors' knowledge, no substantial discrepancies have been noted.[21] The model has also been extended to account for transients in barrier layer thickness and passive current in response to potential step and linear potential sweep perturbations. The model has also been extended to account for electrochemical impedance data and, indeed, optimization of the model on impedance data as a function of frequency and voltage has proven to be a very effective way of determining values for various model parameters. Finally, the PDM has also been used to describe the cathodic formation of metal hydride films on metals, such as Li and Zr, and, again, optimization has proven to be an effective means of determining values for model parameters. Discussion of these topics is beyond the

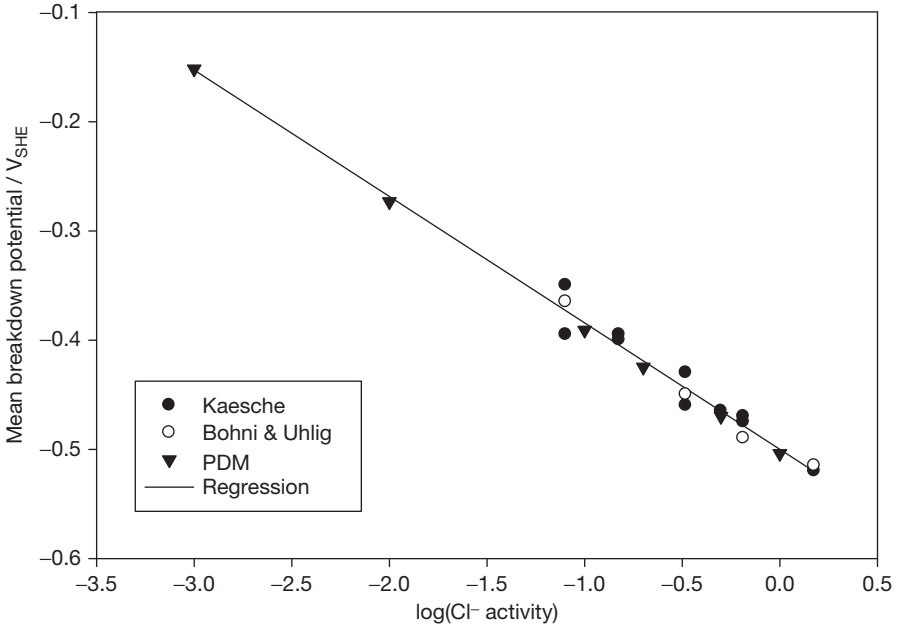

Figure 6 Plot of the mean critical breakdown potential vs. log(Cl^- activity) for aluminum in sodium chloride solutions at 25 °C. Experimental data are taken from Kaesche[45] and Böhni and Uhlig.[46]

scope of the present chapter, and the reader is referred to the literature for additional information.[21]

On any real surface, a large number of potential breakdown sites exist, corresponding to a distribution in the properties of the 'weak spots.' Thus, examination of data reported by Shibata[47] and Fratesi,[48] among others, suggests that the breakdown voltage is nearly normally distributed. The PDM assumes that the breakdown sites, with respect to the diffusivity of cation vacancies, are described approximately by a normal distribution function,[39] that is,

$$\frac{dN(D)}{dD} = -A \exp\left[-\frac{(D-\bar{D})^2}{2\sigma_D^2}\right] \quad [38]$$

Here, $N(D)$ is the number of breakdown sites (per square centimeter) that have diffusivities larger than D, and $\bar{D}$ and σ_D are the average value and the standard deviation, respectively, of the diffusivity for the population of the breakdown sites. The negative sign in eqn [38] means that $N(D)$ decreases with increasing D. Parameter A does not depend on D, so that normalization of the diffusivity distribution using the condition $N(0) = N_{mp,0}$, where $N_{mp,0}$ is the total number of breakdown sites (per square centimeter), yields

$$N(D) = N_{mp,0}\ \mathrm{erfc}\left(\frac{D-\bar{D}}{\sqrt{2}\sigma_D}\right)/\mathrm{erfc}\left(-\frac{\bar{D}}{\sqrt{2}\sigma_D}\right) \quad [39]$$

Because the transport of cation vacancies across the barrier layer from the barrier layer–solution interface to the metal–barrier layer interface occurs primarily by electro-migration, the cation vacancy flux density, $\mathcal{J}_{ca}$, is proportional to the diffusion coefficient of the vacancies, D, that is,

$$\mathcal{J}_{ca} = DB \quad [40]$$

where the function B depends on the external conditions (applied voltage, V_{app}, temperature, T, chloride activity, a_x, etc.) and on the electric field strength within the film. Thus, for the case of passivity breakdown in a solution containing an aggressive anion, X^- (e.g., chloride ion), the PDM yields

$$B = \hat{a}u^{-\chi/2}\exp\left(\frac{\chi F\alpha V_{app}}{2RT}\right)a_x^{\chi/2} \quad [41]$$

where α is the polarizability of the film–solution interface (i.e., dependence of the potential drop across the barrier layer–solution interface on the applied potential), χ is the cation oxidation state in the barrier layer, R is the gas constant, and F is Faraday's constant. In turn, parameters $\hat{a}$ and u are defined as[35]

$$\hat{a} = \chi(F\varepsilon/RT)[N_A/\Omega]^{1+\chi/2}\exp\left(-\Delta G_S^0/RT\right) \quad [42]$$

where parameter u is defined by eqn [36].

Substituting eqns [40] into eqn [32] yields the following criterion for metastable pit nucleation as

$$D \geq D_{cr} = \frac{\xi + \mathcal{J}_m(t-\tau)}{B(t-\tau)} \quad [43]$$

Criterion [43] states that the nucleation of metastable pits occurs within the observation time, t, on those and only those sites that have $D \geq D_{cr}$. From Equations [26], [39], and [43], we have

$$N(t) = N_0\ \mathrm{erfc}\left(\frac{a}{t-\tau}+b\right)/\mathrm{erfc}(b) \quad [44]$$

where $a = \xi/\left(B\sqrt{2}\sigma_D\right)$, and $b = (\mathcal{J}_m/B - \bar{D})/\left(\sqrt{2}\sigma_D\right)$. Accordingly, for the rate of pit nucleation, we obtain the following expression,

$$n(t) = \frac{dN}{dt} = \frac{N_0 2a}{\mathrm{erfc}(b)\sqrt{\pi}}\frac{\exp\left[-\left(\frac{a}{t-\tau}+b\right)^2\right]}{(t-\tau)^2} \quad [45]$$

It is important to note that, in accordance with eqn [28], the maximum pit nucleation rate must be observed at the beginning of corrosion attack, that is, at $t = 0$. On the other hand, in accordance with PDM, as follows from eqn [45], the maximum pit nucleation rate must be observed at

$$t_{max} = a\left(b+\sqrt{b^2+4}\right)/2 \quad [46]$$

Accordingly, if observation time, t (service life t_s), satisfies the condition

$$t \gg t_{max} \quad [47]$$

practically all pits nucleate during a very short period of time at the beginning of the observation time, that is, the PDM predicts the case of instantaneous nucleation. Calculation shows[13] that, in some cases (especially at high concentrations of Cl^-) criterion [47] holds very well and the nucleation of pits on a metal surface may be regarded as an 'instantaneous nucleation' phenomenon. However, t_{max}, increases very sharply with decreasing chloride concentration, leading to the case of progressive nucleation, in which new pits nucleate on the surface as existing pits grow and die (repassivate). The fact that the surface concentration of pits grows at a maximum rate after the appearance of the first pit has been experimentally observed, for example,

the case of the pitting corrosion of passive iron in borate buffer solution containing chloride ion.[49]

2.39.6 Rate of Pit (Cavity) Propagation

The quantitative description of pit (or cavity) growth remains one of the key problems in predicting corrosion damage in many practical systems. This follows from the fact that the calculated corrosion damage that is based only on this (growth) stage can be compared with experiments in many limiting cases. For example, in the case of pitting corrosion, when all pits nucleate 'instantaneously,' or when the induction time for pit nucleation is much smaller than the observation time, it is possible to ignore the initial stage of pit nucleation when estimating the damage. In addition, if the probability of survival of a corrosion defect is sufficiently high, we must take into account the possibility that a stable corrosion defect (pit or crack) nucleates immediately after the start of operation and propagates without repassivation and hence, the same defect that nucleated in the beginning is still active at the end of the observation time. In any case, calculations based only on the growth stage yield the most conservative estimate of the service life, $t_{s,min}$, of the system. We can be sure that if calculation of the service life is based on growth alone, the real service life, t_s, will at least be not less than $t_{s,min}$.

Moreover, it is also natural to assume that the rate of propagation of an individual pit (crack) without neighbors will be greater than that for the same pit (crack) with neighbors (i.e., within an ensemble of pits (cracks)), because the neighboring pits reduce the potential at the surface and multiple, neighboring cracks are expected to reduce the stress intensity factor experienced by a single crack for a given loading stress. Accordingly, the proper modeling of propagation of individual corrosion defects can yield the possible minimum survival time for the system as a whole (e.g., a machine). If this time extends beyond the projected service life of the system, we can be sure that the system will survive under real conditions.

2.39.6.1 General Approach for Calculating Propagation Rates

Apparently, one of the main theoretical problems in describing localized corrosion damage is the prediction of the shape and dimensions of corrosion cavities at any time as a function of the parameters controlling the process (potential of the metal, species concentrations, such as velocity of the electrolyte, thickness of the passive film, diameter of the pit mouth, etc.). It seems obvious that mathematical models describing the pit (cavity) growth should start with the assumption that the pit form and size are not known *a priori*, but should be found during the solution of the appropriate equations.

From the mathematical point of view, the problem of determining the shape and size of a developing pit belongs to the class of Stefan problems.[50] These problems are reduced to the solution of the system differential equations of parabolic or elliptic type with unknown boundary conditions because the velocity of this boundary is connected to the sought after solution by some differential relationship.

The implicit equation $\Phi(t, x_1, x_2, x_3) = 0$ shall describe the pit surface with time, relative to the Cartesian coordinate system x_1, x_2, x_3. This expression fulfills the relation $d\Phi = (\partial\Phi/\partial t + \nabla\Phi \cdot V_s)dt = 0$, where $V_s(t, dx_1/dt, dx_2/dt, dx_3/dt)$ is the velocity of the dissolving metal surface. In this formulation, subscript refers to the electrode surface and subscript ∞ to the bulk of the solution. Let $\vec{n} = \nabla\Phi/|\Phi|$ be a unit vector pointing normally from the solution to the metal surface. According to Faraday's law, $V_s = K_V i_{corr}\vec{n}$, where i_{corr} is the current density for metal dissolution, and K_v is the electrochemical equivalent volume, that is, the volume of dissolving metal when one Faraday of charge (96 487 int. coulombs) passes through the interface.

Introducing the correlation for V_s into the expression for the differential $d\Phi$ yields an equation describing the change of the electrode surface

$$\frac{\partial\Phi}{\partial t} + K_V i_{corr}|\nabla\Phi| = 0 \qquad [48]$$

Equation [48] is frequently used to describe some important processes in electrochemical technology, for example, electrochemical machining of metals, electrochemical shape formation, and so on.[51] Of course, we can also expect that, in the general case, some additional component, not connected with metal dissolution (e.g., due to mechanical spallation at very high fluid velocities or hydrogen embrittlement) should be incorporated into the expression for the V_s, but this issue is not germane to the present discussion and will not be considered further here.

Besides the information about the boundary position in the initial period, $\Phi(0, x_1, x_2, x_3)$, the integration of eqn [48] requires information about the

dissolution current density, i_{corr}, that is, eqn [48] must be solved with a set of nonstationary equations for mass balance for each component in the solution, namely

$$\frac{\partial c_k}{\partial t} = -\nabla \cdot \vec{\mathcal{J}}_k + R_k; \quad k = 1, \ldots, K \qquad [49]$$

where C_k is the concentration of species k, $\vec{\mathcal{J}}_k$ is the flux density of species k, and R_k is the rate of production (source) or depletion (sink) of this species as a result of homogeneous chemical reactions. The current density, $\vec{i}$, in the electrolyte solution is defined as

$$\vec{i} = F \sum_k z_k \vec{\mathcal{J}}_k \qquad [50]$$

In the vast majority of practical applications, dilute solution theory is used to calculate the flux of the species, that is,

$$\vec{\mathcal{J}}_k = -D_k \nabla C_k - z_k F u_k C_k \nabla \phi + C_k \vec{v} \qquad [51]$$

where ϕ is the electrostatic potential in the solution, v is the fluid (hydrodynamic) velocity, and u_k is the mobility of species k, which can be estimated by using the Nernst–Einstein equation:

$$u_k = \frac{D_k}{RT} \qquad [52]$$

In eqn [51], the first term on the right-hand side represents the contributions of diffusion, the second term describes migration, and the third term is a contribution of convection. An additional condition for determining the electrostatic potential is the equation

$$\sum_k z_k C_k = 0 \qquad [53]$$

It must be noted that, generally speaking, the condition of electroneutrality is not a law of nature and can be considered as an approximation of Poison's equation:

$$\nabla^2 \phi = -\frac{F}{\varepsilon} \sum_k z_k C_k \qquad [54]$$

where ε is the dielectric permittivity (dielectric constant multiplied by the permittivity of free space) of the solution. However, due to the large value of the ratio F/ε, an appreciable separation of charge would require unrealistically large electric forces. Visible deviation from electroneutrality can be observed only in a very thin double layer near an electrode surface (which is of the order of 1–10 nm in thickness) or within a doped semiconductor junction that can be taken into account in the boundary conditions for the problem. Accordingly, the electroneutrality approximation is fulfilled very well, and is widely accepted by the electrochemical community.[52] In spite of this fact, some papers where Poison's equation is used directly can be found in the literature.[53] In accordance with our opinion, this approach introduces only unnecessary complications, due to excessive calculational time.

The hydrodynamic velocity, $\vec{v}$, within the framework of dilute solution theory, can be found apart from the solution of the mass transfer problem by using the corresponding mechanical equations (e.g., the Navier–Stokes equations, in the case of laminar flow[52,54]). In the case of turbulent flow, which often exists outside the corrosion cavity, it is convenient to use some effective diffusion coefficient instead of the usual diffusion coefficient, D_k,

$$D_k^{\text{eff}} = D_k + D_t \qquad [55]$$

where diffusion coefficient D_t depends on the distance from the wall, hydrodynamic conditions, and the physical properties of the liquid. Some empirical correlations for D_t can be found in the literature.[52,54,55]

Strictly speaking, eqn [51] for species flux densities is valid in the case of dilute solutions. In the case of concentrated solutions, eqn [51] should be replaced by

$$\vec{\mathcal{J}}_k = C_k \vec{v}_k \qquad [56]$$

where the velocity, $\vec{v}_k$, of species k can be found from the equation of multicomponent diffusion.[52]

$$C_k \nabla \mu_k = RT \sum_i \frac{C_k C_i}{C_T D_{ki}} (\vec{v}_i - \vec{v}_k) \qquad [57]$$

where μ_k is the electrochemical potential of species k, D_{ij} are diffusion coefficients, and C_T, is the sum of all concentrations of all components, including the solvent. However, in the literature, there are no significant applications of the theoretical principles describing transport in concentrated solutions for the case of corrosion, with the exception of the preliminary work of Popov *et al.*[56] The reasons for this state of affairs are the increased complexity of the theory and the lack of appropriate input data for practical application.

However, it is important to note that, in the overwhelming majority of corroding systems, the concentrations of all solute species, C_k, are much smaller than the concentration of the solvent, C_0. Under these

conditions, only one term on the right side of eqn [50] is important. Accordingly, eqn [57] can be rewritten in the following form for the theory of moderately dilute solutions[52]

$$\vec{J}_k = -D_k \nabla \mu_k + C_k \vec{v} \qquad [58]$$

If we present μ_k in the form

$$\mu_k = RT \ln(\gamma_k C_k) + z_k F \varphi \qquad [59]$$

where the activity coefficient, γ_k, depends on the concentration of all species in the solution, the equation of the flux becomes

$$\vec{J}_k = -D_k \nabla C_k - \frac{D_k z_k F}{RT} C_k \nabla \phi + C_k \vec{v} - D_k C_k \nabla \ln(\gamma_k) \qquad [60]$$

This equation for ion flux densities has been used, for example, in Walton *et al.*[57] for describing crevice corrosion. However, the activity coefficients in Walton *et al.*[57] are calculated within the framework of Debye–Hückel theory that, is strictly speaking, applicable only for the case of dilute solutions.

We would like to emphasize that, in many real corrosion systems, the concentration drops within a corroding cavity may be not very high, because corrosion is not a fast process. Accordingly, eqn [1] can be used with sufficient accuracy in relatively concentrated solutions, assuming that D_k is referred to the bulk electrolyte, but not to infinitely dilute solutions.

In accordance with the rules, the homogeneous terms, R_k, in the balance equations can be written in general form as

$$R_k = \sum_{m=1}^{M} \left[-k_m v_{km} \left\{ \prod_{v_{km}>0} C_k^{v_{km}} - K_m \prod_{v_{km}<0} C_k^{-v_{km}} \right\} \right] \qquad [61]$$

where k_m is the rate constant of reaction m, $\sum_k v_{km} M_k = 0$ ($m = 1,2,\ldots,M$), K_m is the equilibrium constant for reaction m, v_{km} is the stoichiometric coefficient for species k in mth chemical reaction, and M_k is the symbol for the chemical formula of species k.

The presence of the chemical terms in balance eqns [49] greatly complicates their solution. First of all, we have practically no information about the rates of homogeneous reactions (usually, we only have information about their equilibrium constants). However, we can reasonably assume that these reactions are fast and they are practically in equilibrium at any given point and time. The most widely applied method for dealing with these problems is to eliminate chemical terms by adding or subtracting balance eqns [49]. The new set of governing equations is then supplemented by equations of equilibrium.[58] The great disadvantage of this approach is as follows. Every time, we want to add or delete from consideration any chemical reaction, we have to completely change the computer code for numerical solution of balance equations because of their change in form. Moreover, the forms of these equations do not coincide with the standard form of the equation of mass balance, and this adds to the complexity of the process of numerical solution.

The alternative approach for modeling the equilibrium state is to keep the governing equation in rate format (i.e., in the form of eqn [49]), and hence to assume that reactions are very fast. As long as reaction rates are large, relative to the rates of mass transport, the reactions will remain at equilibrium, and the solution composition will be independent of the kinetics assumed. All kinetic expressions that are physically consistent (i.e., are stoichiometrically true) yield zero net reaction at equilibrium, change sign as the equilibrium point is crossed, and give sufficiently fast reaction rates that can be used.[59] The choice becomes a matter of numerical stability and convenience. Therefore, Walton[60] used the following expression for the rate of production or depletion of species k by the chemical reaction

$$R_k = \sum_{m=1}^{M} \left[-r_m v_{km} \ln \left\{ \prod_{k=1}^{K} C_k^{v_{km}} / K_m \right\} \right] \qquad [62]$$

which satisfies all of the conditions noted above.

Another alternative approach is the following.[57,61] It is assumed that characteristic times of chemical reactions in aqueous solution are much shorter than those of the mass transport or corrosion processes, which is equivalent to assuming high reaction rates. Accordingly, the set of transport equations are first solved separately from the chemical terms. After that, at the end of each sufficiently small time step, the resulting aqueous solution composition, within each elementary volume, is solved to equilibrium by calling an equilibrium solver. For example Walton *et al.*[57] determined the equilibrium composition of the solution by Gibbs free energy minimization.

The homogeneous terms, R_k, in the balance equations can be written in a general form as: It is assumed that at a point far away from the mouth of a pit or crevice, the concentrations and potentials have their bulk values, that is,

$$C_k = C_{k,\infty}; \phi = \phi_\infty = 0 \quad [63]$$

It is also assumed that the normal fluxes on the solid surface, $\mathcal{J}_{ks}$, can be expressed as a known function of surface temperature, T_s, surface concentrations, C_{ks}, and surface potential, E_{corr}–φ_s, (on the metal surface), that is,

$$-D_k \frac{\partial C_k}{\partial n} = \mathcal{J}_{ks}(E_{corr} - \phi, C_{1,s}, C_{2,s}, \ldots, C_{K,s}, T_s) \quad [64]$$

If some component does not participate in any heterogeneous reaction (chemical or electrochemical), its flux density will be equal to zero. Of course, on an insulator, all fluxes are equal to zero.

In formulating the initial conditions, it would be natural to assume that concentrations of all species and potentials coincide with the corresponding bulk values at $t = 0$. However, simple calculation shows that, under normal conditions, the velocity of the interface is so slow that the steady-state approximation can be used for describing the transport processes for the anodic dissolution of the metal.[50,51] The sense of this approximation is as follows: The movement of the metal surface is so slow that the concentration distribution in the solution is approximately that corresponding to steady flow at a given position of the boundary and for given boundary conditions. In this case, it is possible to omit the derivative over time in balance, eqn [49]. Accordingly, it is possible to separate the solution of the mass transfer problem from the movement of the boundary. After solving the steady-state problem in the region with the fixed boundaries, and after calculating the corrosion current density, the new position of the metal surface is found by using Faraday's law (see eqn [48]). After that, the solution of the steady problem for the new boundary is found, and the process is repeated until the desired time is achieved. Of course, it is not possible to omit the derivative over time in the balance equation in the case of corrosion fatigue, caused by the sharply changing hydrodynamic velocity, which is a result of periodic loading.

However, it must be noted that there are a very limited number of studies where the problem of pit propagation is regarded as a problem having a free boundary in multidimension space. Practically, (in multidimension space) consideration of a moving boundary is limited to the simplest cases, when the system of transport equations can be reduced to the solution of a single Laplace equation for the relative concentration of a single species[62] or electric potential.[63]

On the other hand, such problems are successfully solved in heat transfer studies, for example, in connection with the problem of metal ingot solidification.[64] The presence of migration is the fundamental difference between the problems of ionic transport and those in nonelectrolyte solutions or problems in heat transfer. This difference does not permit the direct use of a wide range of methods and computer programs that have been developed in connection with the problems of heat transfer for solving ion transport problems. As a result, to solve each ion transport problem, for example, using the so-called Newman method,[52] it is necessary to create new programs that require substantial expenditure of time and effort.

It is also possible to use iterative methods to reduce ion transport problems to a sequence of transport problems for nonelectrolyte solutions, which enables one to directly use the methods and even the existing computer programs available in heat engineering.[65–67]

The very useful method of quasipotential transformation for modeling transport processes in dilute electrochemical systems has been developed by Pillay and Newman.[68] It can be shown that, under steady-state quiescent conditions, with equilibrium homogeneous chemical reactions, and for a single electrochemical reaction, the electrostatic potential and all concentration distributions can be represented as a single-valued harmonic function of the quasipotential, q. This harmonic function vanishes at infinity and satisfies the following boundary conditions

$$\frac{\partial q}{\partial \boldsymbol{n}} = 0 \quad [65]$$

at an insulating surface, and

$$-\frac{\partial q}{\partial \boldsymbol{n}} = i \quad [66]$$

at an electrode (conducting) surface, where $\boldsymbol{n}$ is the unit normal vector at the electrode surface pointed towards the solution. Accordingly, the set of coupled second-order, nonlinear partial differential equations governing mass transfer by diffusion and migration in electrochemical systems is transformed into Laplace's equation for the quasipotential and hence, into a set of coupled, first-order nonlinear ordinary differential equations. This method has been applied to the case of the development of an active hemispherical pit.[69] Unfortunately, this method cannot be generalized, for example, for the nonstationary case, for the case of

multiple electrochemical reactions, or for mass transfer in flowing electrolytes.

It is also important to note that, at the present time, commercial software is available for solving transport equations with migration terms with fixed boundaries (see, e.g., COMSOL software),[70] although some algorithms also handle moving boundaries now. Accordingly, the most difficult problem that arises very often during the solution of mass transfer problems is not the solution of the differential equations themselves, but in defining the transport coefficients (e.g., diffusion coefficients) in multicomponent systems, rates of chemical reactions, and especially in establishing real kinetic relations for the species fluxes on the metal surfaces (particularly for the rate of metal dissolution), such as those contained in eqn [64]. The concrete dependencies of the rates of corrosion propagation as a function of potential, concentrations of species near the metal surface, and mechanical conditions for the cases of pitting corrosion, stress corrosion cracking, corrosion fatigue, crevice corrosion, etc. are discussed in the corresponding chapters of this book. Commercial software for calculating transport properties (diffusion coefficients, activities, viscosities, density rates of particular electrochemical reactions on particular metals and alloys) is also available (see, e.g., OLI Systems software).[71]

A detailed review of a great number of papers dealing with mathematical modeling of transport phenomenon in pitting and crevice corrosion is presented, for example, in Turnbull,[58] Sharland,[61] Papavinosan *et al.*[72] In the majority of these models, instead of boundary conditions [64], the boundary conditions of the Type II kind (i.e., prescription of current density on the metal surface) are employed. In the latter case, the principal aim of these models is not to predict corrosion damage (corrosion rates are assumed to be known in advance), but to estimate species concentrations, and the potential distribution in corrosion cavities, as a function of many parameters like cavity dimension, bulk solution composition, temperature, and so on. Very often such models serve to aid in the understanding of results of particular experimental systems. However, at present, the overwhelming majority of the models devoted to estimating the size of a corrosion cavity have adopted the one-dimensional approximation, that is, they are reduced to calculating the depth of the cavity, a, as a function of time, when eqn [48] is reduced to the simplest relation

$$\frac{da}{dt} = K_V i_{corr} \qquad [67]$$

Because of the mathematical complexity of the problem, analyses of the transfer processes occurring within corrosion cavities have generally employed the one-dimensional approximation. For example, it is often assumed, in the case of corrosion pits, that the cavity has a cylindrical shape with a depth a, which is much larger than the radius, r. Likewise, crevices and cracks are often viewed as being one-dimensional slots of length a, such that a is much greater than the opening displacement, w.[57,60,61,73–82] Very often, only metal dissolution at the bottom is assumed. However, two-dimensional analyses of corroding hemispherical pits have been described for the case of a well mixed electrolyte by Newman *et al.*,[83] and for the case of a quiescent system, in which concentration gradients exist.[63,69,84] In many cases, the results obtained by mathematical simulation or by experimental studies of 'ideal' cells (one-dimensional or hemispherical) have been used to describe corrosion processes under real conditions.

In the one-dimensional case, the balance equations are reduced to the form

$$\frac{\partial(wC_k)}{\partial t} = -\frac{\partial w\mathcal{J}_k}{\partial x} + wR_k + \mathcal{J}_{S1} + \mathcal{J}_{S2}, \quad k = 1, 2, \ldots, K \qquad [68]$$

where $\mathcal{J}_k$ is the flux density along the direction down the crevice, x, averaged over the width of the crevice, w; $\mathcal{J}_{S1}$ and $\mathcal{J}_{S2}$ are the flux densities at a metal–solution interface or on the side walls (usually it is assumed that $\mathcal{J}_{S1} = \mathcal{J}_{S2}$). In the case of the cylindrical pit of radius, r, we simply have

$$\frac{\partial C_k}{\partial t} = -\frac{\partial \mathcal{J}_k}{\partial x} + R_k + 2\mathcal{J}_S/a, \quad k = 1, 2, \ldots, K \qquad [69]$$

It must be emphasized that, in the overwhelming majority of the work devoted to describing localized corrosion in the one-dimensional approximation, it has been tacitly assumed that it is possible to neglect the potential drop in the external environment (outside the corrosion cavity), that is, to assume that boundary conditions [56] are fulfilled at the mouth of the crevice. The following section will show that such an approximation is incorrect from the physical point of view and in many cases can lead to significant errors in the estimation of corrosion damage.

2.39.6.2 Coupled Environment Corrosion Cavity Growth Models

Many localized corrosion processes, including pitting, stress corrosion cracking, corrosion fatigue, and crevice corrosion may be described within the framework of the differential aeration hypothesis (DAH), which was first postulated by U. R. Evans in the 1920s.[85] This postulate attributes localized corrosion to a spatial separation of the local anode and local cathode, with the local anode occurring in that region of the system that has the least access to the cathodic depolarizer (e.g., oxygen), while the local cathode occurs in that region that has the greatest access to the cathodic depolarizer. In the case of a pit or a crack, as depicted schematically in **Figure 7**, the local anode exists within the cavity, whereas the local cathode exists on the bold external surfaces.

The voltage difference generated between the cavity and the external surface causes a positive current to flow through the solution from the local anode to the local cathode. Negative electron current flows through the metal in the reverse direction and the two currents mutually annihilate at the external surface via a charge transfer reaction, in this case, the reduction of oxygen. The current is known as the 'coupling current' and is easily measured.[86] The coupling current has been shown to contain a wealth of information concerning the processes that occur within the cavity. The coupling current is generated within the cavity by anodic oxidation of the metal that may be unassisted by mechanical processes (pitting corrosion and crevice corrosion) or assisted by the presence of a constant stress (stress corrosion cracking, SCC) or a cyclic stress (corrosion fatigue, CF). In any event, the flow of positive current out of the cavity occurs because of the existence of a potential gradient in the solution from the cavity tip to the cavity mouth, such that $\phi_t > \phi_m > \phi_\infty$, where ϕ_t, ϕ_m and ϕ_∞ are the corresponding electrostatic potentials in the solution at the cavity tip, cavity mouth, and at a point on the external surface that is at an effectively infinite distance from the mouth (i.e., the 'throwing power,' which turns out to be about 10–20 crack mouth opening displacements, but which also depends upon the conductivity of the environment). The sign of this potential gradient is such that anions are transported into the crack, where they neutralize the positive charge that is injected into the cavity solution in the form of metal cations. The metal cations hydrolyze to produce protons that acidify the environment. The concentration factors for both Cl^- and H^+ from electromigration and hydrolysis, respectively, can exceed 10^4. Thus, for an environment containing 10 ppb of chloride ion and having a pH of 7, the chloride concentration and pH in the cavity may exceed 100 ppm and below 3, respectively. Accordingly, noting the propensity of chloride ions to induce passivity breakdown, the DAH accounts for the development of aggressive conditions within the cavity, even though the external conditions might be quite benign.

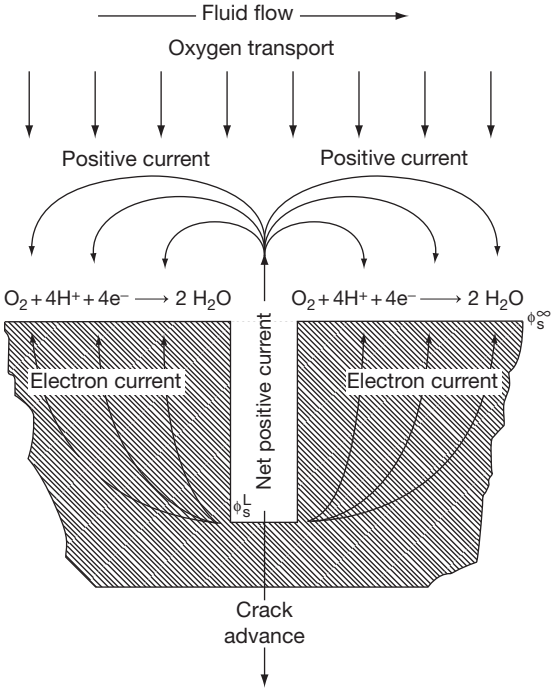

Figure 7 Coupling of crack internal and external environments. Note that in the steady state, the crack can grow only as fast as the positive current flowing from the crack can be consumed on the external surfaces by oxygen reduction. Reproduced from Macdonald, D. D.; Lu, P.-C.; Urquidi-Macdonald, M.; Yeh, T.-K. *Corrosion* **1996**, *52*, 768.

It is evident that, under free corrosion conditions, the conservation of charge requires that the charge passed by the cathodic reaction be matched by the charge passed by the partial anodic reaction (see eqn [25]). Recognizing that, at sufficiently large distances from the crack mouth on the external surface, the net current, $i_N = i_a + i_c$ (i_a and i_c are the local anodic and cathodic partial current densities) must be zero, corresponding to 'free,' general corrosion, the partial current density distributions are such that eqn [25] must be satisfied. Note that eqn [25] does not stipulate that cathodic partial reactions cannot occur within the cavity or that anodic partial reactions cannot occur on the external surfaces; only that, in the 'cathodic' and

'anodic' regions, the net current densities are negative and positive, respectively, and the total currents integrated over the respective areas are equal.

It is also important to glean an understanding of the critical nature of the properties that exist at the crack mouth. Thus, note that solving the entire problem involves solving two closely coupled sub problems, one for the external environment and the other for the crack enclave. These two problems are coupled because they share common boundary conditions in potential, ϕ_m, and in current, i_m. The objective in all coupled environment models (CEMs) developed to date has been to find the appropriate values for ϕ_m and i_m, such that eqn [25] is satisfied. It is the constraint imposed by eqn [25] that imparts determinism to the model.

Traditionally, models for localized corrosion cavity growth have assumed that the electrical potential in the solution at the crack mouth is the negative of the free corrosion potential or that the external environment presents no impedance to current flow (i.e., the current may flow to infinity). Neither postulate is correct. In the first case, no potential gradient would exist in the external environment and hence, the coupling current must be zero, contrary to experimental observation. Indeed, these models actually predict that SCC cannot occur. In the second case, if there exists no impedance for current flow to infinity, then there should be no dependence of the coupling current and crack growth rate on the catalytic properties of neighboring external surfaces, again contrary to experiment. The requirement that the underlying theory must account for all of the experimental observations is therefore not met by both classes of models. However, the authors note that the assumptions may be valuable approximations in solving the mass transport equations for the cavity, but, in doing so, it must be recognized that in ignoring the external environment, the physical description of the system is incomplete. Accordingly, and emphasizing again that a viable model must account for all experimental observations, such an approach would fail to recognize the important impact that catalysis or inhibition of oxygen reduction on the external surfaces has on crack growth rate in sensitized Type 304 SS in high temperature water, as noted above.[87,88]

To date, we[86,89–95] and others[96,97] have developed 'coupled environment' models for stress corrosion cracking (coupled environment fracture model, CEFM[89,90,92,93]), corrosion fatigue (coupled environment corrosion fatigue model, CECFM[94]), pitting (coupled environment pitting model, CEPM[91]), and crevice corrosion (coupled environment crevice model, CECM[95]). Details of the algorithms are not given here as they have been adequately described in the literature. In the interests of space, only a brief outline of some of the results from the CEFM is given. We note that alternate models for crack growth in sensitized stainless steels have been developed by others, most notably by Ford and coworkers,[98,99] Shoji,[100,101] and Vankeerberghen and Gavrilov.[102] Of these models, only the model of Vankeerberghen and Gavrilov[102] constrains the solution by the conservation of charge and hence, can be regarded as being deterministic. The models of Shoji[100,101,103] are essentially mechanical in form, with any electrochemistry being introduced 'inadvertently,' and, like Ford *et al.*'s models,[98,99] while they are 'mechanistic,' they fail to be constrained by the relevant natural law (conservation of charge), recognizing that IGSCC is primarily an electrochemical phenomenon.

The first of the CEMs to be developed was the coupled environment models (CEMs) in 1991.[89] Since then, the model has been extensively developed by the authors and their colleagues as a deterministic model for predicting stress corrosion crack growth rate in a variety of systems, including the coolant circuits of water-cooled nuclear reactors.[104] The models are based upon the following general experimental observations that apply strictly to the growth of intergranular cracks in sensitized Type 304 SS in high temperature water, but that are believed to be general correlations for SCC and other forms of localized corrosion in other systems:

- Localized corrosion generally follows the differential aeration hypothesis, first proposed by Evans in the 1920s.[85]
- A positive coupling current is observed to flow through the solution from the crack mouth to the external surfaces, while an equal but opposite electron current flows through the metal in the reverse direction.[86]
- The crack growth rate increases roughly exponentially with the potential of the metal if it is sufficiently high. At lower potentials, the CGR is potential-independent, corresponding to the mechanical creep (**Figure 8**).[90–101,103]
- The CGR depends upon the electrochemical crack length, which is defined as the shortest distance between the crack front and the exposed external surface. This length is generally different from the mechanical loading crack length.[90,102]

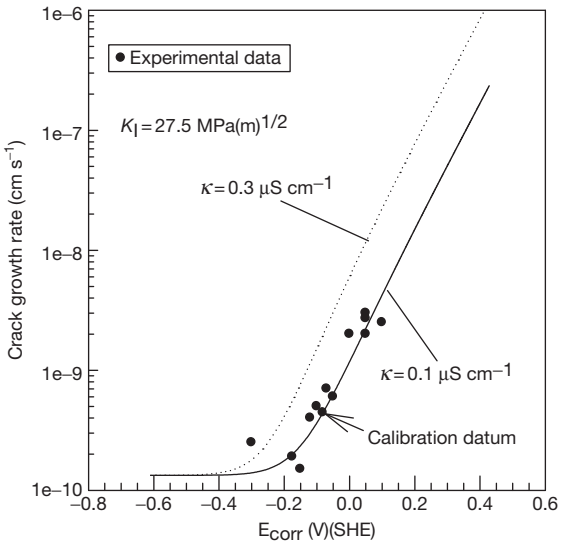

Figure 8 Measured and analytically calculated crack growth rate of sensitized Type 304 stainless steel as a function of corrosion potential. Calculations were done using the Congleton's correlation for the crack-tip strain rate. Experimental data were taken from Ford *et al.*[99]

- The environmentally-mediated CGR is proportional to the magnitude of the coupling current.[87,105]
- Coating the external surfaces with an insulator, and hence inhibiting the reduction of oxygen, causes the coupling current to decrease sharply and stops the crack from growing.[87]
- Catalyzing the reduction of oxygen on the external surface results in an increase in the coupling current and hence, an increase in the CGR.[86,88]
- The crack growth rate passes through a maximum with increasing temperature at about 175 °C.[106]

It is well known that, in the fracture of sensitized stainless steels and nickel alloys in high temperature (250–300 °C), oxidizing aqueous media, the CGR becomes independent of potential at sufficiently negative ECP values (see **Figure 8**) and that the fracture morphology changes from intergranular brittle fracture to ductile failure. The ductile fracture surfaces frequently yield evidence of microvoid coalescence, with ductile tearing of the matrix between the voids. These voids appear to nucleate at intergranular precipitates, such as carbides (e.g., $Cr_{23}C_7$) on the grain boundaries, but nucleation at intragranular precipitates is also observed. Thus, in the CEFM, which was developed originally to describe fracture in sensitized stainless steels in BWR primary heat transport circuits,[83,84,90] it seemed appropriate to describe crack growth at the 'creep' limit in terms of a cavitation model.

A modified version of the cavitation model developed by Wilkinson and Vitek[107] was used to estimate CGR at sufficiently negative potentials, where environmental effects are not evident. A detailed account of the creep model will not be given here and the reader is referred to the original paper by Wilkinson and Vitek[107] and papers by Macdonald *et al.*[90,93,108] describing the application of the model in the CEFM. It suffices to note that the Wilkinson–Vitek model accurately describes creep crack growth in stainless steels over the temperature range of interest (25–300 °C).

The numerical and analytical solutions employed in the CEFM yield very reasonable results for the environmentally assisted and creep fracture of sensitized Type 304 SS,[89] and have yet to yield a prediction of crack growth rate that is at odds (i.e., lies outside the experimental error range) with experiment. The calibration factor appears to take care of a number of simplifying assumptions in the numerical CEFM (e.g., inert crack walls and linear potential drop down the crack) and compensates for some less quantified effects (e.g., parameters associated with the crack tip process). Nevertheless, it is only necessary to calibrate the model with a single crack growth rate under specified conditions (see **Figure 8**) and to choose an appropriate activation energy for the crack tip strain rate (this is actually equivalent to calibrating the model with CGR data at two temperatures), in order to accurately describe crack growth rate in sensitized Type 304 SS over temperatures ranging from 25 to 288 °C.

One of the persistent issues that is raised in debates on the basis of the CEFM concerns the role of the external environment in determining the crack growth rate. If the differential aeration hypothesis (DAH) is accepted as the basis for localized corrosion, including SCC, then the importance of the external environment is unequivocal. That the external environment is intimately involved has been demonstrated experimentally by detecting and measuring the coupling current that flows from the crack to the external surfaces where it is consumed by oxygen reduction.[88,89] Furthermore, unless the cathodic processes are confined to the crack, in which case the measured coupling current would be zero, and hence at odds with experiment,[86] the conservation of charge *requires* consideration of the external environment in any deterministic

description of crack growth. Finally, catalysis[88] and inhibition[87] of the oxygen reduction reaction on the external surface is found to increase and decrease the crack growth rate, respectively. In the case of inhibition, which was affected by depositing Zirconia on the external surfaces, the extent of inhibition was in agreement with that calculated by the CEFM by reducing the exchange current density for the oxygen electrode reaction by the amount indicated by electrochemical impedance spectroscopy measurements of the specific interfacial impedance using a fast redox couple $[Fe(CN)_6^{3-/4-}]$.[87] These studies unequivocally demonstrate the importance, and possibly the dominance, of the processes occurring, on the external surfaces in determining the crack growth rate in sensitized Type 304 SS in high temperature aqueous systems.

The role of the external environment is further demonstrated by the calculated polarization data plotted in **Figure 9**.[93,108] Thus, it is seen that, at low temperatures (e.g., 50 °C), significant polarization is predicted to occur in the external environment (170 mV). As the temperature increases, the polarization in the external environment is predicted to decrease, but nevertheless remains significant at temperatures up to 250 °C. Even at higher temperatures, where the external polarization has been decreased to small values, because of increased conductivity of the external environment and increased rate of oxygen reduction on the external surfaces, the external environment must still be considered because of the need for charge conservation. The temptation has been to assume that, in this case, the potential at the crack mouth can be equated to $\phi_m = -E_{corr}$, and hence to eliminate the need to consider the external environment altogether. However, this would be to assume that no potential gradient exists in the external environment, in which case no coupling current should be detected, again at odds with experiment,[89] leading to the prediction that SCC cannot occur. Finally, it is interesting to note that the decrease in the polarization in the external environment is predicted to be at the expense of an increase in the potential drop down the crack.

As noted elsewhere,[90,104] the CEFM predicts that the crack growth rate for given values of stress intensity, ECP, conductivity, etc. depends upon the crack length. This prediction is consistent with the available experimental data.[19,88,105] In discussing this topic, it is necessary to differentiate between the mechanical crack length (MCL), which is traditionally referred to as the 'crack length' in fracture studies, and the 'electrochemical crack length' (ECL), as noted previously.[19,88,105] The electrochemical

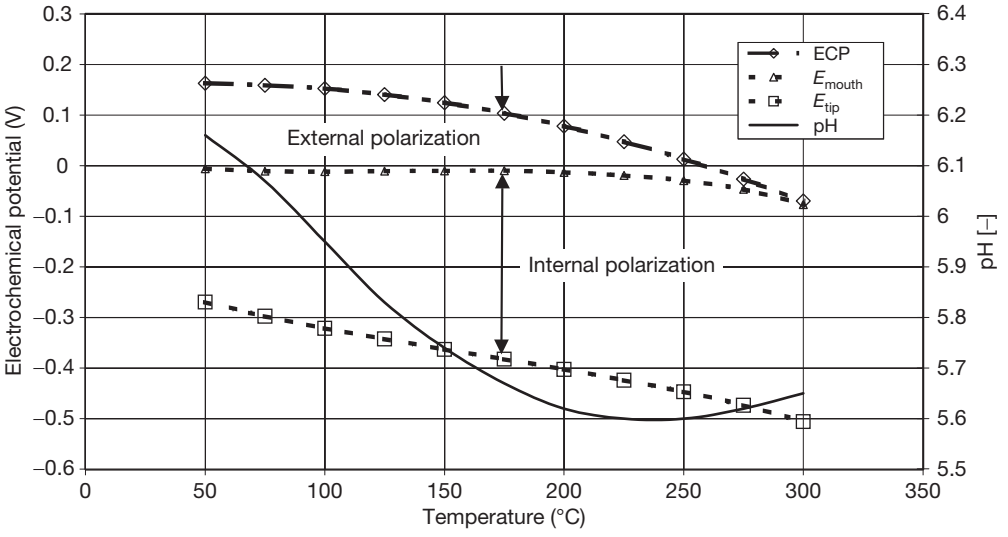

Figure 9 The calculated effect of temperature on the pH of the external environment, the electrochemical potential at the crack tip, E_{tip}, the potential at the crack mouth, E_{mouth}, and on the potential in the external environment (ECP), during crack growth in Type 304 stainless steel in dilute sulfuric acid solution having an ambient temperature (25 °C) conductivity of 0.27 μS cm^{-1} and a dissolved oxygen concentration of 200 ppb. The data were calculated using the CEFM after calibration at 288 °C and assuming a crack tip strain rate thermal activation energy of 100 kJ mol^{-1} (Congleton crack tip strain rate model).[93]

crack length is defined as the shortest path through the solution from the crack front, where the coupling current is generated, to the external surface, where the current is consumed. For a CT specimen, the MCL corresponds physically to the distance between the load line (for example) and the crack tip, and this distance increases as the crack grows through the specimen. On the other hand, because of the through thickness nature of a crack in a CT specimen, the ECL is constant and is essentially independent of the MCL. Furthermore, a CT geometry yields a distribution in ECL, depending upon where the current originates at the crack front. This dependence is such that the crack growth rate is highest at the crack edges (smallest ECL), but is lowest for the coupling current that originates from the crack front in the center of the specimen (largest ECL) by virtue of the dependence of crack growth rate on the electrochemical crack length.[90,102,104] This phenomenon is responsible for the generation of convex crack fronts, when the crack grows by SCC, in contrast to the concave crack front obtained for creep crack growth.[105]

Finally, we note that the CEFM is used extensively in various corrosion damage codes developed by Macdonald and coworkers (DAMAGE PREDICTOR, ALERT, REMAIN, FOCUS)[19,23] to predict stress corrosion cracking damage in BWR primary coolant circuits, as described below. To date, fourteen BWRs have been modeled and, where comparison is possible, the predicted damage is found to be in excellent agreement with that observed in the field.

2.39.6.3 Simplified Approach for Calculating Propagation Rates

It is well known from experiment that the rates of individual pit (crack) propagation as a function of time at constant environmental conditions can be approximated by a relatively simple function of time. Thus, for the case of pitting corrosion, the power function,

$$a = kt^m \qquad [70]$$

has been suggested, where k and m are empirical constants.[11,58,109] Here, a is the characteristic pit size (e.g., pit depth or radius of the pit mouth). Published values of m are very often approximately equal to $1/3$, $1/2$, $2/3$ or 1, but they can also vary over wider ranges.[11,109–111]

However, this dependence of a on t cannot be used directly in mathematical calculations for small times, because of the nonphysical limit

$$V_s = \frac{da}{dt} = kmt^{m-1} \to \infty, \text{at } t \to 0 \text{ for } m<1 \qquad [71]$$

This is why, instead of eqn [70], the following interpolation equation for pit propagation rate, V_s, has been suggested[91]

$$V_s = \frac{da}{dt} = V_0(1 + t/t_0)^n \qquad [72]$$

where $n = m - 1$ and t_0 are constants, and V_0 is the initial, finite rate of pit propagation. Equation [72] yields $V = V_0$ at $t/t_0 << 0$ and $V = V_0(t/t_0)^n$ at $t >> t_0$.

Integration of eqn [72] with the boundary condition $a = 0$ at $t = 0$ yields

$$a = x_0[(1 + t/t_0)^m - 1] \qquad [73]$$

where $x_0 = t_0V_0/m$. For small times, as follows from eqn [73], a can be presented as the linear function of t, $a = V_0t$ and for large times, a takes the form of eqn [70]. In many cases, the period of time over which the approximation

$$V(t)V_0 = \text{Constant} \qquad [74]$$

is valid can be comparable with the observation time (or even with the service life of the system). The reason is that corrosion is, generally speaking, a slow process and under real, practical conditions, values of the critical pit depth of the system, x_{cr}, and typical service life, t_s, impose significant restrictions on the values of the initial and average corrosion current densities and, thus, on the potential and concentration drops that might be observed in a corrosion cavity.[112]

For constant external conditions, the dependence of cavity propagation rate as a function of the cavity depth, x, can be written in the form

$$V_s = \frac{da}{dt} = V_0\varsigma(x) \qquad [74]$$

where function $\varsigma(x)$ satisfies the evident boundary condition $\varsigma(x) \to 1$ at $x \to 0$. For the particular case when eqn [72] holds, $\zeta(x)$ can be expressed in the form:

$$\varsigma(x) = \frac{1}{(1 + x/x_0)^{(1-m)/m}} \qquad [75]$$

where $x_0 = v_0\, t_0/m$.

The general approach based on the numerical solution of the system of mass transfer equations does not present the depth of pit in the form of eqn [70] or [73]. As noted in Turnbull,[58] the mechanistically based models are complex to set up and, at the

present stage of development, are not user-friendly. For us, it is most important that the solution of the full system of mass transfer equations for the ensemble of pits is practically unrealistic for usual systems, from the point of view of the required computation time. One way to deal with this problem is to perform numerous calculations of pit propagation in advance and approximate the obtained results by eqns [70] or [73]. The other way is to try, after some simplification that does not significantly reduce the accuracy of calculations, to develop a model that can yield a cavity propagation law of the form of eqns [70] or [73], and that may even yield analytical expressions for parameters k and m. The principal concept in this simplification is that, if the rate of corrosion reaction depends explicitly only on the local potential and some surface concentrations of particular species (e.g., Cl^- and H^+), the pit growth rate depends only on the concentrations of those species that determine the value of electrostatic potential near the corroding surface.

Below, we will consider the example of such an approach for the simplest (but perhaps the most important, from the practical point of view) case of the corrosion of steels in neutral solutions. Thus, it has been suggested that, in the mathematical simulation of the corrosion of Fe in NaCl solutions, at least six species in the solution must be taken into the account.[91]

$$S_1 \equiv Fe^{2+};\ S_2 \equiv Fe(OH)^+;\ S_3 \equiv Na^+;\ S_4 \equiv Cl^-;$$
$$S_5 \equiv H^+;\ \text{and}\ S_6 \equiv OH^-$$

These species include iron ions from the dissolution process, sodium and chloride ions (for example) that are commonly included to control the bulk conductivity, hydrogen and hydroxyl ions from the dissociation of water, and a metal hydrolysis product (for example). In the simplest case, the following homogeneous hydrolysis reactions are assumed to occur

$$Fe^{2+} + H_2O = Fe(OH)^+ + H^+ \quad [76]$$
$$Fe(OH)^+ + H_2O = Fe(OH)_2(s) + H^+ \quad [77]$$
$$H_2O = H^+ + OH^- \quad [78]$$

with $Fe(OH)_2(s)$ representing the precipitated hydrolysis product. Homogeneous reactions include hydrolysis processes and also precipitation processes. If the degree of supersaturation is sufficiently high, direct precipitation will occur in the solution itself; otherwise, precipitation will tend to occur on the walls preferentially. However, if an appropriate balance is obtained between the rate of production of the hydrolyzing species and the rate of precipitation, general saturation is expected to occur.[60]

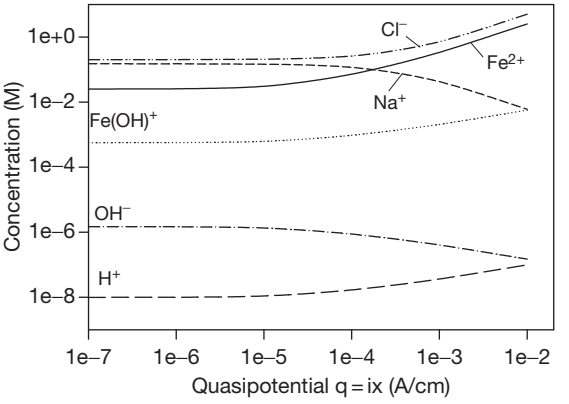

Figure 10 The concentration of species down a corroding cavity (crevice) in 0.1 M NaCl at 25 °C as functions of the quasipotential.

We will assume that a single electrochemical reaction

$$Fe \rightarrow Fe^{2+} + 2e \quad [79]$$

occurs on the walls of the cavity.

Numerical solution of the corresponding boundary problem has been performed[91] by using the values of kinetic parameters from Sharland *et al.*[78] **Figure 10** shows the concentrations profiles as a function of the quasipotential, q.[68] Please note that, for the case of a deep, one-dimensional cylindrical pit with passive walls or for a crevice with parallel passive sides, $q = ix$, where x is the distance down the cavity, and i is the current density in the crevice that is determined by the dissolution rate.[91,112] We can see that there are three species that dominate in the pit, Fe^{2+}, Cl^-, and Na^+, and only these species determine the electrostatic field in the cavity.

Let us now assume in addition, that, the electrodissolution reaction occurring in the cavity due to oxidation of the metal, can be described in terms of the Tafel equation as

$$i = i_0 \exp\left\{\frac{\alpha F(V_m - U_0 - \phi_s)}{RT}\right\} = i^* \exp\left\{-\frac{\alpha F \phi_s}{RT}\right\} \quad [80]$$

Here, i_0 is the exchange current density, α is the anodic transfer coefficient, V_m is the local electrode potential, U_0 is the open-circuit potential (measured on the external surface remote from the pit), ϕ_s is the electrostatic potential in the solution near the

electrode surface, all referred to a reference electrode at infinity, and $i^* = i_0 \exp\{\alpha F(V_m - U_0)/RT\}$ is the current density calculated in the absence of a potential drop in the cell ($\phi_s = 0$ corresponding to the maximum possible current density on the electrode surface at the given potential of the metal).

Hence, if we only want to calculate the potential distribution and rate of corrosion in this system, we can approximate the complete system involving six species (Fe^{2+}, $Fe(OH)^+$, Na^+, Cl^-, H^+ and OH^-) by a reduced system involving only three species (Fe^{2+}, Na^+ and Cl^-).

In this case, the solution of the mass transfer equations for this simplified system can be easily performed even in analytical form. In particular, if the polarization curve for reaction [79] can be described by Tafel's law [80] with the symmetry factor, α, it was shown that the depth of one dimensional pit with passive walls can be described by eqn [73] with

$$m = \frac{\alpha + 1}{2\alpha + 1} \qquad [81]$$

and

$$x_0 = 3FD_1 C^{b}_{Cl^-}/i^*,\ V_0 = K_V i^*,\ t_0 = mx_0/V_0 \qquad [82]$$

where D_1 is the diffusion coefficient of Fe^{2+}, and $C^{b}_{Cl^-}$ is the bulk concentration of chloride ions. Moreover, if $\alpha = 1$ (typical value for corrosion of steels), eqn [81] yields $m = 2/3$.

If, for example, $C^{b}_{Cl^-} = 0.6\,M$ (which corresponds approximately in the case of seawater), $i^* = 10^{-4}$ A cm^{-2} (which corresponds to an initial propagation rate, V_0, of ~1 mm $year^{-1}$) and $D_1 = 0.72\ cm^2/s$, eqn [82] yields $x_0 \approx 12$ cm. Accordingly, if the critical depth of the pit penetration x_{cr} is of the order of 1 cm, as follows from eqns [74] and [75], it is possible to conclude that the pit will propagate at a constant rate because, when x_0 is a large number $\varsigma(x)$ becomes equal to one. The physical reason for this uniform propagation is that the potential (and concentration) drops are very small in this system for the adopted values of dimensions, kinetic parameters, and environmental conditions. We can also state that the mere fact that hemispherical (or approximately hemispherical) pits exist can be explained by the insignificance of the potential drop in the corrosion cavity. Otherwise, the corrosion current density on the edge of the pit becomes higher than that on the bottom, and the pit will quickly assume a shallow ('saucer') form. This initial rate can be determined by using the experimentally measured polarization curves in the region of active dissolution, and can be calculated for certain metals and alloys for different environmental conditions by using available software.[71]

However, it is also possible that pits can propagate with a constant rate, in spite of the fact that significant potential drops may exist down the cavity. In many cases, the rate of corrosion depends on the concentration of aggressive anions (e.g., chloride ions) near the metal surface. This dependence is usually approximated by the following relation[11]:

$$i = k_a C^{\lambda}_{As} \exp\left\{\frac{\alpha F(V_m - U_0 - \phi_s)}{RT}\right\} \qquad [83]$$

where C_{As} is the surface concentration of the aggressive anion, k_a is the rate constant for the reaction proceeding in the anodic direction, and λ is the effective kinetic order of the metal dissolution reaction with respect to the anion concentration. The value of λ is usually restricted to $0 \le \lambda \le 1$.[11] It was shown that, in this case, instead of eqn [81], we can use the alternate equation[91,112]

$$m = \frac{\alpha_{eff} + 1}{2\alpha_{eff} + 1} \qquad [84]$$

where

$$\alpha_{eff} = \alpha - \lambda \qquad [85]$$

It is clear that if $\alpha \approx \lambda$, we have $m \approx 1$, and the pit propagates with an approximately constant rate.

Generally speaking, under real, practical conditions, values of the critical pit depth of the system, x_{cr}, and typical service life, t_s, impose significant restrictions on the corrosion current densities (averaged and initial) and thus on the potential and concentration drops that might be observed in the corrosion cavity. Thus, if x_{cr} does not exceed the order of 1–10 mm, and if the order of t_s is not less than 1 year, initial corrosion current densities in real, open pits cannot exceed values of 10^{-4} to 10^{-3}A cm^{-2}, with the understanding that the polarization curve (corrosion current density versus potential) and the surface concentrations of the species do not change as the pit propagates.[112] Simple analytical expressions for predicting the potential and concentration drops in open corrosion cavities and for predicting cavity propagation rate in systems containing uni- and bivalent anions in stagnant electrolytes under well mixed, external conditions have been obtained.[112]

After the transition of a pit into a crack or into a corrosion fatigue crevice, the total rate of corrosion cavity propagation, V_s, cannot be described simply by Faraday's law, but also has to contain mechanical

and, in the general case, some additional environmental component (e.g., hydrogen embrittlement component). It would be natural to assume that V_s is a known function of the environmental (concentration of species near metal surface, temperature) and mechanical parameters (stress), and so on. The explicit forms of these dependences are discussed in the corresponding chapters of this book. Here, only the most general relations will be discussed.

Figure 8 clearly shows that at low corrosion potential, the crack propagation rate does not depend on E_{corr}, that is, V_s reduces to the mechanical (creep) component. It is also clear that at high values of E_{corr}, crack propagation rate does not depend on creep rate and is described by an exponential dependence of the Tafel type. Accordingly, in the first approximation, we can present V_s as the sum of two contributions

$$V = V_{env} + V_{mech} \quad [86]$$

where V_{env} is the environmental/electrochemical component, which is often determined by Faraday's law, and V_{mech} is the mechanical component (crack advance associated with mechanical fatigue/creep). Of course, in some cases, the synergistic interaction of mechanical and environmental attack can play a role and a simple summation, as expressed by eqn [86], may not be appropriate.[113]

A review of many models for describing environment-induced cracking based directly or indirectly on anodic reaction processes or on hydrogen embrittlement can be found.[114,115] Thus, in accordance with the slip-dissolution model, the average crack growth velocity will be given by

$$V_{env} = K_v i^0_{corr} \Gamma \quad [87]$$

where i^0_{corr} is the current density on the bare surface, and Γ is the ratio of the bare surface of the crack tip to the total geometrical surface. It can be shown that

$$\Gamma = \frac{t_0^n}{(1-n)\varepsilon_f^n}(\dot{\varepsilon}_{ct})^n \quad [88]$$

where ε_v is the fracture strain of the passive film at the crack apex, $\dot{\varepsilon}_{ct}$ is the crack tip strain rate, and t_0 and n are material constants. It is evident that $\Gamma \leq 1$. In turn, the expressions for $\dot{\varepsilon}_{ct}$ can be found as described in Engelhardt *et al.*,[92] Turnbull,[114] and Peng *et al.*[116]

In the case of corrosion fatigue, the crack growth rate is usually expressed in terms of the increment of crack growth during each fatigue cycle, $da/dN = V_s/f$ (where f is the frequency of the applied stress). Very often, this rate follows the well known power-law relationship (Paris' law)

$$\frac{da}{dN} = C(\Delta K)^n \quad [89]$$

for both fatigue (no corrosion) and corrosion fatigue. Here, ΔK is the stress intensity factor range and C and n are empirical parameters that depend, in the general case, on environmental conditions. While the dependencies of the Paris equation parameters on environmental conditions is well recognized through numerous experimental studies, few of the models for corrosion fatigue developed to date incorporate environmental effects in an explicit, mechanistic manner. This is another example of where the underlying (mechanical) theory fails to account for the experimental data, and the resultant models fail to meet the requirements of determinism.

Until now, it has been tacitly assumed that the rate of pit (crack) propagation is unequivocally determined by its depth and by the external conditions, that is, there is no distribution in cavity propagation rate for pit cavities of equal depth. However, as noted above, a distribution in pit (crack) propagation rate might be observed in practical systems because of underlying distributions in system parameters that affect the growth rate. Usually, such problems are considered in the following way. In the case of pitting corrosion, it is assumed that the pit depth is described by eqn [70] with distributed parameters k and m.[117] However, in Turnbull *et al.*,[118] it is assumed for simplicity, that only parameter k is normally distributed; parameter m is assumed to be fixed, and its value is obtained by fitting the model to the experimental data. In contrast, in Harlow and Wei,[3] it is assumed that the pit maintained a hemispherical geometry and grew at a constant volumetric rate. From this fact, it immediately follows that $m = \text{const} = 1/3$. On the other hand, it was assumed that parameter k is described by a Weibull distribution.

Analogously, in Turnbull *et al.*,[118] for the case of SCC, the crack propagation rate was assumed to be given by

$$\frac{da}{dt} = C\sigma^p a^q \quad [90]$$

where σ is the applied stress. It was assumed that parameters p and q are fixed and were determined by fitting eqn [90] to the experimental data, but parameter C was assumed to be normally distributed. Additionally, for example, in Harlow and Wei,[3] for the case of corrosion fatigue, it was assumed that crack propagation is described by eqn [89] with

fixed crack growth exponent, n, and distributed parameter C.

Of course, few of the models that are discussed in this section are 'deterministic' in nature, although they are certainly 'mechanistic' in form. Determinism is readily introduced by first identifying the relevant natural laws and then ensuring that the predictions are constrained by these laws. In many cases, this would be most effectively done by introducing the models, which for the most part, describe the 'anodic' part of the corrosion cell, into a 'coupled environment' framework to impose the conservation of charge. This again illustrates the important difference between 'mechanistic' and 'deterministic' models, with only the latter constraining the output ('predictions') to those that are 'physically real' (i.e., that are consistent with scientific knowledge).

2.39.7 Rate of Pit Repassivation and Transition of Pits into Cracks

As noted above, we assume that the repassivation process obeys a first-order decay law

$$R_a(x,t) = -\gamma f_a(x,t) \qquad [91]$$

where γ is the delayed repassivation ('death') constant (i.e., the rate constant for repassivation of stable pits), and f_a is the differential damage function for active pits. The repassivation constant, γ, is, in general, expected to be a function of the external conditions, including the corrosion potential, temperature, and electrolyte composition. Generally speaking, γ is also expected to be a function of the depth of the pit, x, because the local potential in the solution at the cavity surface depends on the IR potential drop in the cavity, that is, γ might be a function of both the spatial coordinates and time. Of course, if the potential and concentration drops inside the corrosion cavity are insignificant during pit propagation, it is possible to neglect changes in γ (see above). However, the value of this constant still depends on the external conditions, such as potential, pH, and concentration of aggressive species in the bulk electrolyte. Finally, active pits may no longer be viable if the potential, E, at the pit internal surface is less than the repassivation value, E_{rp}. Accordingly, if the value of E_{rp} is reached at some pit depth, x_{rp}, active pits passivate and cannot penetrate further into the metal. The value of repassivation potential E_{rp}, is a function of the metal potential and surface concentrations at the pit tip. It can be calculated, for example, by using methodology described in Anderko *et al.*[119]

Regarding the transition of a pit into a crack, we assume that a pit immediately transforms into a crack if its depth exceeds some critical value $x_{tr.}$ As of now, the most widely accepted set of criteria for the transition of a pit into crack are the Kondo criteria.[120] According to these criteria, two conditions must be satisfied for crack nucleation to take place from a pit, namely,

$$K_I > K_{ISCC}(\text{forSCC}) \text{ or } \Delta K > \Delta K_{th}(\text{forCF}) \qquad [92]$$

and

$$V_{crack} > V_{pit} \qquad [93]$$

Here, K_I and K_{ISCC} are the stress intensity factor and critical stress intensity factor for propagation of a stress corrosion crack, respectively: ΔK is the stress intensity factor range, and ΔK_{th} is the threshold stress intensity factor range for fatigue crack propagation, respectively.

The first requirement defines the mechanical (fracture mechanics) condition that must be met for the prevailing stress and geometry, while the second simply says that the nucleating crack must be able to 'outrun' the pit.

It is important to note the following circumstance. At high values of corrosion potential, E_{corr}, the environmental component of crack propagation rate, V_{env}, could be much higher than the mechanical component, V_{mech} (see. **Figure 8**). Accordingly, the crack propagation rate, V_{crack} will practically coincide with its environmental part, V_{env}.

In accordance with the slip dissolution model, the crevice tip is partially blocked by the passive film. Accordingly, for a given set of tip conditions (metal potential, pH, etc.), V_{env}, must be smaller than that corresponding to the pit propagation rate, V_{pit}, with the tip surface being bare (see eqn [87]). This means that, under these conditions, the transition from a pit into a crack occurs if (1) the depth of the pit exceeds some critical length, x_{mech} (where $K_I \geq K_{ISCC}$ or $\Delta K_I \geq \Delta K_{I,th}$); and (2) the pit is passivated (when V_{pit} is very small). Thus, this latter criterion suggests that cracks will nucleate only from 'dead' pits. This example shows how important repassivation phenomena may be for predicting corrosion damage.

2.39.8 Statistical Properties of the Damage Function

There exists a close correspondence between damage function analysis (DFA), which has been described at some length above, and extreme value statistics (EVS). The latter technique has been used extensively to extrapolate damage (maximum pit or crack depth) from small samples in the laboratory to larger area samples in the field. Furthermore, DFA provides a means of calculating the central and scale parameters and their time-dependencies in EVS from first principles, and hence represents a unification of the two prediction philosophies.

From a statistical point of view, all distributed properties of the system are completely determined by the cumulative distribution function (CDF), $\Phi(x)$. By definition, $\Phi(x)$ is the probability that the depth of a randomly selected pit (crack) is $\leq x$. We postulate that the pit distribution on the metal surface is uniform. Accordingly, the total number of nucleated pits in the entire system is $SN(t)$, where S is the area of the system and, from the definition of the integral damage function, F, the number of pits that have the depth $\geq x$, is $S[N(t) - F(x,t)]$. Accordingly, from the definition of probability, we have

$$\Phi(x,t) = \frac{S[N(t) - F(x,t)]}{SN(t)} = 1 - \frac{F(x,t)}{N(t)} \qquad [94]$$

We see that the CDF for a given observation time, $\Phi(x,t)$, can be predicted if we know (can calculate) the integral damage function of the system (note that the number of nucleated, stable pits, $N(t)$ simply equals $F(0,t)$). This relationship can be regarded as being the bridge between the statistical and deterministic approaches for estimating the accumulation of localized corrosion damage on a surface.

As noted above, from the practical point of view, the most important value for characterizing corrosion damage is the failure probability, P_f, of the system. By definition, P_f, is the probability that at least one corrosion event in any form (pit, crevice, stress corrosion crack, or fatigue crack) reaches a depth, x, at a given observation time, t, where x, in this case, is the critical dimension. It can be shown[14] that

$$P_f(x,t) = 1 - \exp\{-SF(x,t)\} \qquad [95]$$

Equation [95] allows us to calculate the probability of failure if the integral damage function, F, is known. The latter function can be found as a solution of eqn [4]. However, here we will reject the equal velocities for all pits with a given depth assumption that was adopted previously (see eqn [9]). Thus, it is well known that the morphology of pits on any given surface can vary significantly, with some shapes favoring more rapid mass and charge transfer, and hence, a greater propagation rate.[121] In addition, some pits will initiate at metallurgical features that may favor more rapid propagation, for example, at MnS inclusion.[121] The distribution in pit propagation rate might also be explained, for example, by the spatial distribution in electrochemical activity of the anodic and cathodic sites on the corroding surface.[122]

Here, we will assume that the pits that propagate with initial rate V_0 are nucleated in accordance with the equation.

$$n(t) = \int_0^\infty \lambda(t, V_0)\mathrm{d}V_0 \qquad [96]$$

The function $\lambda(t,V_0)$ yields the number of pits (per square centimeters) that have initial propagation rates between V_0 and $V_0 + \mathrm{d}V_0$ and that nucleate in the period of time between t and $t + \mathrm{d}t$. Further propagation of the pits takes place in accordance with eqn [74]. It can be shown that, in this case, the expression for the flux of active pits can be expressed in general form as[123]

$$j_a(x,t) = \int_0^\infty \exp[-\gamma g(x)/V_0]\lambda(t - g(x)/V_0, V_0)\mathrm{d}V_0 \qquad [97]$$

where

$$g(x) = \int_0^x \frac{\mathrm{d}x'}{\varsigma(x')} \qquad [98]$$

(compare with eqn [9]). Accordingly, the expressions for the differential damage functions for active and passive pits and the integral damage function have the following forms[123] as solutions of eqn [4]

$$f_a = \int_0^\infty \frac{\exp[-\gamma g(x)/V_0]\lambda[t - g(x)/V_0, V_0]}{V_0\varsigma(x)}\mathrm{d}V_0 \qquad [99]$$

and

$$f_p = \int_0^\infty \frac{\gamma\exp[-\gamma g(x)/V_0)\Lambda[t - g(x)/V_0, V_0]}{V_0\varsigma(x)}\mathrm{d}V_0 \qquad [100]$$

Furthermore, for the case of pitting corrosion, the total integral damage function, F, is[123]

$$F = \int_0^{\infty} \exp[-\gamma g(x)/V_0)\Lambda[t - g(x)/V_0, V_0]\mathrm{d}V_0 \quad [101]$$

where $\Lambda(t, V_0) = \int_0^t \lambda(t', V_0)\mathrm{d}t'$ yields the number of pits (per square centimeters) that have initial propagation rates between V_0 and $V_0 + \mathrm{d}V_0$ and nucleate in the period of time between 0 and t. F is the sum of the integral damage functions for active and passive pits for the given case.

Let us assume that the distribution in initial pit propagation rate does not depend on time, that is,

$$\lambda(t, V_0) = n(t)\psi(V_0) \quad [102]$$

To move further, we must assume a distribution function, $\psi(V_0)$, for the pit growth rate, in order to account for those factors that result in a distribution in growth rate that is not captured by the (present) deterministic models. For our purposes, it is most convenient to approximate $\psi(V_0)$ by Laplace's distribution function

$$\psi(V_0) = \frac{\exp(-|V_0 - \bar{V}_0|/\beta)}{2\beta} \quad [103]$$

where $\bar{V}_0$ is the mean initial pit propagation rate and $\sigma^2 = 2\beta^2$ is the dispersion.

If eqn [102] holds, we have, for the integral damage function and the cumulative damage function, the following expressions

$$F(x,t) = \int_0^{\infty} N[t - g(x)/V_0)\exp[-\gamma g(x)/V_0)\psi(V_0)\mathrm{d}V_0 \quad [104]$$

and

$$\Phi(x,t) = 1 - \int_0^{\infty} N[t - g(x)/V_0)]\exp[-\gamma g(x)/V_0)\psi(V_0)\mathrm{d}V_0/N(t) \quad [105]$$

respectively. In particular, for the case of instantaneous nucleation, we have

$$\Phi(x,t) = 1 - \int_{x/t}^{\infty} \exp[-\gamma g(x)/V_0]\psi(V_0)\mathrm{d}V_0 \quad [106]$$

As has been shown experimentally, in many practical cases, the asymptotic behavior (for large values of x) of the CDF can be described by the exponential relationship[58,121]

$$\Phi(x,t) = 1 - \exp[-(x-u)/\alpha] \quad [107]$$

where u is the central parameter (the most frequent value), and α is the scale parameter, which defines the width of the distribution. Accordingly, as follows from eqn [107], the extreme value distribution (EVD), $\psi(x,t)$ (the probability that the largest value of pit depth $\leq x$), is described by a double exponent (Gumbel Type I extreme value distribution) in the form[58]:

$$\Psi(x,t) = 1 - P_f = \exp[-\exp(-y)] \quad [108]$$

where

$$y = (x - h)/\alpha \quad [109]$$

and $h = u + \alpha \ln(SN)$.

Numerical calculation[14] shows that the dependencies of ln(1 − CDF) on pit depth, x, can be approximated by straight lines, at least for sufficiently large values of x, and therefore provide a theoretical basis for applying the Type I extreme value distributions to real corrosion systems. In some cases, parameters α and h can be expressed in analytical form. Thus, for the case of instantaneous nucleation and constant pit propagation rate, these parameters can be presented in the form[14]:

$$\alpha = \frac{\beta t}{1 + \gamma\beta t/\bar{V}_0} \quad \text{and} \quad h = \frac{[\bar{V}_0 + \beta Ln(0.5SN_0)]t}{1 + \gamma\beta t/\bar{V}_0} \quad [110]$$

We see that, for small values of t, the parameters α and h can be described by $\alpha = \beta t$ and $h = [\bar{V}_0 + \beta Ln(0.5SN_0)]t$, that is, they are proportional to time. Such dependencies were actually observed, for example, for the case of the pitting corrosion of manganese steel in CO_2–acidified seawater.[122] On the other hand, for large observation times, the parameters α and h approach the following limits

$$\alpha = \bar{V}_0/\gamma \quad \text{and} \quad h = [\bar{V}_0 + \beta Ln(0.5SN_0)]t\bar{V}_0/\gamma \quad [111]$$

that are independent of time. This fact can be regarded as being physically evident, because at sufficiently large times, all pits become passive (the damage function becomes 'frozen'), and further propagation of damage cannot occur, provided that $\gamma > 0$. This conclusion concerning the achievement of limiting pitting depth also follows from a formal statistical treatment of experimental data for underground carbon steel pipelines.[11] The 'freezing' of damage functions can also be seen in the propagation of corrosion damage on aluminum in tap water.[10]

Equation [110] with eqn [108] can be used for calculating the probability of the failure of a system. Unfortunately, very often it can be the case that not

all, or even none, of the kinetic parameters that determine the pit (crack) nucleation rate, pit propagation rate, and pit repassivation rate, are known. However, unknown parameters are determined by comparing the results of analytical or numerical calculations of the depths of the deepest pits (cracks) with the corresponding experimentally observed values for short-term experiments. After determining values for the unknown parameters, the depths of the deepest pit (crevice) for the total system (i.e., for the system with arbitrary surface area) for long-term exposure are predicted.

Usually therefore, in the case when none of the kinetic parameters are known, the following expression, based on the Gumbel type-I distribution is used for predicting perforation probability in the large systems with the total area, S, by using the results of measurements of the depth of the deepest pits on the series coupons with area, s[124]

$$P_f = 1 - \exp\{-\exp[-(d - u + \alpha\ln(S/s))/\alpha]\} \quad [112]$$

where d is the thickness of the wall.

For predicting probability of failure in long-term experiments by using the results of measurements in short-term experiments, it is necessary to assume some functional dependence of the location parameter, u, and scale parameters, α, on time. For the case when eqn [110] is valid, these parameters are described by hyperbolic relations of the form

$$u = \frac{a_1 t}{1 + a_2 t}, \quad \alpha = a_3 u \quad [113]$$

where, a_1, a_2, and a_3 are unknown parameters that must be fitted by using the short term experiments. The procedure of such fitting by using the maximum likelihood method is described in Laycock *et al.*[125] **Figure 11** illustrates the applicability of the hyperbolic dependencies for predicting the results of experiments measuring the depth of the deepest pits in the corrosion of aluminum Alloy 2S-O in Kingston tap water.[10] The mean depth of the deepest corrosion event, X_m, and standard deviation of this value, σ, can be calculated by using the following relations[125]:

$$X_m = h + \alpha[\mathrm{E} + \ln(S/s)] \quad \text{and} \quad \sigma = \pi\alpha/\sqrt{6} \quad [114]$$

We see that applicability of the hyperbolic functions can be considered as being very satisfactory. Note that only the data for $t = 1$ week and 1 month were used for calibration and hence, for prediction over a period of up to 1 year, providing accurate extrapolation over a range of 12 times that of the calibration range.

However, the typical time-relations that are usually used for estimating the location and scale parameters in extreme value distributions are of the power law type:

$$h = a_1 t^{a_2}, \quad \alpha = a_3 h \quad [115]$$

or logarithmic:

$$h = a_1 \log(t) + a_2, \quad \alpha = a_3 h \quad [116]$$

Figure 12 shows that application of the power law functions for fitting experimental data to the short

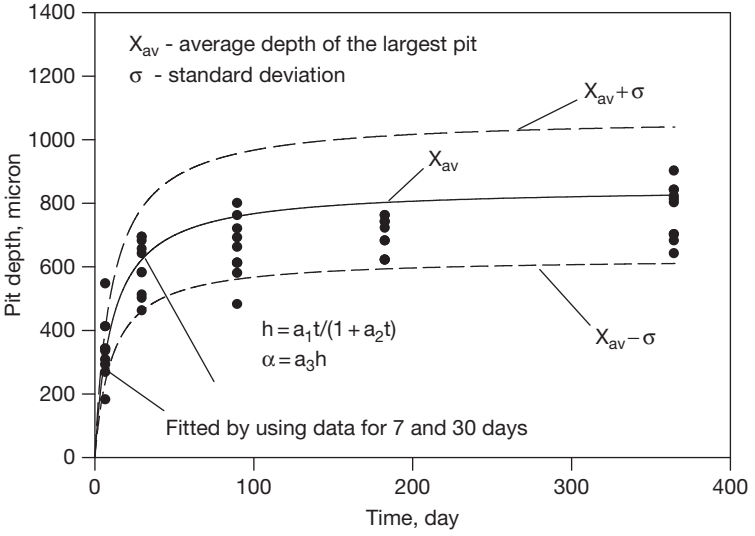

Figure 11 The mean depth of the deepest pit as a function of time. Fitting to experimental data (black circles) has been performed by using the hyperbolic dependencies [113].

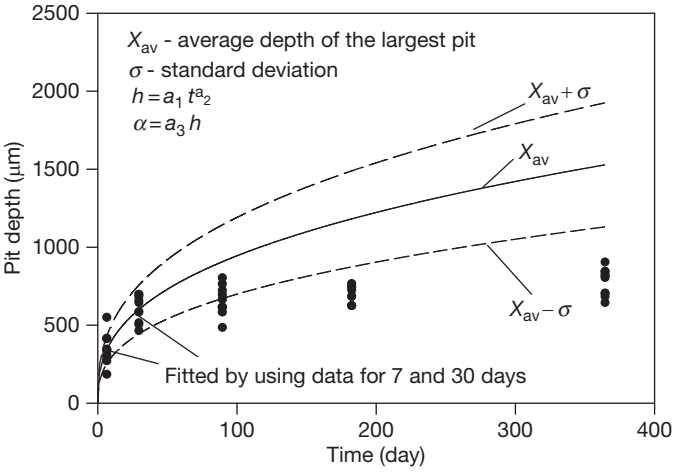

Figure 12 Fitting to experimental data (black circles) has been performed by using power law dependencies [114].

term experiments yields results that are not as good as application of hyperbolic law, at least for the considered experimental data. This happens, because the power law [115] does not take into account the repassivation of pits that plays a substantial role in determining the results of Aziz's experiments.

From the above, it is evident that the application of the logarithmic law yields much more acceptable results than does the application of the power law (**Figure 13**). However, at present, there is no physical model that could explain a logarithmic law of pit growth. In reality, if we assume that the growth law of individual pits can be described by a logarithmic function, it can be easily shown that the rate of the pit growth must decrease in accordance with the exponential law ($da/dt \sim \exp(-\zeta a)$). This dependence is substantially stronger that the maximum possible decrease of the rate of open pit growth under diffusion control when $da/dt \sim 1/a$. Accordingly, it might be suggested that the logarithmic dependence of pit growth is formally introduced for effectively describing pit propagation in the presence of repassivation phenomena.

A generalization of the hyperbolic function [113] in the form

$$h = \frac{a_1 t^{a_4}}{1 + a_2 t^{a_4}}, \quad \alpha = a_3 h \qquad [117]$$

appears to offer some advantages. The principal advantage of the general hyperbolic dependence [117] is that it coincides with the power law at short times and yields the accurate transition: $u, \alpha \rightarrow$ constant as $t \rightarrow \infty$ as it must, due to the repassivation. It is interesting to note that calculation

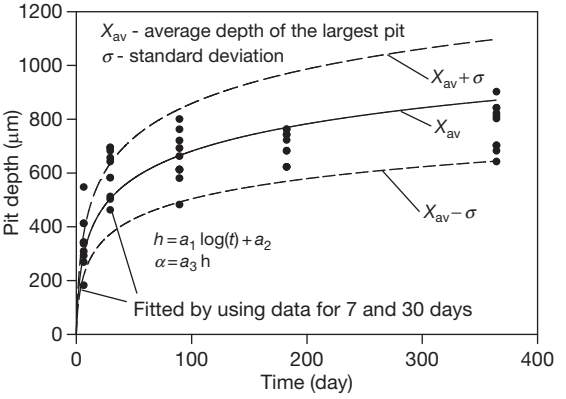

Figure 13 Fitting to experimental data (black circles) has been performed by using logarithmic dependencies [116].

shows that the parameter $a_4 = 1.0093 \approx 1$, that is, fitting by using the general hyperbolic dependencies yields, for the given case, practically the same results as the simple hyperbolic dependencies.

2.39.9 Monte Carlo Simulation

The existence of deterministic models to describe nucleation, propagation, and repassivation of localized corrosion processes allows us to replace the current DFA, which reduces to the direct solution of the balance eqns [2], with an alternative approach – Monte Carlo simulation of corrosion damage. However, it is worthwhile to develop this alternative

approach for describing corrosion damage for the following reasons. It is important to note that, frequently, under real conditions, only a few pits (or cracks), or sametimes only a single pit (or crack), may be alive (propagating) on the corroding metal surface (see the upper extremes in **Figure 1**). In this case, the differential equations for the damage function, which are equivalent to a balance equation for particles in discontinuous media, lose their strict physical meaning.

The main idea of the Monte Carlo method is to keep track of each stable pit (or crack) that nucleates, propagates and repassivates on the metal surface. A great advantage of this method lies in the fact that it allows us to take into account the interactions between particular individual pits (cracks) in an explicit manner. By doing so, it becomes possible to reduce the number of unknown parameters that describe the interaction between individual pits (cracks). Preliminary calculation shows that both approaches (DFA and Monte Carlo) yield the same results, if the same physical assumptions are made for describing the propagation of corrosion damage. At this point, it is important to note that, in the Monte Carlo method described here, the stages in the life of an individual pit or crack are described deterministically (i.e., in terms of models whose predictions are constrained by the natural laws), while the ensemble of pits is described statistically in terms of a Monte Carlo algorithm. Below, the current version of the deterministic Monte Carlo simulation (DMCS) algorithm that has been developed for predicting the accumulation of localized corrosion damage will be briefly described.

Let us denote by N_0 the total number (not per square centimeters) of stable pits that can nucleate on a metal surface having a total area of S. We number these pits by the index $k = 1, 2, \ldots, N_0$, and we will track each of these pits individually. Initially, we suggest that there are no stable pits on the metal surface. We proceed by calculating the probability that a pit will nucleate in stable form during the time step dt as

$$P_{\text{nucl}} = \frac{N(t + dt) - N(t)}{N_0 - N(t)} \qquad [118]$$

where, $N(t)$ is the number of stable pits that nucleate within the time interval between 0 and t. (Note that P_{nucl} is defined as a ratio of the number of pits that nucleate in the time interval between t and $t + dt$ to the number of available remaining sites at moment t).

For each pit, k, that has not yet been born, we generate a random number $0 \leq G_k \leq 1$. If $G_k \leq P_{\text{nucl}}$, a pit is proclaimed to have been born with a depth of penetration $x = 0$; otherwise, it is considered not to have been born and will be interrogated in the following step. In the case of instantaneous nucleation, all pits in the amount of N_0 are born during the first time step. In the more general 'progressive nucleation' case, the function $N(t)$ can be calculated by using, for example, the PDM, as noted above. The Cartesian coordinates of the centers of the nucleated pits, X_k and Y_k, are also established by using the random number generator, but this will be modified in the future to correspond to particular metallurgical, microstructural, and microchemical features on the surface (e.g., emergent precipitates or second phase particles) that may not be randomly distributed (e.g., $Cr_{23}C_7$ precipitates on emergent grain boundaries in stainless steels). This innovation will introduce, surface structural factors for the first time, in the deterministic prediction of localized corrosion damage. Practically, if the surface is rectangular with area $a \times b$, the Cartesian coordinates X_k and Y_k are declared to be $X_k = G_a$, and $Y_k = G_b$, where $0 \leq G \leq 1$ is a random number. If the surface is not rectangular, we insert the surface into a sufficiently large rectangle so that all points on the actual surface are included, and then repeat the described procedure. However, in this case, we declare X_k and Y_k as a center of a newly-born pit only if the point (X_k, Y_k) lies inside the actual surface. Otherwise, the procedure is repeated until success is achieved, that is, until (X_k, Y_k) lie inside the actual surface.

At each time step, the depth of the j-th stable, living pit, a_j, is calculated sequentially by using Faraday's law

$$a_j(t + dt) = a_j(t) + K_V i_j(t) dt \qquad [119]$$

We assume that i_j is described by Tafel's law for the active metal dissolution current density as a function of potential, that is,

$$i_j = i_0 \exp\left(-\frac{\alpha F \Delta\phi_j}{RT}\right) \text{ at } \Delta\phi_j < \Delta\phi_{\text{cr}} \text{ and}$$

$$i_j = 0 \text{ at } \Delta\phi_j \geq \Delta\phi_{\text{cr}} \qquad [120]$$

where $\Delta\varphi_j$ is the averaged potential drop on the active surface (relative to a point that is remote from the hemispherical pit of index j), α is the transfer coefficient of the metal dissolution reaction, i_0 is the corrosion current density at the corrosion potential, T is the Kelvin temperature, F is Faraday's constant, and R is

the gas constant. The physical meaning of the value $\Delta\varphi_{cr}$ is as follows. We can assume that the pit should continue to grow (be alive) if the metal potential at the bottom of the pit, E, is larger than the repassivation potential, E_{rp}, that is, at $E = E_{corr} - \Delta\varphi_j > E_{rp}$ or at $\Delta\varphi_j < E_{corr} - E_{rp}$. In other words $\Delta\varphi_{cr} = E_{corr} - E_{rp}$ is the difference between corrosion and repassivation potentials. Of course, it is assumed that $E_{corr} > V_{crit}$, which in turn is greater than E_{rp}, otherwise pitting corrosion cannot be initiated.

It can be shown[126] that the average potential drop on the active surface of a hemispherical pit (relative to a point far away from it), $\Delta\varphi_j$, can be estimated by the following relation

$$\Delta\phi_j = \frac{ba_j i_j}{\kappa} + \sum_{k\neq j} \frac{i_k a_k^2}{\kappa d_k} \qquad [121]$$

Here, the index k denotes the pits on the surface (the pit of interest is denoted by the index j), a_k is the radius of the hemispherical pit, i_k is the average current density inside the pit, κ is the conductivity, and $b \approx 2.1$ is a constant. Equation [121] can be obtained as an approximate solution of Laplace's equation for the electrical potential for the ensemble of hemispherical pits embedded in a plane under the condition that pits are far apart, that is, when the contribution of each pit can be considered independently. Noting that $\Delta\phi_j$ corresponds to the potential drop from some point within the pit and a remote point on the external surface, the first term in eqn [121] describes the contribution of the central pit to the total potential drop; this contribution can be found, for example, by using the method described in Pistorius and Burstein.[32] The second term describes the contribution of all other pits on the corroding surface.[50]

Accordingly, i_j is calculated by using eqn [121], where $\Delta\varphi_j$ is determined by a numerical solution of the equation

$$\Delta\phi_j = \frac{ba_j i_0}{\kappa} \exp\left(-\frac{\alpha F \Delta\phi_j}{RT}\right) + \sum_{k\neq j} \frac{i_0 a_k^2}{\kappa} \exp\left(-\frac{\alpha F \Delta\phi_k}{RT}\right) \qquad [122]$$

By solving this equation, we assume that all $\Delta\varphi_k$ in the second term on the right-hand side of eqn [122] are known and are equal to their previous (in the iteration sense) values.

After each time step, the repassivated (dead) pits are excluded from the population of actively growing pits. A pit is considered dead if $\Delta\varphi_j > \Delta\varphi_{cr}$. In addition, if two pits touch each other, that is, if

$$d_{i,j} \leq a_i + a_j \qquad [123]$$

where $d_{i,j}$ is the distance between the centers of the ith and jth pits, the smallest pit is declared repassivated (dead). A more correct assumption might be that, instead of two touching hemispherical pits, we have a single ellipsoidal pit with the depth of the deepest pit and a dimension obtained, for example, from the condition $\pi a^2 = \pi a_i^2 + \pi a_j^2$. Also, the entities that encroach on one another are the 'hemispheres of influence' (HOI), such that the pits begin to compete for the same resources (oxygen reduction). However, such an approach would substantially complicate the problem, but these factors will eventually be included in the analysis. To justify the adopted simplification, we note that the total area occupied by the active pits, S_a, must be much smaller than the area of the sample, S, in order to sustain differential aeration. Accordingly, overlap of the pits must be a relatively rare event. Moreover, our simplification can only decrease the value of $\Delta\varphi_j$ for any given pit j. Thus, if interactions between pits were substantial in the corrosion process, the conclusion would be all the more true than without the simplification.

In addition, we consider the probability that pits can repassivate accidentally (by chance). It is assumed that the probability of a pit repassivating during each time step is proportional to the magnitude of this step, that is, $P_\gamma = \gamma\, dt$, where γ is the delayed repassivation constant. Practically, for the jth living pit in each time step, we generate the random number $0 \leq G \leq 1$. If $G \leq P_\gamma$, the pit is declared to be dead (passivated) and is excluded from the further consideration; otherwise, the pit is considered to be alive on entering the next time step. We see that our Monte Carlo simulation method describes all three stages of the pit propagation damage – nucleation, propagation, and repassivation of stable pits.

Table 2 Parameter values for model calculations

i_0	1.5×10^{-2} A cm^{-2}
K_v	3.44×10^{-5} cm^3 C^{-1}
α	1
κ	$0.3 \times 10^{-3}\ \Omega^{-1}$ cm^{-1}
$\Delta\varphi_{cr}$	200 mV
T	25 °C
τ	3 days
a	3.65 days
b	1
γ	0.066 day^{-1}

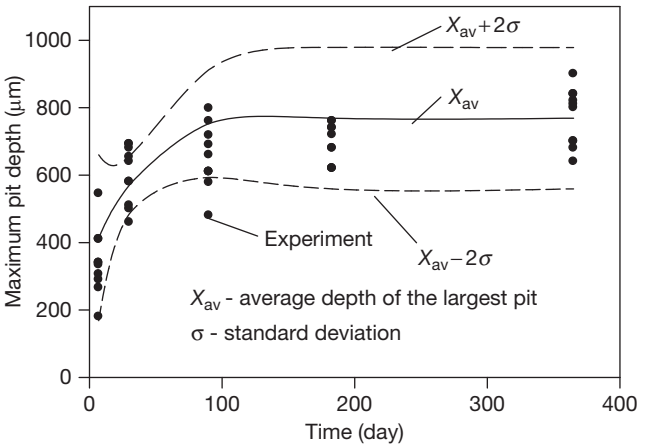

Figure 14 The mean depth of the deepest pit as a function of time. Experimental data are taken from Aziz[10] and are for aluminum alloy Alcan 2S-O in Kingston, Ontario tap water. Note that no calibration was performed on short term data, as was the case for **Figure 11**.

As an example of the application of this Monte Carlo simulation method within DFA, we consider again, the corrosion of aluminum alloy Alcan 2S_O in Kingston, Ontario tap water.[10] In this paper, for the purpose of numerically simulating the accumulation of pitting damage on the alloy surface, we will assume the values of various model parameters that are shown in **Table 2**. The parameters for the PDM (τ, a, and b) were chosen somewhat arbitrarily. The aim was only to ensure that, by the end of two weeks, practically all stable pits had nucleated, as indicated by the experimental data.[10] The value of K_V corresponds to that for aluminum and the value of κ corresponds to that typically assumed for tap water. The value for the delayed repassivation constant, γ, was chosen to ensure that, by the end of 2 months, the bulk of the pits represented by the bell-shaped curve have ceased to grow (see **Figure 1**). The value of α has been chosen as being typical for metal dissolution, and only the value of i_0 has been fitted to the experimentally measured values of maximum pit depth at $t = 1$ week after metal exposure.[10] Finally, the sample is considered to be rectangular with the dimensions 7×18 cm and $N_0 = 450$.[10]

Figure 14 shows a comparison of results of the Monte Carlo simulation with experimental data.[10] For a given observation time, t, we perform M simulations as described above and, accordingly, receive M values $x_1^*(t), x_2^*(t), \ldots, x_M^*(t)$ for the depth of the deepest pits. After that, we calculate the average (mean) value of the depth of the deepest pit as

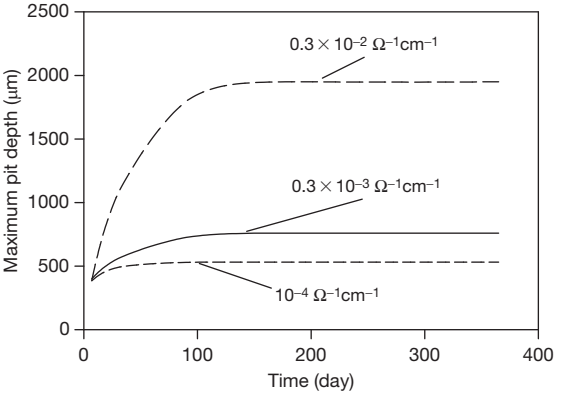

Figure 15 The mean depth of the deepest pit as a function of time for different conductivities of the electrolyte for aluminum alloy Alcan 2S_O in Kingston, Ontario tap water. Reproduced from Aziz, P. M. *Corrosion* **1956**, *12*, 35–46.

$$X_{av}(t) = \frac{1}{M}\sum_{m=1}^{M} x_m^*(t) \qquad [124]$$

and the standard deviation as

$$\sigma(t) = \sqrt{\frac{1}{M-1}\sum_{m=1}^{M}\left(X_{\mathrm{av}}(t) - x_m^*(t)\right)^2} \qquad [125]$$

For the sufficiently large value of M ($M \geq 40$, in our case), the results do not depend practically on the value of M. Because 95% of all experimental measurements usually lie in the interval ($X_{\mathrm{av}} - 2\sigma$, $X_{\mathrm{av}} +$

2σ), we posit that excellent agreement is observed between the experimental and simulation results.

It is important to emphasize that **Figures 11** and **14** were obtained by using absolutely different approaches. While **Figure 11** was obtained as a result of extrapolating data from short term experiments, without any assumption of kinetic parameters, **Figure 14** was obtained assuming that we have the complete set of required parameters without directly using data of short term experiments.

As noted previously, the main advantage of deterministic models over the statistics-based models lies in the fact that deterministic models allow us to make predictions for environmental conditions that lie beyond the available experimental (calibration) data, because the predictions are analytic and based upon a sound physical model and because the prediction is constrained by the natural laws to that which is physically real. As an example, **Figure 15** shows the influence of electrolyte conductivity on the mean depth of the deepest pits from multiple, identical sample areas on the surface as a function of time. It is seen that the mean of the deepest pits on multiple, but equal, areas on the alloy surface is a very sensitive function of the external environment conductivity; this probably reflects primarily an enhanced throwing power of the coupling current from the pit mouth to the external surface where it is consumed by oxygen reduction. Thus, increasing the conductivity of the external environment allows the coupling current to be thrown a greater distance from the mouth because of the lower IR potential drop in the solution, with the result that the pit can access a larger area for oxygen reduction. Because the pit growth rate is related to the magnitude of the coupling current through Faraday's law, the pit depth is also predicted to increase. It is also important to note that, in all cases, the mean of the deepest pits on the surface is predicted to become constant after ~100 days of exposure, simply reflecting that, at longer times, all the pits on the surface are 'dead' (repassivated). The critical question then is whether the deepest dead pits are sufficiently deep to nucleate cracks under the prevailing loading conditions.

The version of the Monte Carlo model that is described above deals only with the propagation of pitting corrosion damage. The example of Monte Carlo simulation that considers the transition of a pit into a crack can be found, for example, in Turnbull *et al.*[118] This model is based on mechanistic equations for pit and crack propagation rates (see eqns [70] and [90]), with statistically distributed input parameters, and no models were assumed for the pit or crack growth processes. These unknown parameters are fitted to the available experimental data, and accordingly, it will be impossible to use this model for predicting corrosion damage under different environmental conditions.

It is important to note that, in the models that consider deterministically the propagation of ensemble of cracks, it would be necessary, in the general case, to take into account the possible mechanical interactions between multiple cracks.[127]

2.39.10 Examples of Deterministic Prediction of Corrosion Damage in Complicated Industrial Systems

In this section, we present two examples of the deterministic prediction of corrosion damage in complex industrial systems. The two systems chosen are both from the electric power industry, where corrosion has proven to be an important factor in determining the availability of the power generating facilities. Indeed, it has long been recognized that the management of

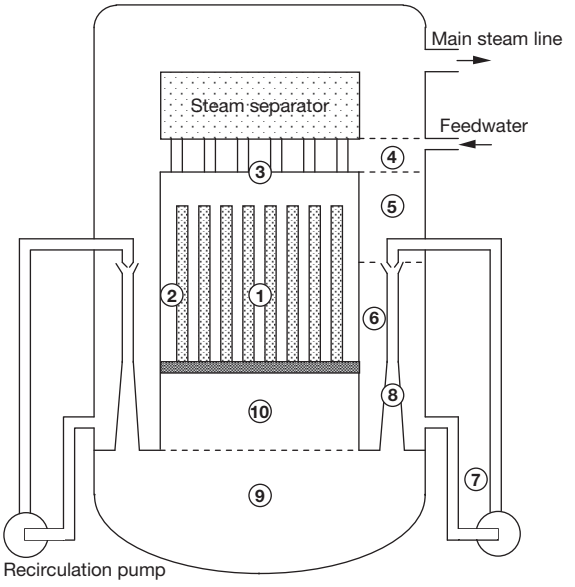

Figure 16 Schematic of the primary coolant circuit of a BWR having external coolant pumps. The regions are identified as (1) core channels; (2) core bypass; (3) upper plenum; (4) mixing plenum; (5) upper downcomer; (6) lower downcomer; (7) recirculation system; (8) jet pump; (9) bottom of lower plenum; (10) top of lower plenum. Reproduced from Macdonald, D. D.; Balachov, I.; Engelhardt, G. R. *Power Plant Chem.* **1999**, *1*, 9–16.

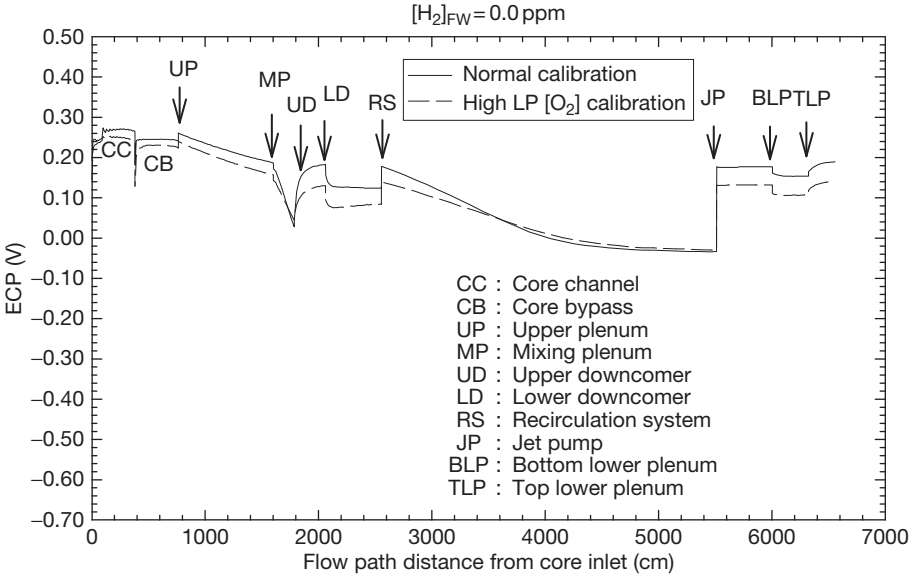

Figure 17 Calculated ECP (versus SHE) for the primary coolant circuit in the Leibstadt BWR operating under 'normal water chemistry' conditions (no hydrogen added to the feedwater). Reproduced from Macdonald, D. D.; Urquidi-Macdonald, M. *Corrosion* **1992**, *48*, 354–366.

the accumulation of corrosion damage, such that maintenance can be performed during scheduled outages, is an effective strategy for enhancing availability and for life extension. The primary purpose, here, however, is to convince the reader that the deterministic prediction of damage is practical and that such models may form the basis for the effective management of damage.

2.39.10.1 Cracking in Nuclear Reactors

The first example of the application of deterministic modeling of damage localized corrosion that we have chosen to describe in our work on modeling the accumulation of damage due to intergranular stress corrosion cracking (IGSCC) in sensitized Type 304 SS in the primary (liquid water) coolant circuit of a BWR.[23] This case is important because it illustrates the integration of the damage over the CEP taken by the reactor during normal operation. The reader will recall that the CEP is the path taken by the system in terms of those independent variables that have a significant impact on the rate of accumulation of damage as the system changes from the present state to the future state.

A schematic of the primary coolant circuit of a BWR with external coolant pumps is shown in Figure 16, and the various components and regions in the flow circuit are identified in the caption.[128]

Plotted in Figure 17 is the ECP calculated using the MPM (see Section 2.39.4) by first calibrating the radiolysis model (not the MPM) on Dresden II (a completely different reactor in Illinois) field data for the oxygen content of the coolant during operation and on another reactor (Duane–Arnold); these two reactors define the extremes of the US fleet of BWRs in their response to hydrogen added to the reactor feedwater.[20,31,99] These calculations predict that the ECP varies by about 250 mV around the entire coolant circuit when no hydrogen is added to the feedwater.

On the other hand, if significant hydrogen is added to the feedwater (e.g., 0.5 ppm), the corrosion potential is predicted to vary by about 0.9 V around the circuit. The Nuclear Regulatory Commission (NRC) has proposed a critical potential for intergranular stress corrosion cracking (IGSCC) in sensitized Type 304 SS of -0.23 V_{SHE}; if the corrosion potential lies below this value, no cracking will occur but for more positive values, cracks will nucleate and grow, and the utility cannot take credit for a 'no cracking environment.' In the case of 'normal water chemistry (NWC)' (Figure 17, zero feedwater hydrogen), all components in the primary (liquid water) coolant circuit are predicted to be susceptible to IGSCC. Under 'hydrogen water chemistry (HWC)' (Figure 18, $[H_2]_{FW} = 0.50$ ppm), significant regions of the coolant circuit are protected by the added hydrogen, including much of the recirculation piping system

and the Lower Downcomer, while other regions are not. This example demonstrates how modern modeling techniques (i.e., reaction kinetic analysis, RKA) can be used to specify the conditions that must be achieved in a complex chemical system in order to protect components against corrosion.

As indicated above, the CEP describes the path taken by the system in terms of the independent variables that have a significant impact on the process, resulting in corrosion damage as the system changes from the present state to the future state. Once this path is defined, the corrosion rate is integrated along the path to yield the integral damage. This concept is illustrated below with reference to intergranular stress corrosion cracking in the core shroud of a boiling water nuclear reactor. (The shroud is a stainless steel drum that surrounds the core containing the fuel rods. The shroud contains a circumferential weld (the 'H-3 weld') at the top, and the steel adjacent to the weld, in the so-called heat-affected zone, HAZ, is sensitized and hence is susceptible to IGSCC. The phenomenon of IGSCC has been responsible for billions of dollars of losses in the nuclear power industry during a period extending over 30 years.) For IGSCC in sensitized Type 304 SS, the important independent variables in determining the crack growth rate are stress, degree of sensitization (DOS), crack length, temperature, conductivity of the water, oxygen, hydrogen, and hydrogen peroxide concentrations (all produced by the radiolysis of water or added, as in the case of H_2, for a reactor operating on hydrogen water chemistry), and water flow velocity. In turn, the concentrations of the redox species (H_2, O_2, and H_2O_2) determine the electrochemical corrosion potential (ECP), upon which the crack growth rate is exponentially dependent. Accordingly, the independent variables defining the CEP for the crack in the shroud ID surface within the HAZ of the weld are temperature, degree of sensitization (DOS) of the steel, crack length, tensile stress (residual and operational), water conductivity, ECP, and flow velocity. Thus, the CEP is defined in terms of the variations in each of these quantities as the reactor changes during the ten years of operation.

Figure 19 shows the operating history of the reactor in terms of reactor power (which defines the temperature and the bulk coolant flow rate) and hydrogen added to the feedwater (H_2 has a large impact on the ECP – see **Figures 17** and **18**). This generic reactor was operating on HWC, with hydrogen being added only when the reactor is operating, not during shutdown, and the damage, in terms of the crack length, was calculated by integrating the crack growth rate over the CEP for a period of 10 years.

The predicted damage is summarized in **Figure 20**, in which are plotted crack length (in centimeters) versus time curves for three operating protocols:

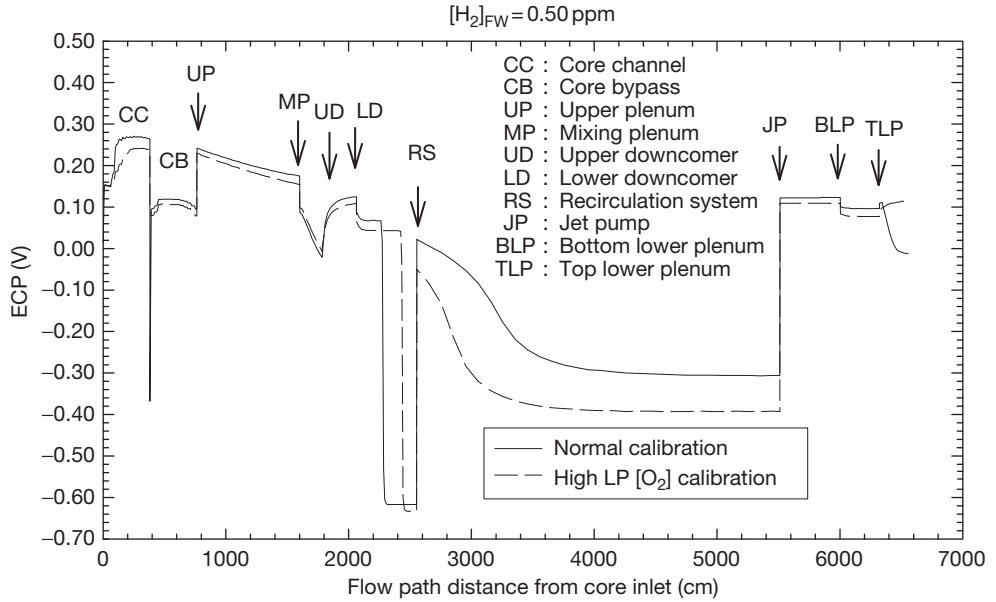

Figure 18 Calculated ECP (vs. SHE) for the primary coolant circuit in the Leibstadt BWR operating under 'hydrogen water chemistry' conditions (0.50 ppm hydrogen added to the feedwater). Reproduced from Macdonald, D. D.; Balachov, I.; Engelhardt, G. R. *Power Plant Chem.* **1999**, *1*, 9–16.

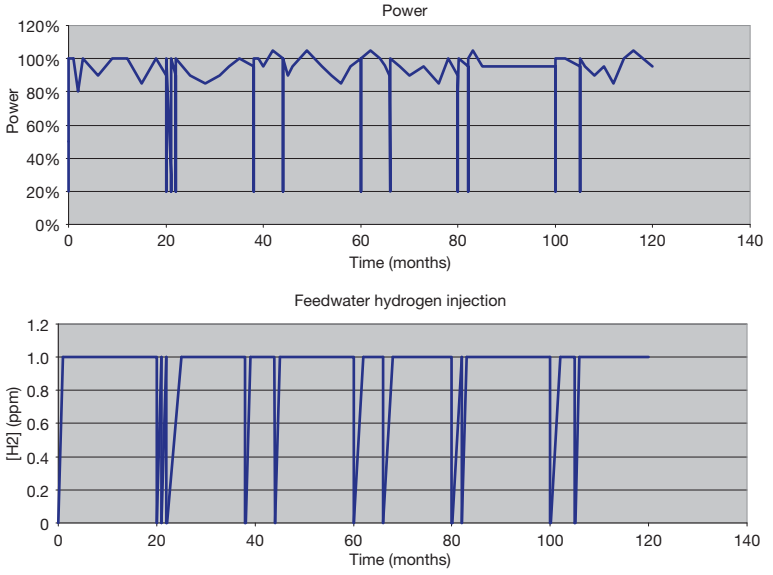

Figure 19 Corrosion evolutionary path (CEP) defined in terms of the prime variables of reactor power and hydrogen added to the reactor feedwater. Reproduced from Macdonald, D. D.; Balachov, I.; Engelhardt, G. R. *Power Plant Chem.* **1999**, *1*, 9–16.

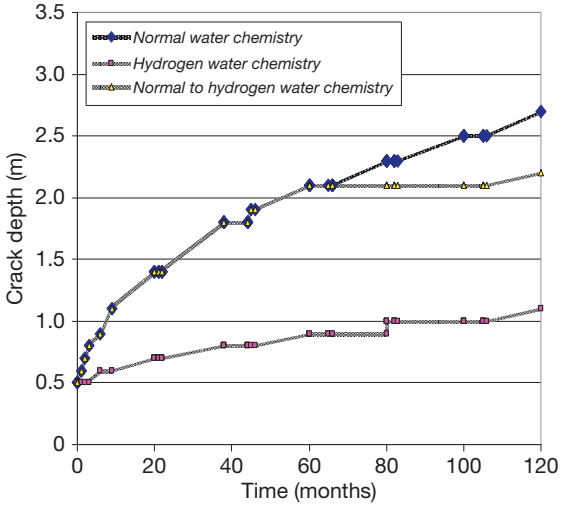

Figure 20 Integrated damage functions (crack length) versus reactor operating time for three operating scenarios: (1) normal water chemistry, (2) hydrogen water chemistry (1 ppm H_2 in the reactor feedwater), (3) NWC for 5 years followed by HWC for the remaining 5 years. Reproduced from Macdonald, D. D.; Balachov, I.; Engelhardt, G. R. *Power Plant Chem.* **1999**, *1*, 9–16.

(1) normal water chemistry (NWC), where no hydrogen is added to the reactor coolant (diamonds), (2) hydrogen water chemistry (1 ppm H_2 in the reactor feedwater over the entire 10-year operating period, squares), and (3) NWC for 5 years followed by HWC for the remaining 5 years (triangles). The various 'jigs and jogs' in the data are not artifacts caused by imprecise calculation, but represent changes in crack growth rate with the changing conditions along the CEP, particularly when the reactor is shut down and started up. During entering and exiting a shutdown period, some of which occur for refueling of the reactor, the hydrogen concentration, coolant conductivity, temperature, coolant flow velocity, and stress (although the stress on the crack was assumed to be primarily residual and hence, is assumed to be constant in the simulations described above) change markedly, but the impact on the overall damage is only small, because the shutdown and start up periods are short. It is seen from **Figure 20** that the crack growth rate (gradient of the curve) decreases with time. This is the consequence of coupling between the internal and external environments of the crack, as postulated in the coupled environment fracture model (CEFM) (see Macdonald *et al.*[23] and citations therein and the corresponding section of this article). Thus, as the crack grows in length under constant potential conditions, a larger IR potential drop occurs down the crack, resulting in a lower potential drop being available on the external surface for the reduction of oxygen or the evolution of hydrogen, thereby resulting in a reduction of the coupling current and hence, a lower crack growth rate. (Note that the crack cannot grow faster than the coupling current can be consumed on the external surface by oxygen reduction and/or hydrogen evolution, and it has been established experimentally

that the crack growth rate is linearly related to the coupling current.)

Under NWC, the crack is predicted to grow by about 2.2 cm over the 10 years of operation (note that we assume an initial crack length of 0.5 cm). If HWC (where 1 ppm of H_2 is added to the reactor coolant water only during operation, see **Figure 19**), the crack is estimated to grow by only 0.6 cm over the 10-year operating period, a substantial reduction in the damage. If, on the other hand, the reactor operated for the first 5 years on NWC (no added hydrogen) and then switched to HWC, the damage (increase in crack length) is predicted to be 1.7 cm. The progression of damage is clearly governed by the 'law of decreasing returns,' in that the damage avoided in the last 5 years by implementing HWC (0.5 cm) is substantially less than that incurred under NWC in the first 5 years (1.6 cm). This is entirely due to the dependence of the crack growth rate on crack length, a dependence that was never previously recognized in crack growth-rate studies. Clearly, predictions of this type are of considerable value, because they allow the benefits to be defined in a cost/benefit analysis. The cost of installing HWC in a BWR is significant because of the need to store considerable amounts of hydrogen on site and because of the need to shield personnel against the production of radioactive $^{16}NH_3$ that forms by neutron bombardment of oxygen in water ($^{1}n_0 + {}^{16}O_8 \rightarrow {}^{16}N_7 + {}^{1}p_1$) under the reducing conditions that exist in the coolant circuit under HWC operating conditions. Note that $^{16}N_7$ is a strong γ-photon emitter.

At this point, it is worthwhile to enquire how accurate the prediction might be for a system that is as complex as an operating BWR. Data published by Tang *et al.*[129] (see also Macdonald *et al.*[23]) for a crack adjacent to the H-3 weld in a reactor operating in Taiwan affords an opportunity to assess the accuracy, as depicted in **Figure 21**. The depth of the crack was assessed by inspection at times of 10 and 20 months after Outage 11 and the ALERT code was fit to the datum for the shorter time, essentially by adjusting the time of nucleation of the crack, such that the calculated and measured crack depth coincided. ALERT was then used to calculate the crack depth at the longer, 20-month time after Outage 11, and the comparison with the measured value is displayed in the figure. Excellent agreement is obtained, with the small residual difference being attributed to uncertainty in the operating history of the reactor.

This example has been presented because it illustrates the application of damage function analysis (DFA) to the deterministic prediction of damage in a complex industrial system. It also illustrates the role of, and the need for, careful characterization,of the CEP. It is the opinion of the authors that a water-cooled nuclear reactor is comparable in complexity to, say, an oil production system, and that meaningful damage prediction calculations are possible on the basis of DFA (or any other deterministic protocol), provided that the CEP is carefully defined.

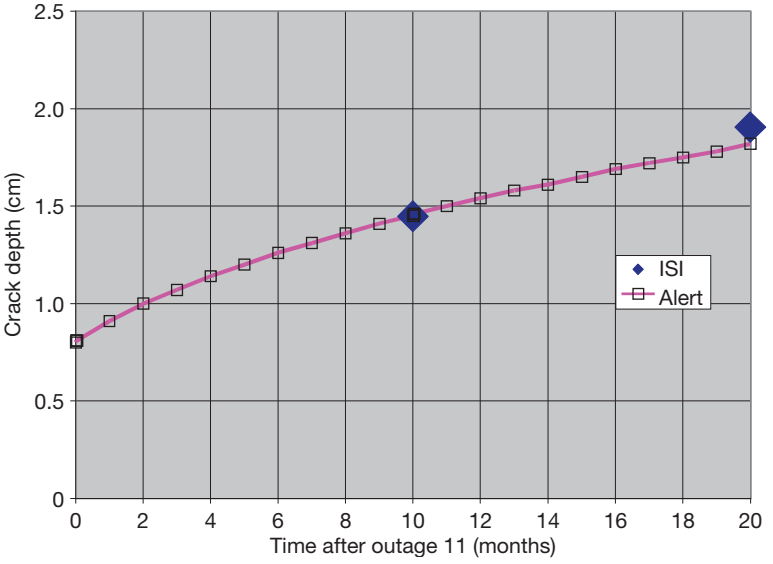

Figure 21 Depth of a crack at the H3 weld in the shroud as a function of time after Outage 11. (♦) Values calculated by ALERT.[19,23] Experimental data reported by Tang *et al.*[129]

Of course, the reward for being able to make such calculations is that it then becomes possible to answer the all-important 'what if' questions, such as: 'What damage will I incur if I operate in this manner?' or 'If I take this corrective measure, can I operate with reasonable certainty to the next outage?' Answers to questions of this type can have significant economic implications.

2.39.10.2 Low Pressure Steam Turbines

Another complex industrial system that has been modeled deterministically with regard to the accumulation of localized corrosion damage is low pressure steam turbines (LPSTs). Failure of LPSTs generally occurs via the cracking of the rotor, disk, or blades, from cracks that nucleate at pits.

Below we will show some results of calculating the probability of failure, P_f, of LPSTs by using the deterministic Monte Carlo simulation method that has been described above.[130] By definition, P_f is the probability that at least one corrosion event in any form (pit, stress corrosion crack, or fatigue crack) reaches a depth, a_{cr}, at a given observation time, t, where a_{cr}, in this case, is the critical dimension (e.g., the stress corrosion crack length at which unstable, rapid mechanical fracture and sudden failure occurs). Using the Monte Carlo simulation method, we can calculate P_f in a straightforward way. Let us assume that we make M calculations of the depth of the deepest corrosion event, x^*, and, in M_f cases ($M_f \leq M$), $x^* > a_{cr}$ for a given observation time, t. In this case, $P_f(a_{cr}, t)$ is defined as

$$P_f = \frac{M_f}{M} \qquad [126]$$

for sufficiently large M.

In particular, it was found that the failure probability is a very sensitive function of the conditions that exist in a low pressure steam turbine (LPST) during shutdown, including the oxygen concentration, chloride concentration, and the fraction of the time spent under shutdown versus operation, if the shutdown environment is not deaerated, and the steel

Table 3 Assumed operational cycle parameters for the development of corrosion fatigue in low pressure steam turbine blades

Shutdown	*Operation cycle*
$t = 100$ h	$t = 500$ h
$\sigma = 0$	$\sigma = \sigma_m + 0.5\ \Delta\sigma \sin(2\pi ft)$
	$\sigma_m = 84$ ksi, $\Delta\sigma = 4$ ksi, $f = 60$ Hz
$T = 25\,^{\circ}$C	$T = 95\,^{\circ}$C
$[O_2] = 8$ ppm	$[O_2] < 1$ ppb
$[Cl^-] = 3500$ ppm	$[Cl^-] < 100$ ppm
pH = 6	pH = 6

Table 4 Assumed operational cycle parameters for the development of corrosion fatigue in low-pressure steam turbine discs

Shutdown	*Operation cycle*
$t = 100$ h	$t = 500$ h
$\sigma = 0$	$\sigma = 95$ ksi
$T = 25\,^{\circ}$C	$T = 160\,^{\circ}$C
$[O_2] = 8$ ppm	$[O_2] < 1$ ppb
$[Cl^-] = 3500$ ppm	$[Cl^-] < 100$ ppm
pH = 6	pH = 6

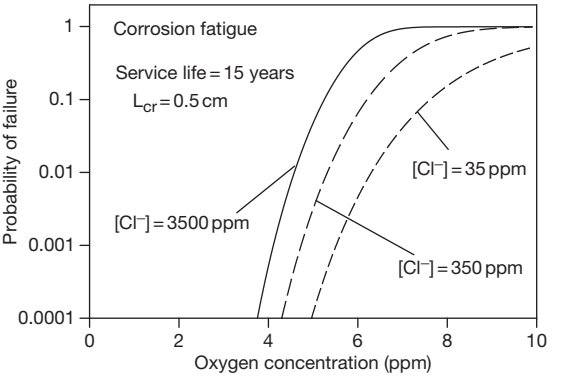

Figure 22 Calculated failure probability for LP steam turbine blades as a function of oxygen concentration for different chloride concentrations in the electrolyte film during the shutdown period. Other parameters are the same as in Table 3.

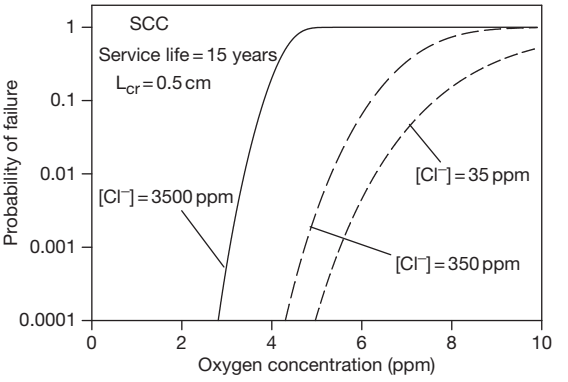

Figure 23 Calculated failure probability for LP steam turbine discs as a function of oxygen concentration for different chloride concentrations in the electrolyte film during the shutdown period. Other parameters are the same as in Table 4.

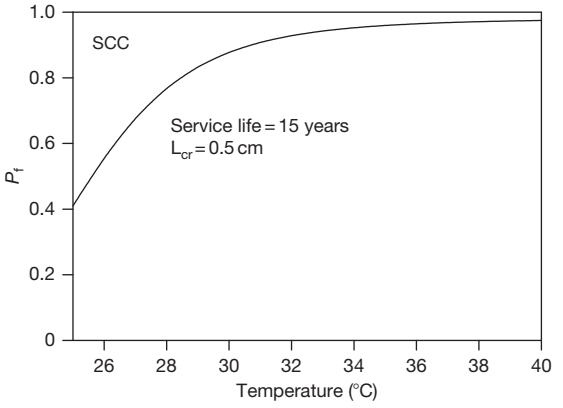

Figure 24 Probability of failure of a turbine disk as a function of temperature during the shutdown period. The oxygen concentration during shutdown period is 4.5 ppm. Other parameters are the same as in **Table 4.**

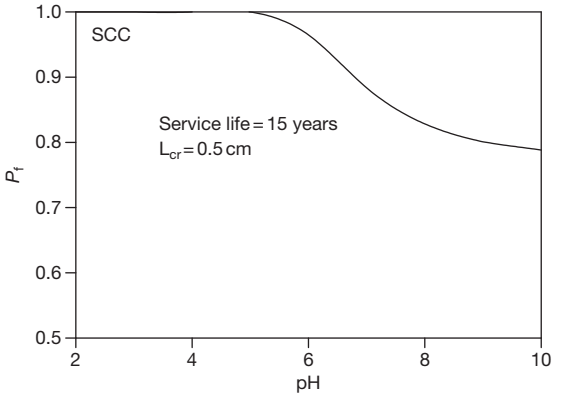

Figure 25 Probability of failure of a turbine disk as a function of pH during the shutdown period. The oxygen concentration during shutdown period is 5.2 ppm. Other parameters are the same as in **Table 4**.

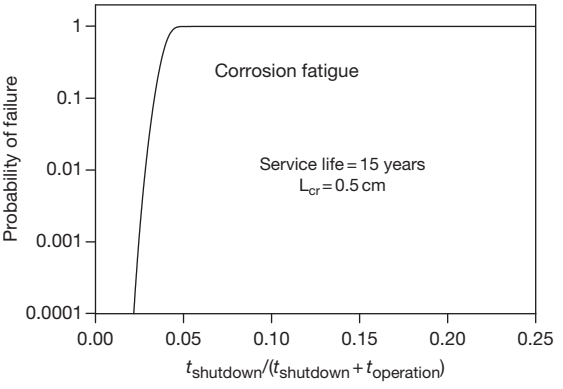

Figure 26 Calculated failure probability for LP steam turbine blades versus the fraction of the time spent in shutdown.

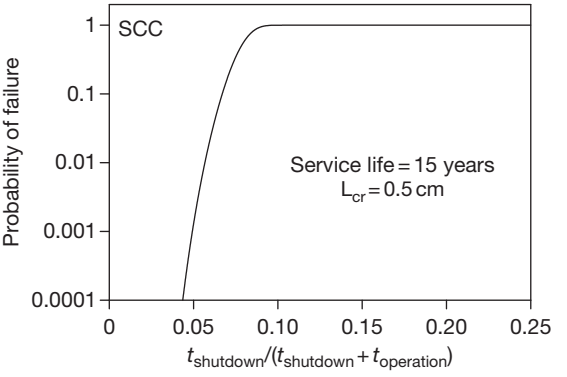

Figure 27 Calculated failure probability for LP steam turbine discs versus the fraction of the time spent in shutdown.

surfaces are not washed free of chloride ion. It is important to note that the calculations were made by using experimentally determined electrochemical parameters for Type 403 SS in the case of determining failure in blades (where CF takes place) and A470/471 steels in the case of determining failure in discs and rotors (where SCC takes place).[131]

For illustrative purposes, we present below only some examples of the influence of environmental parameters on the probability of failure of blades and discs in low pressure steam turbines. The assumed operating cycle parameters for the case of stress corrosion cracking can be found in **Tables 3** and **4**. This information defines the CEP.

The failure probabilities plotted in **Figures 22–27** as a function of $[O_2]$, $[Cl^-]$, temperature, pH, and fraction of the time spent in shutdown under aerated conditions all during the shutdown period, were calculated for 219 shutdown–operation cycles over 15 years, assuming instantaneous nucleation (all pits nucleating during the first shut down) and that all cycles are identical. This particular CEP was chosen for modeling convenience; more complicated CEPs, in which the cycle time and other parameters are varied over realistic ranges, are easily enacted. The critical crack length was assumed to be 0.5 cm, and crack growth was determined to occur primarily by mechanical fatigue during operation.

The calculated failure probabilities plotted in **Figures 22** and **23** are clearly sensitive functions of both the oxygen concentration and the chloride concentration in the condensate on the blade or disk surface left over from operation. Increasing the oxygen concentration under open shutdown (i.e., opening the turbine to the atmosphere) displaces the corrosion potential in the positive direction and hence

increases the pit nucleation and propagation rates, thereby resulting in enhanced pitting damage. Upon subsequent startup, the pits act as stress-raisers for the nucleation of cracks (SCC and corrosion fatigue) and hence lead to an increase in the failure probability. The important lesson to be learned from this plot, and from many simulations of this type, is that deaeration of the turbine upon shutdown should be an effective method of protecting low pressure steam turbines against blade and disc failure after subsequent start-up.

Figures 22 and **23** also show that the failure probability, P_f, decreases sharply to a very low value (essentially zero) as $[Cl^-]$ is lowered below 35 ppm. This provides a second strategy for reducing, or even eliminating the failure of discs and blades, reducing the chloride concentration of Cl^- on the surfaces immediately upon shutdown. This would be most easily instituted by washing the blade and disc surfaces with pure (chloride-free) water immediately upon shutdown of the turbine. In fact, an even more effective strategy would be to combine turbine surface washing with nitrogen blanketing. Given that turbine failure costs anywhere between \$10 million and \$100 million per event, depending upon the nature of the failure, an incentive certainly exists for the utilities to explore the strategies identified above.

The temperature of shutdown is also predicted, in certain situations, to have a visible effect on the failure probability (see **Figure 24**), primarily through the pit growth rate. While this is a substantial reduction, the investment in the necessary facilities to cool a turbine after shutdown is possibly too great to be cost effective, but the desired effect might be achieved through conventional air conditioning.

The remaining environmental variable that is amenable to change is the pH. This variable may be changed by doping the boiler water of the steam with pH buffers, including ammonia, various amines, and systems such as boric acid–hydroxide systems. However, our predictions are that pH has relatively little impact on the failure probability (see **Figure 25**). Thus, the gain that might be achieved in turbine service life possibly would not warrant instituting a major chemistry change upon the basis of enhancing turbine blade and disc life alone.

Figures 26 and **27** clearly show that the probability of failure increases rapidly with the time spent under aerated conditions during shutdown. That is why the reduction of this time could be an effective method of protecting low pressure steam turbines against blade and disc failure.

It must be emphasized that prediction of the probability of failure in LPTS can also be done on the basis of damage function analysis. Examples of the corresponding calculations can be found in Engelhardt *et al.*[132] and Engelhardt and Macdonald.[131]

2.39.11 Conclusions

The purpose of this chapter is to introduce the reader to deterministic methods that have been developed to predict the accumulation of corrosion damage in complex industrial systems. That such predictions can be made is now well beyond question, and it is expected that determinism will rapidly develop as the philosophy of choice in making damage predictions. Because practicing scientists and engineers have seldom taken a course on the philosophies of prediction, few have been exposed to the modeling choices that are available, ranging from empiricism, to 'mechanistic models,' to models that are characterized by varying degrees of determinism. This latter caveat recognizes that, in practice, 'determinism' is an ideal concept that is seldom, if ever, achieved in modeling in pure form. From a practical viewpoint, however, determinism offers a methodology that means minimal calibration, because the dependent/independent variable relationships are captured within the constitutive equations of the model, rather than by calibration, as is the case for an empirical model. As noted above, failure in industrial systems is, by and large, a very rare event, so that almost no chance exists for establishing reliable dependent–independent variable relationships by direct calibration.

Another great advantage of deterministic models is that they draw upon the wealth of scientific experience by constraining the solutions of the constitutive equations to that which is 'physically real' via the natural laws. This feature cannot be overemphasized, as it greatly reduces the need for calibration, provides a condition that must be satisfied and does not arise from the model itself (the model is described by the constitutive equations). If the constraints are absent, or are not imposed, the model may still be 'mechanistic,' but it clearly lacks the predictive power offered by determinism.

In making predictions with any model, be it empirical or deterministic, it is essential to define the CEP, which is the path taken by the system in terms of those independent variables that have a significant impact on the damage accumulation rate as the system changes from the present state

to the future state. Because, the future cannot generally be predicted with certainty, the CEP is most often synthesized to present 'what if' scenarios of operation. These scenarios coupled with economic analyses, may be used to identify the most cost-effective modes of operation and hence, are a valuable financial planning tool. Similarly, the CEP may be designed to ascertain the probability that failure will not have occurred by the time of the next scheduled inspection, which, given the deleterious cost of unscheduled outages, again becomes a valuable financial planning tool. Finally, it is evident that the tools discussed in this chapter are capable of providing valuable input to the design of complex industrial systems, particularly in the light of the fact that corrosion issues are seldom, if ever, given more than cursory examination.

One of the significant advantages of integrating the damage along the CEP to yield the damage function (DF) is that the process may be applied to historical data from which the CEP may be defined with considerable accuracy. In this mode, the predicted damage function becomes a means of accessing the veracity of the model and the damage prediction process. In fact, this type of calculation should always be performed, if for no other reason than that it affords a means of customizing the algorithm to the system of interest. Customization may require the adjustment of values for poorly known parameters in the model or may even require modification of the code itself. In any event, the code becomes the 'alter ego' of the system and provides a means of accurately predicting the accumulation of damage under conditions where the CEP can be defined with historically accuracy.

References

1. Macdonald, D. D.; Urquidi-Macdonald, M. *Corrosion* **1992**, *48*, 354–366.
2. Kowaka, M.; Tsuge, H.; Akashi, M.; Masamura, K.; Ishimoto, H. *Introduction to Life Prediction of Industrial Plant Materials: Application of the Extreme Value Statistical Method for Corrosion Analysis*; Allerton Press, 1994.
3. Harlow, D. G.; Wei, R. P. *AIAA J.* **1994**, *32*, 2073–2079.
4. Harlow, D. G.; Wei, R. P. *Eng. Fract. Mech.* **1998**, *59*, 305–325.
5. Harlow, D. G.; Wei, R. P. *Fatigue Fract. Eng. Mater. Struct.* **2001**, *22*, 427–436.
6. Harlow, D. G.; Wei, R. P. *Fatigue Fract. Eng. Mater. Struct.* **2001**, *24*, 523–535.
7. Harlow, D. G.; Wei, R. P. *Model. Simul. Mater. Sci. Eng.* **2005**, *13*, R33–R51.
8. Macdonald, D. D.; Liu, C. In *Proceedings of the 12th International Corrosion Congress*; NACE International, Houston, TX, 1993; Vol. 5A, pp 3446–3459.
9. Liu, C.; Macdonald, D. D. *J. Press. Vessel Technol.* **1997**, *119*, 393–400.
10. Aziz, P. M. *Corrosion* **1956**, *12*, 35–46.
11. Freiman, L. I. In *Progress in Science and Technology. Corrosion and Corrosion Protection* VINITI, 1985; Vol. 11, pp 3–71 [in Russian].
12. Macdonald, D. D. *Proceedings of Corrosion and Prevention-2000*; Australasian Corrosion Association: Auckland, NZ, Nov 2000; pp 19–22; Paper **42**.
13. Engelhardt, G. R.; Macdonald, D. D. *Corrosion* **1998**, *54*, 469–479.
14. Engelhardt, G. R.; Macdonald, D. D. *Corros. Sci.* **2004**, *46*, 2755–2780.
15. McCartney, L. N. *Int. J. Fract.* **1979**, *15*, 477–487.
16. Turnbull, A.; McCartney, L. N.; Zhou, S. *Corros. Sci.* **2006**, *48*, 2084–2105.
17. Polyanin, A. D.; Zaitsev, V. F.; Moussiaux, A. *Handbook of First Order Partial Differential Equations*; Taylor & Francis: London, 2002.
18. Wagner, C.; Traud, W. *Z. Elektrochem.* **1938**, *44*, 391–402.
19. Macdonald, D. D.; Urquidi-Macdonald, M. In *Encyclopedia of Electrochemistry*; Bard, A. J., Stratmann, M., Eds.; Wiley-VCH: Weinheim, 2006; *Electrochemical Engineering*, Vol. 5, Macdonald, D. D., Schmuki, P., Eds., pp 665–720.
20. Macdonald, D. D. *Corrosion* **1992**, *48*, 194–205.
21. Macdonald, D. D. *Pure Appl. Chem.* **1999**, *71*, 951–978.
22. Selman, J. R.; Tobias, C. W. *Advan. Chem. Eng.* **1978**, *10*, 211.
23. Macdonald, D. D.; Balachov, I.; Engelhardt, G. R. *Power Plant Chem.* **1999**, *1*, 9–16.
24. Anderko, A.; Young, R. D. *Corrosion* **2000**, *56*, 543–555.
25. Anderko, A.; McKenzie, P.; Young, R. D. *Corrosion* **2001**, *57*, 202–213.
26. Sridhar, N.; Brossia, C. S.; Dunn, D. S.; Anderko, A. *Corrosion* **2004**, *60*, 915–936.
27. Nordsveen, M.; Nešić, S.; Nyborg, R.; Stangeland, A. *Corrosion* **2003**, *59*, 443–456.
28. Nešić, S.; Cai, J.; Lee, K.-L. *Corrosion/2005*; NACE International: Houston, TX, 2005; Paper no. 05556.
29. Davydov, A. D.; Shaldaev, V. S.; Engelhardt, G. R. *Russian J. Electrochem.* **2006**, *42*, 121–128.
30. Davydov, A. D. *Russian J. Electrochem.* **2008**, *44*(7), 835–839.
31. Stewart, J.; Williams, D. E. In *Advances in Localized Corrosion*; Isaacs, H. S., *et al.* Eds.; NACE International: Houston, TX, 1990; pp 131–136.
32. Pistorius, P. S.; Burstein, G. T. *Philos. Trans. R. Soc. Lond. A* **1992**, *341*, 531–559.
33. Williams, D. E.; Stewart, J.; Balkwill, P. H. *Corros. Sci.* **1994**, *36*, 1213–1235.
34. Williams, D. E.; Westcott, C.; Fleischmann, M. *J. Electrochem. Soc.* **1985,** *132,* 1796, 1804.
35. Lin, L. F.; Chao, C. Y.; Macdonald, D. D. *J. Electrochem. Soc.* **1981**, *128*, 1194.
36. Macdonald, D. D.; Urquidi-Macdonald, M. *Electrochim. Acta* **1986**, *31*, 1079.
37. Macdonald, D. D.; Urquidi-Macdonald, M. *J. Electrochem. Soc.* **1987**, *134*, 41.
38. Macdonald, D. D.; Urquidi-Macdonald, M. *J. Electrochem. Soc.* **1989**, *136*, 961.
39. Macdonald, D. D.; Urquidi-Macdonald, M. *J. Electrochem. Soc.* **1992**, *139*, 3434–3449.

40. Uhlig, H. In *Passivity of Metals*; Frankenthal, R. P., Kruger, J., Eds.; The Electrochemical Society: Princeton, NJ, 1978; p 1.
41. Engell, H. *Electrochim. Acta* **1977**, *22*, 987.
42. Macdonald, D. D. *J. Electrochem. Soc.* **2006**, *153*, B213–B224.
43. Kong, D-S.; Chen, S-N.; Wang, C.; Yang, W. *Corros. Sci.* **2003**, *45*, 747.
44. Tsuchiya, H.; Fujimoto, O.; Chinara, O.; Shibata, T. *Electrochim. Acta* **2002**, *47*, 4357.
45. Kaesche, H. *Z. Phys. Chem. (Neue Folge)* **1962**, *34*, 87.
46. Böhni, H.; Uhlig, H. H. *J. Electrochem. Soc.* **1969**, *116*, 906–910.
47. Shibata, T. *Trans ISIJ* **1983**, *23*, 785.
48. Fratesi, R. *Corrosion* **1985**, *41*, 114.
49. Reuter, M.; Heusler, K. E. *Electrochim. Acta* **1990**, *35*, 1809–1814.
50. Carslaw, H. S.; Jaeger, J. C. *Conduction of Heat in Solids*, 2nd ed.; Oxford Press: London, 1959.
51. McGeough, J. A. *Principles of Elecrochemical Machining*; Chapman and Hall: London, 1974.
52. Newman, J.; Thomas-Alyea, K. E. *Electrochemical Systems*, 3rd ed.; Prentice Hall: Englewood Cliffs, NJ, 2004.
53. Chang, H.-Y.; Park, Y.-S.; Hwang, W.-S. *J. Mater. Process. Technol.* **2000**, *103*, 206–217.
54. Bird, B. R.; Stewart, W. E.; Lightfoot, E. N. *Transport Phenomena*, Wiley: New York, 2002.
55. Davis, J. T. *Turbulence Phenomena*; Academic Press: London, 1972.
56. Popov, Yu. A.; Alekseev, Yu. V.; Kolotyrkin, Ya. M. *Sov. Electrochem.* **1979**, *14*, 1260.
57. Walton, J. C.; Grangolino, G.; Kalandros, S. K. *Corros. Sci.* **1996**, *38*, 1–18.
58. Turnbull, A. *Br. Corros. J.* **1993**, *28*, 297–308.
59. Lasaga, A. C.; Kirkpatrick, R. J. *Kinetics of Geochemical Processes*; Mineralogical Society of America: Washington, 1981.
60. Walton, J. C. *Corros. Sci.* **1990**, *30*, 915–928.
61. Sharland, S. M. *Corros. Sci.* **1992**, *33*, 183.
62. Engelhardt, G. R.; Strehblow, H.-H. *Corros. Sci.* **1994**, *34*, 1171–1725.
63. Laycock, N. J.; White, S. P. *J. Electrochem. Soc.* **2001**, *148*, B264–B275.
64. Yao, L. S.; Prusa, J. *Adv. Heat Transfer* **1989**, *19*, 1.
65. Engelhardt, G. R.; Davydov, A. D. *Russian J. Electrochem.* **1994**, *30*, 865.
66. Engelhardt, G. R.; Strehblow, H.-H. *J. Electroanal. Chem.* **1994,** *365,* 7.
67. Engelhardt, G. R.; Strehblow, H.-H. *J. Electroanal. Chem.* **1995,** *394,* 7.
68. Pillay, B.; Newman, J. *J. Electrochem. Soc.* **1993**, *140*, 414.
69. Verbrugge, M. V.; Bakker, D. R.; Newman, J. *J. Electrochem. Soc.* **1993**, *140*, 2530.
70. COMSOL software, www.comsol.com.
71. OLI Systems software, www.olisystems.com.
72. Papavinosan, S.; Revie, W.; Friesen, W. *Corrosion Reviews* **2006**, *24*, 173–230.
73. Isaacs, H. S. *J. Electrochem. Soc.* **1973**, *120*, 1456.
74. Doig, P.; Flewitt, E. J. *Metall. Trans. A* **1981**, *12*, 927.
75. Ateya, D. G.; Pickering, H. W. *J. Appl. Electrochem.* **1981**, *11*, 453.
76. Gravano, S.; Galvele, J. R. *Corros. Sci.* **1984**, *24*, 517.
77. Sharland, S. M.; Tasker, P. W. *Corros. Sci.* **1988**, *28*, 603.
78. Sharland, S. M.; Jackson, C. P.; Diver, A. J. *Corros. Sci.* **1989**, *29*, 1149.
79. Sharland, S. M. *Corros. Sci.* **1992**, *33*, 183.
80. Alkire, R.; Sittary, D. *J. Elecrochem. Soc.* **1979**, *126*, 15.
81. Galvele, J. R. *J. Electrochem. Soc.* **1976**, *123*, 464.
82. Galvele, J. R. *Corros. Sci.* **1981**, *21*, 551.
83. Newman, J.; Hanson, D. B.; Vetter, K. *Electrochim. Acta* **1977**, *22*, 829.
84. Harb, J. N.; Alkire, R. C. *J. Electrochem. Soc.* **1991**, *138*, 2594.
85. Evans, U. R. *J. Inst. Met.* **1923**, *30*, 239.
86. Manahan, M. P.; Macdonald, D. D.; Peterson, A. J. *Corros. Sci.* **1995**, *37*, 189.
87. Zhou, X.; Balachov, I.; Macdonald, D. D. *Corros. Sci.* **1998**, *40*, 1349.
88. Yeh, T-K.; Tsai, C-H.; Chang, C-Y. In Proceedings of the 11th International Symposium on Environmental Degradation of Materials in Nuclear Power Systems – Water Reactors : ANS, WA, USA, 10–14, August 2003; pp 500–511.
89. Macdonald, D. D.; Urquidi-Macdonald, M. *Corros. Sci.* **1991**, *32*, 51.
90. Macdonald, D. D.; Lu, P.-C.; Urquidi-Macdonald, M.; Yeh, T.-K. *Corrosion* **1996**, *52*, 768.
91. Engelhardt, G. R.; Urquidi-Macdonald, M.; Macdonald, D. D. *Corros. Sci.* **1997**, *39*, 419–441.
92. Engelhardt, G. R.; Macdonald, D. D.; Urquidi-Macdonald, M. *Corros. Sci.* **1999**, *41*, 2267–2302.
93. Vankeerberghen, M.; Macdonald, D. D. *Corros. Sci.* **2002**, *44*, 1425.
94. Engelhardt, G. R.; Macdonald, D. D. In *Corrosion/ 2000,* Orlando, FL, March 2000, Paper no. 00227, pp 1–12.
95. Engelhardt, G. R.; Macdonald, D. D.; Millet, P. *Corros. Sci.* **1999**, *41*, 2165–2190.
96. Turnbull, A. *Corros. Sci.* **1999**, *41*, 2267.
97. Gavrilov, S.; Vankeerberghen, M.; Deconinck, J.; Vereecken, J. In 4th Workshop LWR Coolant Water: Radiolysis and Electrochemistry Avignon: 2002, 26 April France.
98. Ford, F. P. In *Corrosion sous contrainte-phénoménologie et mécanismes*; Desjardins, D., Oltra, R., Eds.; Bombannes, 1990.
99. Ford, F. P.; Taylor, D. F.; Andresen, P. L.; Ballinger, R. G. Corrosion-assisted cracking of stainless and low-alloy steels in LWR environments, EPRI Final Report NP-5064M, Project 2006-6; Palo Alo: Electric Power Research Institute, CA, 1987.
100. Shoji, T. Quantitative prediction of environmentally assisted cracking based on crack tip strain rate *American Society of Mechanical Engineers, Pressure Vessels and Piping Division (Publication) PVP* **1985**, *Vol. 99*, 127–142.
101. Shoji, T.; Moriya, S.; Arai, H.; Higashi, M. In *Fracture Mechanics Applications;* American Society of Mechanical Engineers, Pressure Vessels and Piping Division (Publication) PVP, 1994; Vol. *287*, pp 107–113.
102. Vankeerberghen, M.; Gavrilov, S. In EUROCORR 2001, Riva del Garda: Italy, 30 September–4 October 2001.
103. Peng, Q. J.; Kwon, J.; Shoji, T. *J. Nucl. Mater.* **2004**, *324*, 52.
104. Macdonald, D. D.; Lvov, S. N.; Kelkar, G.; Magalhaes, J. F.; Kwon, H.-K.; Wuensche, A.; Biswas, R.; Ahmad, Z.; Engelhardt, G. R.; Urquidi-Macdonald, M. The development of deterministic methods for predicting corrosion damage in water-cooled nuclear reactors, Final Report EP93–33 Empire State Electric Energy Research Corporation (ESEERCO): New York, NY, November 1996.

105. Wuensche, A.; Macdonald, D. D. In CORROSION 2001, Houston, TX, 2001, Paper no. 01236.
106. Andresen, P. L. *Corrosion* **1993**, *49*, 714.
107. Wilkinson, D. S.; Vitek, V. *Acta Metall.* **1982**, *30*, 1723.
108. Macdonald, D. D. In Proceedings of the Chimie 2002 (French Nuclear Society) Avignon: France, April 2002.
109. Szklarska-Smialowska, Z. *Pitting Corrosion of Metals*; National Assosiation of Corrosion Engineers: Houston, TX, 1986.
110. Engell, H. J.; Stolica, N. D. *Z. Phys. Chem., NF* **1959**, *20*, 113.
111. Macdonald, D. D.; Lui, C.; Urquidi-Macdonald, M.; Stickford, G. H.; Hindin, B.; Agrawal, A. K.; Krist, K. *Corrosion* **1994**, *50*, 761.
112. Engelhardt, G. R.; Macdonald, D. D. *Corros. Sci.* **2004**, *46*, 1159–1187.
113. Wei, R. P. In *Fracture Mechanics: Microstructure and Micromechanics*; Nair, S. V., *et al.* Ed.; ASM International: Metals Park: OH, 1989.
114. Turnbull, A. *Corros. Sci.* **1993**, *34*, 921–960.
115. Unger, D. J. *Analytical Fracture Mechanics*; Academic Press: San Diego, 1995.
116. Peng, O. J.; Kvon, J.; Shoji, T. *J. Nucl. Mater.* **2004**, *324*, 52–61.
117. Turnbull, A.; Zhou, S. *Corros. Sci.* **2004**, *46*, 1239–1264.
118. Turnbull, A.; McCartney, L. N.; Zhou, S. *Corros. Sci.* **2006**, *48*, 2084–2105.
119. Anderko, A.; Sridhar, N.; Dunn, D. S. *Corros. Sci.* **2004**, *46*, 1583–1612.
120. Kondo, Y. *Corrosion* **1989**, *45*, 7–11.
121. Marsh, G. P.; Bland, I. D.; Tailor, K. J. *Br. Corros. J.* **1988**, *23*, 157.
122. Strutt, J. E.; Nicholls, J. R.; Barbier, B. *Corros. Sci.* **1985**, *25*, 305.
123. Engelhardt, G. R.; Macdonald, D. D.; Zhang, Y.; Dooley, B. *PowerPlant Chem.* **2004**, *6*, 647.
124. Shibata, T.; Akoshi, M.; Ikematsi, K.; Nakajima, H.; Tsuge, H. *Corros Eng.* **1988**, *37*, 699–705.
125. Laycock, P. J.; Cottis, R. A.; Scarf, P. A. *J. Electrochem. Soc.* **1990**, *137*, 64–69.
126. Engelhardt, G. R.; Macdonald, D. D. In CORROSION/2008, New Orleans, April 2008; Paper no. 08270.
127. Kamaya, M.; Totsuka, N. *Corros. Sci.* **2002**, *44*, 2333.
128. Yeh, T. K.; Macdonald, D. D.; Motta, A. T. *Nucl. Sci. Eng.* **1995**, *121*, 468–482.
129. Tang, J. R.; Kao, L.; Shiau, D.-Y.; Chao, L.-Y.; Yao, C.-C.; Chiang, S. C. *Nucl. Technol.* **1998**, *121*, 324–336.
130. Engelhardt, G. R.; Macdonald, D.; Dooley, B. *PowerPlant Chem.* **2007**, *9*, 454–462.
131. Engelhardt, G. R.; Macdonald, D. D. Development of code to predict stress corrosion cracking and corrosion fatigue of low pressure turbine components, EPRI Report 1004190, 2004.
132. Engelhardt, G. R.; Macdonald, D. D.; Zhang, Y.; Dooley, B. *PowerPlant Chem.* **2004**, *6*, 647–662.